The influence of installing UTES boreholes on the bearing capacity of pile foundations

P. Griffioen

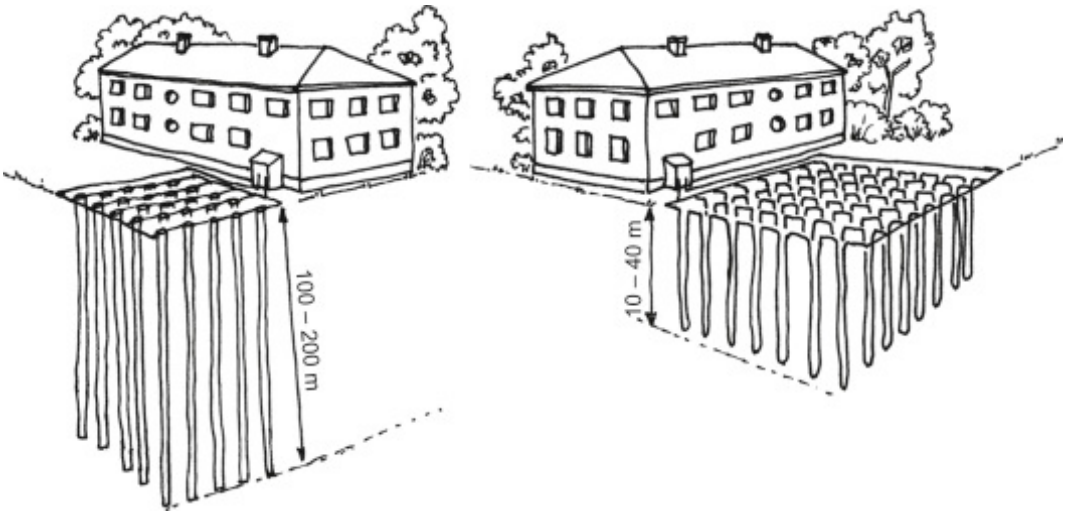

TU Delft

FUGRO

The influence of installing UTES boreholes on the bearing capacity of pile foundations

by

Pieter Jelle Griffioen

to obtain the degree of Master of Science
in Applied Earth Sciences, Geo-Engineering
at the Delft University of Technology,
to be defended publicly at January 13, 2021 at 3 p.m.

Thesis committee:

Dr. P.J. Vardon, TU Delft, Geoscience and Engineering (Chair)

Ir. P.R.M. Ammerlaan, TU Delft, Geoscience and Engineering

Prof. K. Gavin, TU Delft, Geoscience and Engineering

Dr. J.M. Bloemendal, TU Delft, Hydrology

Ir. M. Profittlich, Fugro NL

Ir. F. Hoefsloot, Fugro NL

an electronic version of this thesis is available at http://repository.tudelft.nl/.

Preface

Hereby I would like to present to you my master's thesis "The influence of installing UTES boreholes on the bearing capacity of piles". This thesis was written to obtain the degree of Master of Science in Geo-Engineering in Applied Earth Sciences at the Delft University of Technology. A cooperation with Fugro NL was set for the completion of this report. After one and a half years of attending classes and making exams, writing a thesis was an interesting final journey towards my graduation.

First of all, I would like to thank my committee members from the TU Delft for the support and feedback during the last seven months. In general, I want to thank you all for the positive and progressive thoughts during my meetings. Phil, thank you for always pushing me into the right direction even when I thought I was completely stuck. Thanks also for the great availability and the quick responses on my emails in these times of long-distance communication. Martin, thanks for the detailed feedback on the many different types of BTES, BHE, ATES and UTES systems, which still can get me quiet confused. Patricia, thanks for the help with everything that had to do with piles and your practical insights in PLAXIS simulations of which I thought way too complicated. Ken, despite your busy agenda and little personal feedback, a lot of your feedback probably still reached me through Phil, thanks.

A lot of feedback and practical help was given by my committee members from Fugro as well. Despite the strange times that we have been living in since the start of this thesis project, you did everything possible to manage me through it. Maarten, I want to thank you for arranging all the materials, meetings, feedback and everything else that was necessary to finish this project even though personal contact was not always possible. Flip, thanks for providing incredible technical help and feedback and the never changing 'online' status on Teams which made it possible for me to call whenever I got PLAXIS errors or needed help. Also, sorry for being a bit stubborn in my choices for the PLAXIS model types.

Last but not least I want to thank all my roommates, in this extraordinary times, for thinking along and being so quiet during my many meetings. Also I want to thank all my friends and family for being so supportive and friendly.

Pieter Griffioen
Amsterdam, December 2020

Abstract

The transition to renewable energy has lead to many new ways of energy production, such as wind and solar energy. For solar energy power, there is an excess of energy during summer and an deficiency of it during winter, which is reversed for the energy consumption. In order to amend this problem, there is an introduction of new ways of energy storage in the form of heat for domestic and industrial use. One of these is the use of Underground Thermal Energy Storage (UTES). These systems make use of the underground to store heat during summer and extract heat during winter by using a fluid as the heat transferring agent. There are many different ways of UTES installation, however there are two which are widely used in the Netherlands: 1) Aquifer Thermal Energy Storage (open systems) which are based on heat-transfer by convection and 2) Borehole Heat Exchangers (closed systems) which are based on heat-transfer by conduction. While the way of transferring heat differs, they both need vertically drilled boreholes to reach a certain storage depth. These boreholes are drilled close to, or underneath, pile-founded buildings. The drilling of boreholes influence in-situ soil stresses around them, which might influence the bearing capacity of the piles. The aim of this thesis is to investigate the influence of installing UTES systems on the bearing capacity of piles. This is done by: 1) investigating the stress changes in sand due to the drilling of boreholes (stress analysis) and 2) the influence of these stress changes on the bearing capacity of piles (bearing capacity analysis). All of the modelling was done in PLAXIS, by using the 2D-axisymmetric model for the first part and the 3D plane strain model for the second part. An advanced soil model for sand was used, with soil mechanical behavior according to the Hardening Soil small strain model. The stress analysis consists out of a parameter sensitivity analysis, including the key parameters: backfill grout shrinkage and expansion, Over-Consolidation Ratio and Relative Density. After this, the influence of the borehole fluid pressure and borehole diameter on the stress states were investigated. As not all boreholes are drilled perfectly, the last part of the stress-analysis takes into account drilling complications. The bearing capacity analysis includes simulations of static pile load tests of non-displacement piles. Load-displacements curves are produced for several scenario's: 1) perfectly drilled boreholes, 2) boreholes with drilling complications, 3) influence of a soft soil layer and 4) displacement piles and the influence of a varying installation phasing. The results indicate no large effects of perfectly drilled boreholes on bearing capacity of piles located outside a zone of 1.5 times the borehole diameter. For boreholes with drilling complications, the bearing capacity is influenced for piles located in a zone of influence of only several meters (2-6m), depending on the severity of the complication. At last, loaded piles of existing buildings are extremely sensitive for stress changes due to the drilling process, which will cause severe loss of bearing capacity.

Contents

List of Figures

List of Tables

Nomenclature

BTES = Borehole Thermal Energy Storage

BHE = Borehole Heat Exchanger (closed system)

ATES = Aquifer Thermal Energy Storage (open system)

Hoop stress = stresses acting tangential to the borehole wall (σ_{yy})

Radial stress = stresses acting perpendicular to the borehole wall (σ_{xx})

Vertical stress = stresses acting in the vertical direction of the borehole wall (σ_{zz})

Tangential stress = stresses acting tangential to the borehole wall, equal to hoop stress

Zone of influence = radial zone around the borehole wall in which the stress state is less than 95 percent its initial value (at the same depth)

MC model = Mohr-Coulomb model

HSs model = Hardening Soil Small Strain model

HS model = Hardening Soil model

LE model = Linear-Elastic model

CPT = Cone Penetration Test

1

Introduction

1.1. Project Relevance

The quick and definite depletion of fossil fuels and the adventitious global warming gave rise to a demand for new ways of energy sources during the late 20^{th} century. These new energy sources attempt to decrease the carbon dioxide emission and find alternatives for fossil fuels, called renewable energy sources. Two of those renewable energy sources with high potential are from wind and solar sources.. The total share in wind and solar power in the Netherlands has manifolded by a factor 3 from 2016 to 2019 (CBS, 2019 and Schoemaker et al., 2020). Next to this, the governmental cabinet has set agreements to meet the goals of the Paris Climate Agreement and decrease the emission of greenhouse gasses. One of these agreements for the heating of domestic houses is to fully knock off the use of gas and strive for new systems to heat houses (Ministry of Economic Affairs and Climate Policy, 2020).

Solar energy sources are becoming increasingly popular for the supply of domestic heat as an alternative for fossil fuel based energy resources. One of the main problems that arises from using solar energy for domestic heat supply, is the seasonal variability between energy power and heat demand. During winter, the heat demand is extremely high while the solar energy power is relatively low. This is the exact opposite for the summer period. In order to amend this seasonal variability, an efficient way of energy storage is needed. In this way, the surplus solar power can be stored in terms of heat. One of the popular and relatively payable storage systems is by using Underground Thermal Energy Storage (UTES) systems. In Europe, an increase of 50 percent of usage of UTES systems was seen from 2004 to 2006 (Gao et al., 2015). In the Netherlands, this trend was more or less equal and kept growing strongly until 2010. A growth of 10 percent per year was seen for the past three years (CBS, 2019). The use of UTES systems to store energy is popular for both domestic and industrial energy demands. Many existing buildings switch from fossil fuel heated systems to heat from solar energy power in combination with UTES systems.

As these UTES systems are used in different geological settings, they exist in many different forms. For all of them, vertically drilled boreholes are used for the transport of a

heat carrying fluid, which is transported to a certain depth. At this required depth heat exchange can occur in many different forms. In the Netherlands, however, two main types of UTES systems exist: 1) the Borehole Heat Exchange systems (BHE systems) or closed systems in which the subsurface is used to exchange heat by means of conductivity and 2) the Aquifer Thermal Energy Storage systems (ATES systems) or open systems in which heat is exchanged by convection in an aquifer (Nilsson, 2020). Due to a high variety in groundwater aquifers in the Netherlands, ATES (open systems) are favoured over closed systems. Next to this, ATES systems are mostly used for higher energy power demands (Fleuchaus et al., 2020). In order to make these systems economically feasible, a lot of investigations and studies focus on the efficiency of the systems. These studies give a clear picture of how the technical aspects of the systems need to be installed in varying geotechnical circumstances to reach a high efficiency (Fleuchaus et al., 2020, Rad and Fung, 2016, Welsch et al., 2016, Gao et al., 2015 and Reuss, 2015). The studied technical aspects include: spacing, depth, the amount of boreholes per array and which kind of system is used (open or closed). All of these studies do not focus on the effects of the installation process of the UTES boreholes on the subsurface. There is knowledge on how the drilling of boreholes for wells in petroleum engineering change the stress states in cemented, highly consolidated and often rocky sand formations (Press et al., 1993, Zhang, 2019, Vaziri and Byrne, 1990 and Aadnøy and Looyeh, 2019). However, these studies focus more on rock mechanics instead of poorly consolidated sand and soft soil layers in the shallow subsurface. This shallow subsurface is of such relevance because piles for foundations are embedded in these layers and the in-situ stress states will determine the bearing capacity of the piles. The UTES systems for domestic and industrial use are often installed close to the pile foundations.

1.2. Problem

In the close future, many new UTES systems are used for domestic and industrial heat. A lot of these systems need to be installed in old neighbourhoods were free space is scarce and houses are constructed at small spacing. This means that the boreholes that are drilled for both systems are drilled close to, or underneath, the existing houses or buildings. Next to this, a great portion of the new residential areas built in the future will have a UTES system for energy storage. This is why a better understanding of the influence of borehole drilling processes on the direct subsurface is required. Many of the houses built on soils containing soft layers, a large percentage of buildings are constructed on piles. Previous studies only pay scarce attention to potentially negative effects of the borehole drilling process on the bearing capacity of pile foundations. Only a rough and outdated rule of thumb is used for the required spacing between borehole and piles exist (Spegelaere M., 2019). A better understanding of the influence of borehole drilling on the bearing capacity of piles will help to improve security and available knowledge.
There are several different aspects contained by this specific problem. It is known that the drilling of boreholes causes changes in the stress state and strength of the surrounding soil. The exact effects are still very unexplored in literature and are part of this study. Next to this, drilling complications can occur during the borehole drilling process, aggravating the changes in stress state and strength. The bearing-capacity of pile foundations depends on complicated soil features, which are influenced by both short- and long-term processes. Next to this, the difference of displacement and non-displacement piles play an important role. In addition, the phasing of the installation of these piles are an important factor in these processes. The combination of the effects caused by the borehole and pile construction is an extensive study, which depends on many different input parameters and geotechnical

features. To obtain a better understanding of this problem, all of these factors need to be studied separately first after which the influence on the individual factors need to be investigated.

1.3. Research objective and questions

The main goal of this study is to investigate the influence of boreholes for UTES systems on the bearing capacity of pile foundations. As mentioned above, this influence is determined by many different input parameters and geotechnical features. This is why the problem must be considered conceptually in order to understand the complex problem. After this understanding was obtained, an extended model has been designed in the software program PLAXIS. in this extended model, every parameter and feature can be investigated separately. This is done by means of a study focusing on the key parameters and their influence on the stress states around boreholes. After this, the stress states around boreholes are investigated for different drilling processes and borehole diameters. At last, the influence of these changes in stress states on the bearing capacity of piles is needed. In this way, a qualitative and quantitative understanding of the problem is obtained. Next to this, an understanding of which parameters and stress redistribution have what effect on the bearing-capacity of piles is acquired.

The main aim of this study is contained in the main research question:

What is the influence of the installation of shallow BHE and ATES systems on the bearing capacity of piles?

In order to answer this research questions, the following supporting sub-questions are answered:

1. *What is the influence of drilling boreholes for ATES and BHE systems on the stress-strain state and strength of soils and how is this influenced by*:

    a. Over-Consolidation Ratio
    b. Shrinkage or expansion of grout bodies
    c. Relative Density
    d. Borehole diameter
    e. Drilling complications

2. *What is the influence of the installation of ATES and BHE systems on the bearing capacity of piles and how is this influence by:*

    a. Drilling complications
    b. Installation type of pile
    c. Different soil types

3. *Can the extended models developed in this research be validated with a practical case in the Netherlands ?*

2

Literature study

2.1. Principles of ATES and BHE systems

The BHE and ATES systems are also called seasonal thermal energy storage systems, which make use of the difference in seasonal energy power. During summer, there is a surplus in solar energy power which is used to warm up a heat carrying fluid. This relatively warm fluid is then pumped down to a certain depth. Heat is stored at this specific depth by different means (depending on the type of system). At this depth in the subsurface, temperatures are relatively constant over time allowing for a relatively efficient way of heat storage. The heat is extracted whenever needed by means of inverting the system.

For BHE systems, heat is transferred by conduction, warming up a volume of soil or rock surrounding the boreholes. This is achieved by pumping a heat carrying fluid, normally a mix of water and glycerol against the freezing, to a depth of around 30-200m in vertically drilled boreholes. This depth depends on the location of a suitable rock or soil formation and the system geometry. The most important geotechnical features to suit a BHE system are (Rad and Fung, 2016):

- Drillable soil or rock
- Groundwater favourable
- High heat capacity
- High thermal conductivity
- Low hydraulic conductivity
- Suitable rock or soil formation within 30-200 m depth

For ATES systems, the fluid (groundwater) is pumped down to an aquifer where heat is transferred by means of convection, warming up volume of pore water around the BHE. Due to small energy losses over time, this warmth can be used in winter by extracting heat from this aquifer volume. During summer, cool groundwater can be pumped up in order to cool down the building. For these systems in the Netherlands, spacing is highly situation depend and the depth varies between the 50 - 200m (CBS, 2019). In addition, the most important geotechnical features for ATES systems are Fleuchaus et al., 2020:

- Drillable soil or rock
- Low hydraulic conductivity
- Confined aquifer (thickness depends on energy demand)

Usually, the storage volume can be described by the approximate volume of soil or rock confining the part where heat exchange occurs. For BHE systems this is the entire area surrounding the array of vertical boreholes. For ATES systems, this is the aquifer volume surrounding the BHE.

The efficiency of the system is mainly determined by the heat loss from the storage field. The magnitude of this heat loss is determined by many parameters like: the storage geometry (size and shape), average store temperature, soil properties and the borehole spacing (for closed systems)(Nilsson, 2020). As spacing is important for this research, more information is given in chapter 2.1.2.

2.1.1. Open and closed systems

The storage volume can be used in two different ways. As an open system, in which the heat carrying fluid is in direct contact with the storage medium and is transferred by convection. And as a closed system, in which the heat is transferred from the heat carrying fluid to the storage medium by means of heat conductivity.

The open system makes use of a large diameter HDPE pipe running through the borehole. The annulus between the pipe and the borehole wall is then back-filled with gravel. A borehole diameter of 0.3m and 1.0m is used (SIKB, 2019). In order to exchange water from the storage medium (aquifer) to the boreholes a Borehole Heat Exchanger is used. This is installed over the complete aquifer length and transfers water from the system to the aquifer. It is of great importance that this is installed properly. This type of system is only used in specific sand aquifers. Due to environmental reasons, this system is only used in formations where there is no leakage to the environment and when pure and clean water can be used as heat transfer fluid. In the Netherlands, open systems exist out of two borehole wells with a minimal horizontal spacing of 50-100m (SIKB, 2019). Due to seasonal differences in temperature a warm and a cold well is generated. Warm water is extracted from the warm well, while cold water is injected in the cold well during winter. In the summer season this is completely reversed, as can be seen in fig. 2.1.

In the case of closed systems, double U-pipes, single U-pipes or concentric pipes are installed in the borehole, as illustrated in fig. 2.2. For a double U-pipe system there are two inlet and outlet pipes while for a single U-pipe system there is only one of each of them. These pipes are made of synthetic material (like HDPE) due to its high thermal conductivity. For the double U-pipe installation type, boreholes have an overall diameter is 0.2m. For the single U-pipe installation type, the borehole diameter differs between 0.1 and 0.2m. As can be seen in fig. 2.2, after the installation of the pipes, the boreholes are back-filled with thermally enhanced grout. This allows for proper heat conduction in order to extract heat from the soil surrounding the boreholes. The soil surrounding the boreholes is also called the storage volume. In order to generate a large storage volume, multiple borehole wells are drilled to a large depth. The amount, exact depth and spacing depend on the required heat extraction and available project area. During summer times, warm water is injected in the

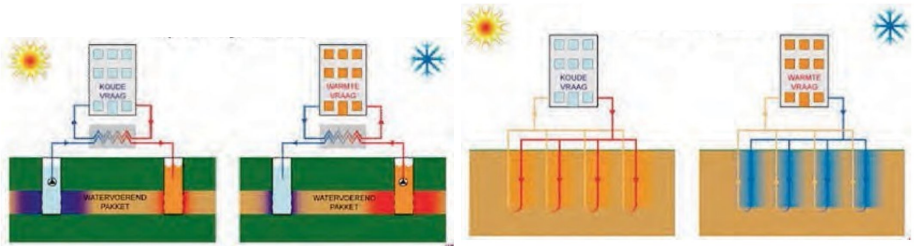

Figure 2.1: Left: Open system making use of two borehole wells. Right: Closed system making use of multiple borehole wells (WKO Nederland, 2020)

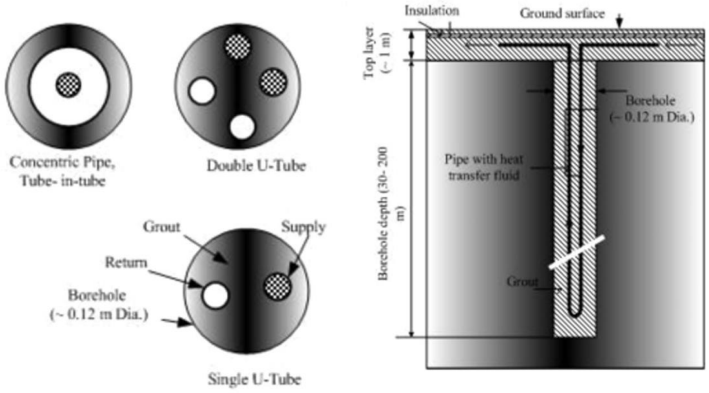

Figure 2.2: Left: Concentric pipe, Double U-pipes and Single U-pipes. Right: Overview of BTES system (Rad and Fung, 2016)

storage medium, generating a warm storage volume. During winter, this heat is extracted from the storage volume. During winter, heat depletion might occur which allows for cold water extraction during summer, as can be seen in fig. 2.1 (Rad and Fung, 2016).

2.1.2. Borehole spacing

The spacing between two boreholes for the open systems is between 50-100m, which means spacing is not a relevant parameter. For the closed systems, parametric studies are performed to find the highest efficiency of the system. The spacing and the amount of the boreholes determines the total storage volume and highly influences the thermal interaction between the boreholes. When borehole spacing is very large, the temperatures in the storage volume do not reach the required height for extraction. On the other hand, when borehole spacing is very small, efficiency drops due to lost potential energy for storage. In fig. 2.3 can be seen that for six different cases (each having different input parameters), the BHE efficiency has a peak between 3-4m (Nilsson, 2020). This spacing is confirmed by other studies, like by Welsch et al., 2016.

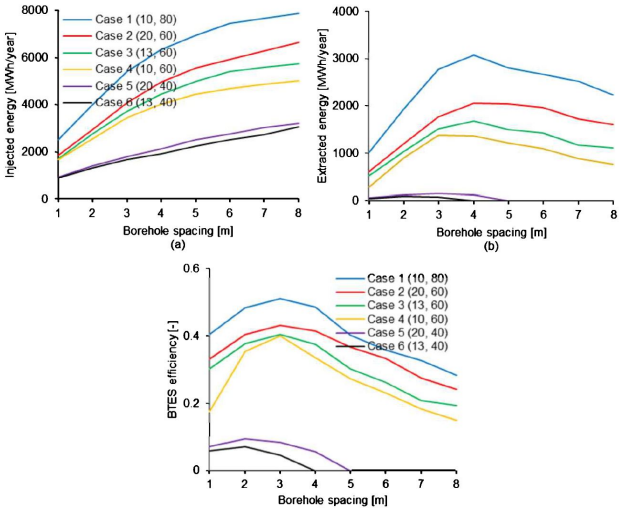

Figure 2.3: Borehole spacing versus: a) injected energy (MW); b) extracted energy (MW); c) Borehole efficiency (Nilsson, 2020)

2.2. Boreholes for ATES and BHE systems

For both systems, vertically drilled boreholes are necessary to reach a certain storage depth. Both systems have a different way of drilling and finalizing the boreholes. In this section, the drilling techniques for both systems are considered. At finalization of the boreholes consists out of the back-filling process, which is explained afterwards. Next to this, the stress changes in the soil around a drilled boreholes are discussed. Drilling complications are an important factor for the research and are included at last.

2.2.1. Drilling techniques

The companies installing BHE and ATES systems hire drilling companies to do research on the possibilities of installations considering the soil characteristics, the soil structure and the accessory way of drilling. These drilling companies do not focus on the heat exchange of the system but on the borehole stability. In the Netherlands, there are many different techniques of drilling holes. The most well-known drilling techniques are: straight-flush rotary drilling, reversed-flush rotary drilling and pulse drilling (J. Desmedt, 2009).

Not all drilling techniques are applicable for all types of soils. Straight-flush rotary drilling and reversed-flush rotary drilling are applicable in most types of soils, but not in rock formations. Pulse drilling is not applicable in very stiff clay layers or rock formations.

During straight-flush rotary drilling. the drilling fluid is pumped down through the drilling-bit. The drilling-bit destroys the soil which is forced upwards between the shaft of the drilling-pipe and the borehole wall. This upward moving water takes along the destroyed sediments and, most of all, provides borehole stability due to water pressure and cementing of the borehole wall by clay particles or grout suspension (J. Desmedt, 2009). An overview is given in fig. 2.4. The drilling-pipe consists out of segments. This means that during drilling a new

segment of drilling-pipe has to be connected to the existing drilling-pipe. For the drilling of boreholes for closed systems (BHE), only relatively small diameter boreholes are drilled, varying from 100-200mm. Next to this, a large amount of boreholes need to be drilled. This is why the drilling speeds are of great importance due to economic reasons. For this reason, the straight-flush rotary drilling method is used for the drilling of closed system boreholes (J. Desmedt, 2009).

For reversed-flush rotary drilling, the drilling fluid is pumped in the reversed direction. It is pumped down between the shaft of the drilling-pipe and the borehole wall and is forced up within the drilling-pipe. In this way, the drilled sediments stay more or less intact, allowing for a better logging of the drilled soil. This drilling technique can reach higher depths and larger diameters due to the application of air-lifting. Next to this, it can be noticed whenever the aquifer is reached due to soil logging (SIKB, 2019). This is extremely important for the drilling process of open systems. Next to this, it required relatively large diameter boreholes. Due to these requirements the reversed-flush rotary drilling mechanism is needed.

A third method is pulse-drilling. This method is problematic when drilling stiff clay formations and does not reach the required depth (J. Desmedt, 2009). This is why it is almost never used in the Netherlands.

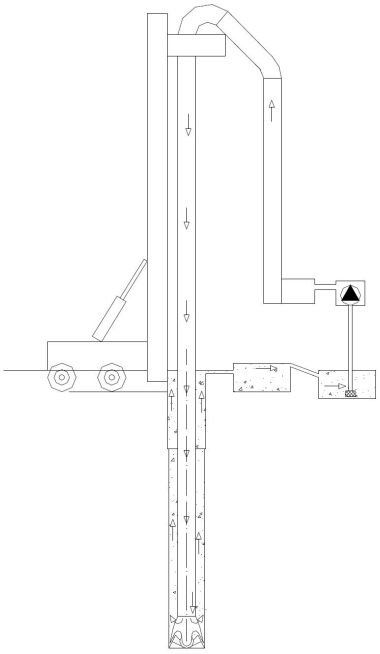

Figure 2.4: A schematic overview of straight-flush rotary drilling (J. Desmedt, 2009)

2.2.2. Back-fill boreholes

In order to keep the borehole stable on the long-term and to allow for the continuity of aquitards, boreholes are back-filled with soil-like material after borehole drilling is complete.

For open systems, the drilling process is completed by installing an HDPE pipe which has a slightly smaller radius than the borehole. A small annulus exists between the HDPE pipe and the borehole wall, which is back-filled with soil. This can be either gravel, sands or clayey material, dependent on the accessory sedimentary layer at a specific depth. In general, soil layers consisting out of aquifers are back-filled with gravel. The aquitards are back-filled with a material with more or less equal properties, like mikolit. It is attempted to obtain soil mechanical properties of the back-fill material that is equal to the surrounding soil layer. The drilling companies mainly focus on the continuity of aquitards rather than the soil stiffness and strength. The back-fill material always exists out of less stiff and strong material than its initial material before drilling.

For closed systems, all boreholes are completely back-filled with grout. The grout material has to be thermally conductive because this is the heat-exchanging process active in the closed systems. These types of grout material consist out of cement and bentonite which are mixed by water. Silica sands and graphite are added to the grout mixture for thermal enhancement (Lee et al., 2010). Due to the mixing of water, an emulsion is formed which is easy to inject in the borehole. After injection a cementitious hardening process causes a strong and stiff material to form. The thermally-enhanced types of grout are relatively new with no laboratory research on physical characteristics. For many other types of grout there are, like in the studies of Rostislav and Magdaléna, 2018 and Afzal et al., 2014, shrinkage and expansion strains occur between -10 and +10 volumetric strains (ε_{vol}). This is dependent of the exact material and the hardening process. In the contrary, more practical knowledge from drilling companies show no visible grout shrinkage of the grout body.

2.2.3. Stress state around a borehole

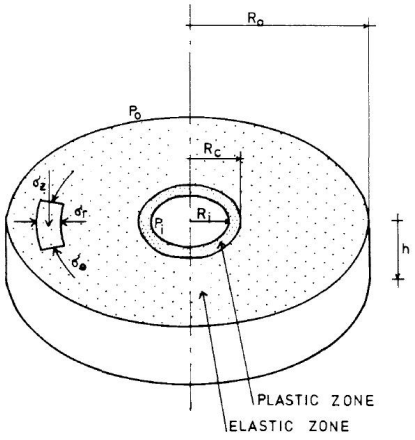

Figure 2.5: The zone of disturbed soil around a borehole in sand with: R_i = radius of the borehole, R_0 = radius from borehole center to outer-boundary, R_c the radius from borehole center to plastic-elastic boundary (Risnes et al., 1982)

Many studies focus on the stress state around boreholes in rock formations and thus are infeasible for this research. The stress state around a borehole in sand can be explained analytically by the study of Risnes et al., 1982.

This analytical model relies on a simplification of real-life conditions. The following assumptions are made in the analytical model:

- Stresses around the wellbore are isotropic and perfectly elasto-plastic
- A homogeneous sand with fully saturated pores is used
- The Coulomb failure criterion is used
- The stresses and deformations around the wellbore are stead-state

A horizontal circular section of the sand is chosen, as illustrated in fig. 2.5.

The initial stress states inside the soil is in equilibrium and normally consolidated. When drilling a cylindrical hole through this soil, the radial stress of this soil decreases while a same amount of the hoop stress (tangential) increases. This stress redistribution depends on the soil properties, the in-situ stresses, the pore water pressure and the operational techniques of drilling. Next to this, the stress-strain state in the soil changes, causing two distinct zones around the borehole to occur: 1) a plastic zone (R_i<r<R_c) and a 2) a non-linear elastic zone (R_c<r<R_o). The used input parameters are for sand formations at great depth and stress values are not realistic for this research, as this research focuses on the shallow subsurface.

A distinction can be made between uncased and cased boreholes, which affect the extend of the plastic zone significantly. For uncased boreholes, the hoop, radial and horizontal stresses all decrease to the level of the drilling fluid pressure at the borehole wall. This means that the extend of the plastic and non-linear zone will be high as seen in fig. 2.6.
For cased boreholes, the stresses at the borehole wall increases which will decrease the extend of the plastic and non-linear elastic zone, as seen in fig. 2.7.

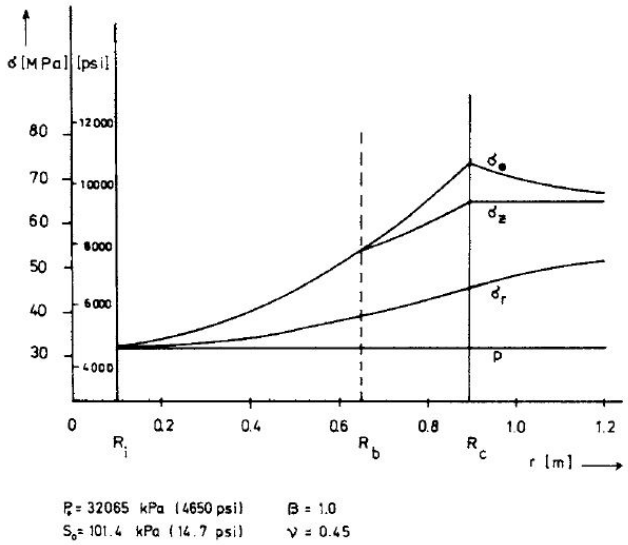

Figure 2.6: Stresses versus radial distance from borehole wall for uncased boreholes (Risnes et al., 1982)

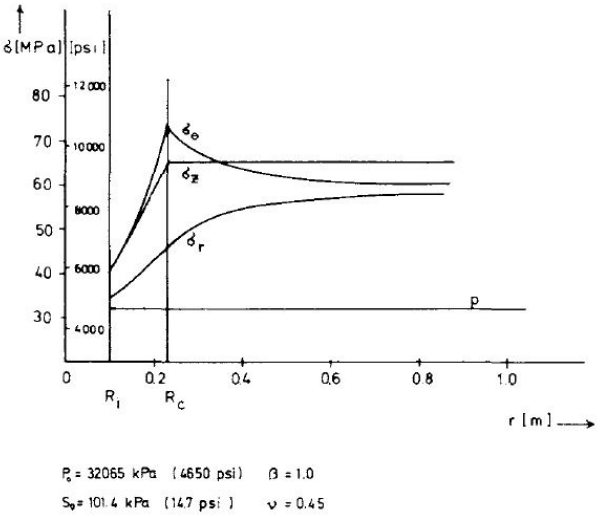

Figure 2.7: Stresses versus radial distance from borehole wall for cased boreholes (Risnes et al., 1982)

Another possibility is the condition in which the mud pressure inside of the borehole is less than the pore pressure in the sand. In this case, the pore fluid will flow into the borehole, changing stress states in the sand and extending the plastic zone.

A change in soil strength, expressed in terms of inherent shear strength, will affect the extend of the plastic zone as well. An inherent shear strength of ten times the initial value will decrease the extend of the plastic zone to almost the situation with a cased borehole, as seen in fig. 2.8.

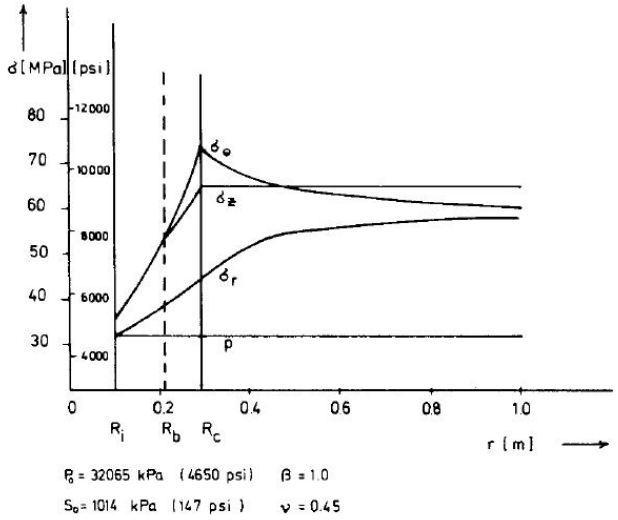

Figure 2.8: Stresses versus radial distance from borehole wall for a high inherent shear strength (10 times initial value) (Risnes et al., 1982)

In general, the following conclusions can be made considering this analytical approach to stresses around a borehole. The extend of the plastic zone decreases significantly for the situation with a: cased borehole, high inherent shear strength and high pore pressures in the borehole. The distribution of the stresses in the plastic zone will change for changes in soil parameters like the Poisson's ratio. By using this analytical model, the influence of soil parameters on the stress state can be investigated. It must be stressed that this research is meant for wellbores in petroleum engineering and that many assumptions are made for deep boreholes.

2.2.4. Drilling complications

During the perfect drilling of a borehole, the stress redistribution will be as given in chapter 2.2.3. In order to perfectly drill a borehole, the pressure of the drilling-fluid inside the borehole is more or less equal to the horizontal total stress in the soil (Press et al., 1993). In practice, however, this is almost never the case. Two types of drilling complications can occur during the drilling of a borehole in sediments, namely circulation problems and mechanical problems. Mechanical problems come in many different forms and usually cause complete failure of the drilling process. Additionally, these problems are severe and are likely to be noticed by the drilling master. Circulation problems, on the other hand, occur in many

different extents and are less likely to be noticed by the drilling master. In this way, it can imperceptibly change the stress state around the borehole. The following consequences of circulation problems might occur:

- A water-pressure drop can occur due to a water channel break-down or during the installation of a new drilling-pipe segment, as explained in 2.2.1. This can cause partial collapse of the borehole. During a severe water pressure drop, sediments will pile up. In this case, over-pressure must be applied to flush away the piled up sediments causing erosion of the borehole wall.
- An over-pressure can occur due to the overestimation of in-situ stresses. In this case, an excess of sediment is drilled away increasing the borehole diameter or it produces hydraulic fracturing of the borehole wall.

All of the above mentioned drilling complications occur during drilling and occur due to: 1) a pressure differential between the wellbore and the formation and 2) a formation with flow channels or holes (Austin and Austin, 1983). These flow channels or holes can be present naturally, in the form of highly permeable, unconsolidated or fractured zones within stronger sediments. Next to this, the channels can be induced due to earlier stages of the drilling process, which are then aggravated. The way of fracturing can occur in many different forms which is dependent on soil characteristics, as given in fig. 2.9.

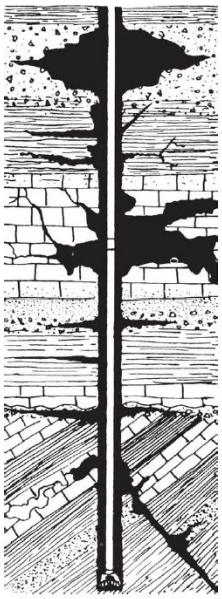

Figure 2.9: An overview of different types of fracturing (Austin and Austin, 1983).

Drilling complications might also occur in different stages of the UTES borehole installation process. Partial collapse or full collapse can occur in the time between the drilling of the borehole and the back-filling of the boreholes. Severe collapses can be measured by the drilling master by measuring and comparing the borehole depth.

For all these complications, higher amount of stress re-distributions (2.2.3) occur due to higher amounts of excavated or lost soil. Next to this, deformations can occur in the soil around the boreholes due to this lost material. The exact extend of drilling complications are not exactly known because drilling companies do not scan the borehole wall after drilling to look for excess lost material. Next to this, the collapse and fracturing might occur in many different forms. This means, that boreholes that seem stable and did not collapse completely are mostly seen as successful by the drilling companies.

2.3. Pile foundations

2.3.1. Type of piles

The material of the piles used for foundations depend on the type of material available, the magnitude of the loading, the soil type and the environment in which the piles are installed (e.g. chemical soil properties). The following types of piles are found (Budhu, 2010), with an overview given in fig. 2.10:

Concrete piles

There are different types of concrete piles which are used for many different environments and loading magnitudes. The cast-in-place concrete piles are constructed by installment of a steel shell into the soil after which they are filled with concrete. The steel shell only has constructional purposes and does not contribute to the bearing capacity of the pile. Normally steel is only added to the pile construction when moments and lateral forces are involved. There are two ways of installment of these steel shells: 1) screwing, which is done for the Fundex-piles and 2) driving, which is done for Vibro-piles.
The most well-known pile in the Netherlands is the prefab concrete pile (or similar) which is used when the exact depth of the piles is known before installment, which is driven into the soil.
Micro-piles are (grouted) piles with an maximum diameter of 340mm, which are mostly used in Belgium and France. In the Netherlands, these piles are less frequently used and mainly for foundation recovery projects.

Steel piles

Steel pipes come in many different shapes like cylindrical and H-profiled. These piles can have an open or closed pile tip when driving in weak soils or a conical tip when driving in soils with boulders or rocks that have to be penetrated. When the piles are driven and the loading capacity has to be increased the soil plug is excavated and filled with concrete, as shown in fig. 2.10c. In the Netherlands, small diameter steel piles are often used for foundation improvement.

Timber piles

Timber piles are not widely used due to their moderate length of around 12m. Next to this, they are very susceptible to environmental features like rotting and degradation by (micro-)organisms. However, many historical houses in the Netherlands have timber piles as foundation.

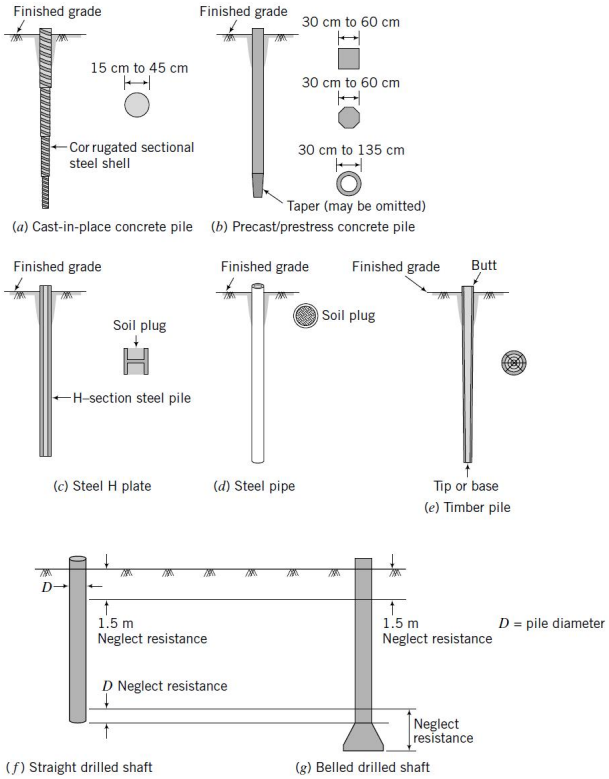

FIGURE 13.2 Pile types.

Figure 2.10: Different types of piles each with their: diameters, shaft resistance and cross-sections (Budhu, 2010)

Pile installation types

There are many different installation techniques from driving piles. For now, we consider the end-spectra of the different types. The way of installing a pile determines the stiffness of the soil underneath a pile and the soil disturbance around the shaft of the pile. The following types are distinguished:

- *Displacement piles*: these are closed-end or precast reinforced piles (Prezzi and Basu, 2005). Due to there closed-end they displace soil laterally when driving them into the ground. This means that the stress-strain circumstances will change and a plastically deformed zone will occur around the shaft of the pile. Next to this, the soil underneath the piles will behave stiffer than there initial state before driving.

- *Non-displacement piles*: these are bored piles or drilled shafts (Prezzi and Basu, 2005). A cylinder of soil is removed after which, for example, concrete or other reinforcement material is put in place. These types of piles will have more settlement after loading due to less stiffer soil underneath it combined with lower skin friction .

2.3.2. Soil disturbance due to the installation of piles

As mentioned in chapter 2.3.1, displacement piles cause significant soil disturbances during installation. This disturbance is caused by the driving of the pile into the soil, changing the stress-strain state of the surrounding soil. There are two main regions in which soil disturbance takes place: 1) in the lateral direction influencing a radial area around the pile and 2) underneath the tip of the pile. Next to this, a displacement pile can be either pushed or driven into the soil. For the pushing of the pile a static axial stress is applied at the pile. A dynamic axial stress is applied for driven piles.

Changes in stress underneath base of pile

For a displacement pile, the stress condition at this base is due to the installation of the pile and the loading after installment. The installation can be performed continuous in which the pile is pushed or it can be dynamic in which the pile is driven. The driving of a pile involves impact loading, unloading and impact reloading. During impact loading the element of soil beneath the pile would deform plastically and soil will flow towards the edges of the pile. However, overburden pressures restrict this movement of soil towards the edges and pushes the soil into the radial direction. The deformation into the radial directions depends on the soil characteristics but is normally very contained due to the expanse of the soil in the lateral directions. During unloading, the soil behaves perfectly elastic and will force the pile to rebound. This movement is restrained by the self-weight of the pile and the possible negative skin friction formed by reconsolidation of the soil along the pile skin. In this way, there is a certain residual stress kept in the soil during unloading. The amount of this residual stress (from A to O in fig. 2.2.3) depends on the swelling stress (rebound stress) of the soil.

So, for a displacement pile, the soil underneath the soil is pre-stressed to point B in fig. 2.12. When the displacement pile is loaded the stress-strain response of the soil is very stiff util the load reached point B. After that this, the stress-strain response continues to be elasto-plastic, from B to D in fig. 2.2.3. The extent of D depends on the amount of loading and the design of the pile foundation. In general, driven piles densify loose soils and loosen dense soils around the pile tip (Beijer Lundberg et al., 2013).
For non-displacement piles, the stress conditions changes are only due to loading after installment, which means they do not experience the loading and unloading behavior. No pre-stressed soil occurs at the pile of a non-displacement pile. Next to this, they do not displace soil during installment, so the soil at the base does not harden or soften (Prezzi and Basu, 2005).

When the soil underneath displacement piles consists out of a fine-grained soil with a low hydraulic conductivity, the excess negative pore pressures that are built up during installation will not dissipate quickly. This means that during the short-term installation process, the saturated mass of soil acts as an incompressible mass. This is due to the built up of negative excess pore pressure underneath the base of the pile which leads to an increase in effective stress (Verruijt, 2010) during driving. This can lead to an overestimation of the load capacity of the pile for the long-term. This has to be considered when performing a single pile load test. Also, it is an important feature for the long-term due to consolidation processes in which the excess pore pressure might dissipate causing settlements. These processes determine the base displacement in the long-term.

Changes in stress around pile shaft

Next to the changes in stress around the pile tip, there are changes in lateral direction when installing displacement piles. As the pile is driven or pushed into the soil, a shear zone is developed between the pile shaft and the soil. High shear stresses built up for vertical pile displacements due to skin friction. For fine-grained soils, dilatancy occur at some point extending the shear zone and allowing for smaller shear stresses acting on the pile shaft. After complete installation of the pile, a filly expressed shear zone has developed around the pile shaft. Due to this shearing a zone around the pile is deformed, as illustrated in fig. 2.13. Due the installation of displacement piles the mobilized shear strength is high, which means that the shaft resistance is high for small pile displacements during the first loading stages (Fleming et al., 1985).

For non-displacement piles the shear zone between pile and soil exists out of a shear band parallel to the pile wall. No shearing exists between the concrete and the soil, which has to do with the interlocking of the in-situ placed cement and the soil particles. This means that the mobilized shear strength is low after installation and required relatively high pile displacements for high mobilized shaft resistance (Fleming et al., 1985).

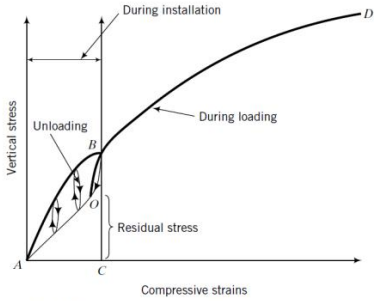

(a) Idealized vertical stress–compressive strain response of soil element under pile base.

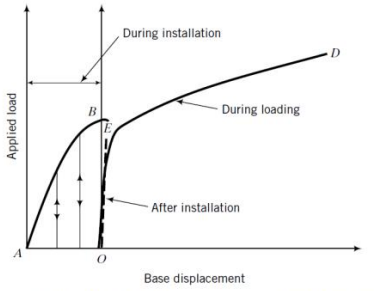

(b) Idealized load–base displacement response of soil element under pile.

Figure 2.11: a) Vertical stress versus compressive strains. b) Applied load versus base displacement (Budhu, 2010)

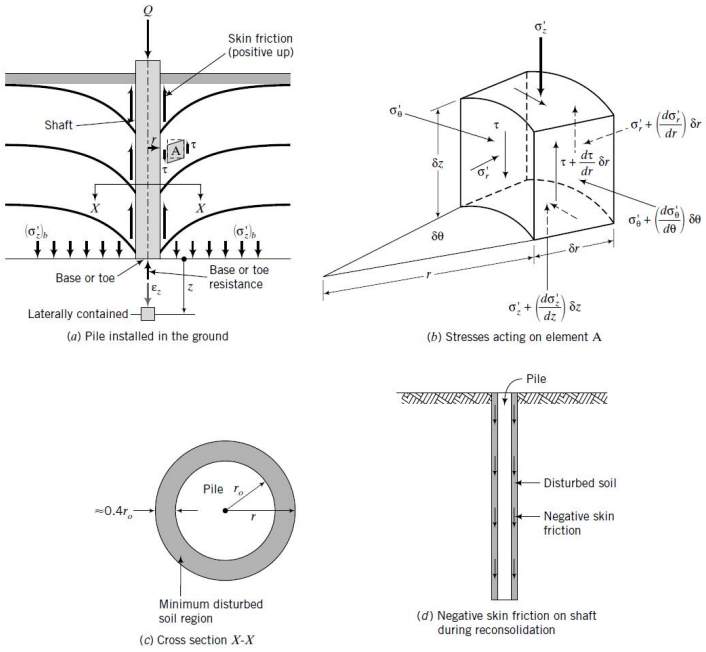

Figure 2.12: Overview of stresses acting on pile shaft and pile tip

2.3.3. Bearing capacity of a single pile

The total bearing capacity of a single pile consists out of the following resisting components: the shaft resistance, which is built up due to the skin friction between the pile shaft and the soil and the tip resistance, which is due to the stiff soil underneath the tip of the pile. This can be summarized in the following general formula for the bearing capacity of a single pile (Briaud, 2013):

$$F_{ult} = F_{shaft,positive} + F_{tip,rest} - F_{shaft,negative} \tag{2.1}$$

It is clear that the sum of the two components make up the total bearing capacity of the pile. However, the distribution between shaft en tip resistance depends on: the initial effective stresses in the soil, the mechanical characteristics of the soil, the physical characteristics of the foundation and the way in which the pile is installed (Meyerhof, 1951).

Tip resistance

The tip resistance is due to the mobilization of soil strength during loading of the pile. For the end-bearing of piles, the plastically deformed soil around the pile tip is illustrated in fig. 2.13. This plastically deformed zone will create a shear zone and obtains strength for the end-bearing of the pile from mobilization shear strength. The ultimate limit state of the tip resistance is reached when the soil in this zone is at critical state. The magnitude of this ultimate state of tip resistance depends on soil and pile characteristics (Meyerhof, 1951).

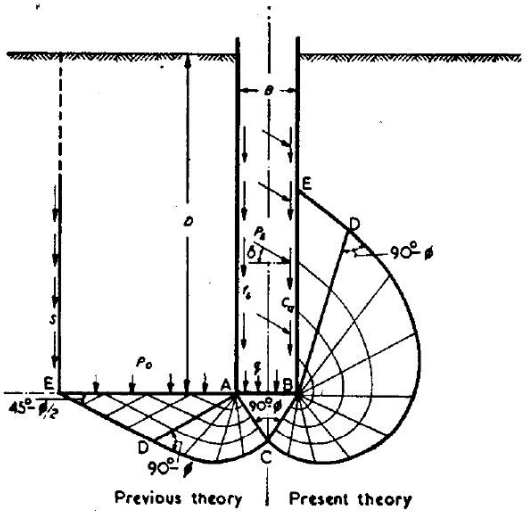

Figure 2.13: The plastic soil deformation as a result of mobilized end-bearing for a single pile (ignore "Previous Theory") (Meyerhof, 1951)

The first way of determining the tip resistance is by means of the Koppejan Method (Verruijt, 2010) which is used and prescribed for soils in the Netherlands (Normalisatie-Instituut., 1995). This Koppejan Method is based on analytical studies and relies on the plasticity theory by Meyerhof, 1951, as given in fig. 2.13. This plastic zone around the pile tip is described by the 4D/8D rule. This rule subdivides the plastic zone into three different zones, as illustrated in fig. 2.14, each having different averaged values of CPT cone resistance.

Zone I and II extend 0.7 to 4 times the pile diameter below the tip. Zone III extends 8 times the pile diameter above the pile tip. The total tip resistance as calculated by the Koppejan method is contained in the following formulas (Verruijt, 2010):

$$p_{tip} = \frac{1}{2} \times \alpha \times \beta \times s[\frac{1}{2}(q_{c1} + q_{c2}) + q_{c3}] \tag{2.2}$$

$$R_{tip} = A_{tip} \times q_{tip} \tag{2.3}$$

In which q_{c1}, q_{c2} and q_{c3} are the average cone resistance values for zones I, II and II respectively. The factors: α, β and s take into account the variety of pile characteristics.

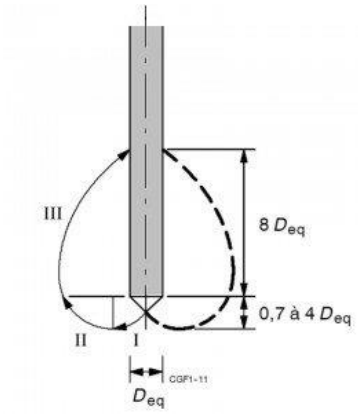

Figure 2.14: A simplified presentation of the soil deformation due to the mobilization of end-bearing of a single pile according to the Koppejan Theory. I: Zone 1; II: Zone 2; III: Zone 3 (Verruijt, 2010)

Next to a determination by means of CPT data, a static analysis can be performed. This was done by multiple researchers, like Brinch-Hansen and Vesic, 1975, given by equation (2.4) and (2.5) respectively.

$$p_{tip} = i_c s_c c N_c + i_q s_q q N_q + i_\gamma s_\gamma \frac{1}{2} \gamma B N_\gamma \tag{2.4}$$

Formula (2.4) is based on the cohesion (c), weight of foundation (B) and the volumetric weight of the soil (γ). Next to this, it includes correction factors for the inclination of the foundation ($i_{c,q,\gamma}$) and for the shape of the loaded area ($s_{c,q,\gamma}$).

$$p_{tip} = \eta q (N_q - 1) d_q \tag{2.5}$$

Formula (2.5) takes into account a correction factor for the depth of the foundations in a sand layer (d_q). The factors N_q, N_c and N_γ correct for the bearing capacity and all depend on the internal friction angle of the bearing sand layer. The sub-equations belonging to equations (2.5) and (2.4) are given in appendix A, together with values for the correction factors.

Shaft resistance

The shaft resistance arises from the skin friction between the pile material and the soil. Most of the times, the skin friction has a high contribution to the total bearing capacity in sandy soils while in soft, clayey soils the contribution of skin friction to the total end bearing is very unreliable (Verruijt, 2010). The skin friction can be positive, acting upwards and thus contributing to the total bearing capacity of the pile or it can be negative, acting downwards and counteracting the total bearing capacity. Positive skin friction in sand is mobilized because the soil around the pile shaft has a lower vertical displacement than the pile which causes frictional forces acting upward. For clayey soils, this is due to the adhesion between the pile material and the soil. The magnitude of this friction depends on the soil properties. Negative skin friction can be mobilized by consolidation processes in sandy soils while in soft, clayey soils this is mobilized by means of settlements after installation.
For displacement piles in sandy soils, reconsolidation of the soil around the pile causes negative skin friction. Due to the lateral compression during the driving of the piles, excess

negative pore pressures built up. After some time (depending on the hydraulic conductivity of the soil) the excess pore pressure dissipates creating a negative skin friction which reduces the load capacity of the pile. However, the soil strength increases due to the increase in effective stress after the dissipation of excess pore pressures (Budhu, 2010).
For displacement piles in soft, clayey soils, settlements after installation called downdrag, may cause negative skin friction. Downdrag occurs when the soil around the upper part of the pile shaft has a larger vertical displacement than the pile itself. The so-called neutral point can be found where there is no relative settlement between pile and soil. This is the point where negative skin friction shifts to positive skin friction again (2.15) (Briaud, 2013). This depends on the relative settlements between pile and soil as explained earlier.

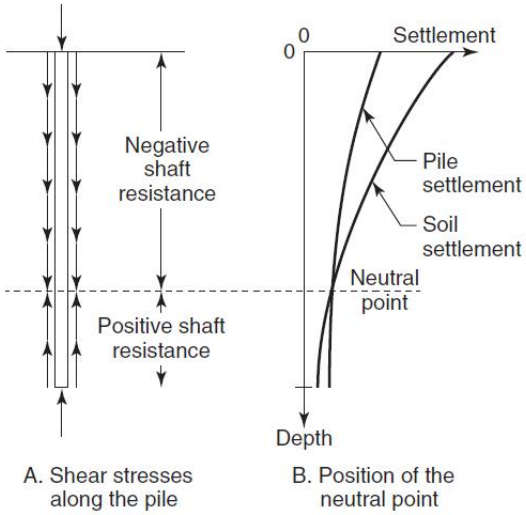

Figure 2.15: a) Shear stresses along the pile shaft. b) Position of the neutral point (Budhu, 2010)

The full shaft resistance is mobilized when a displacement pile has reached a vertical displacement between 2.5 and $10mm$. For non-displacement piles this vertical displacement has to be higher due to no mobilization of shaft resistance during installation. The amount of vertical displacement is dependent on the stiffness and strength of the soil. This does not mean, however, that with an vertical displacement of $10mm$ the full end bearing resistance of the pile is mobilized. Usually this is achieved when the vertical displacement is about 10% of the pile diameter for displacement piles (Budhu, 2010). For non-displacement piles this is about 20% of the pile diameter.

The contribution of the shaft resistance to the bearing capacity is determined by means of CPT cone resistances. As above mentioned, the shaft resistance is divided into positive and negative magnitudes, which are determined by means of formula (2.6) and (2.7) respectively (Normalisatie-Instituut., 1995).

The positive shaft friction is determined by the means of the cone resistance (q_c) and a correction factor (α_p), which takes into account the difference between in installation type:

$$p_{shaft,pos} = \alpha_s \times q_c \tag{2.6}$$

The negative skin friction is dependent on the tip resistance as this increases the drag load. The slip method is used for the determination of this dragload, in whichδ depends on the internal friction angle. Some values for δ are given in appendix A. The negative skin friction is given by:

$$p_{shaft,neg} = K_0 \times tan\delta \times \sigma'_v \tag{2.7}$$

This skin friction is mobilized over the complete shaft of the pile and thus depends on the total surface of the pile. Next to this, the positive and negative skin friction will counteract each other and need to be subtracted. This is explained in Normalisatie-Instituut., 1995 and is contained in formula (2.8):

$$R_{tip} = A_{pile} \times (p_{shaft,neg} + p_{shaft,pos}) \tag{2.8}$$

The influence of soil structure on bearing capacity

The contribution of the mobilized shaft resistance and tip resistance to the bearing-capacity depends on the soil structure in which the pile is installed. There are three main types of soil structures important for bearing-capacity calculations (Tomlinson and Boorman, 1995):

1. A completely soft soil in which most of the bearing capacity is mobilized by the shaft resistance.
2. A soft soil with a relatively stiff soil at the base of the pile in which the bearing capacity is mobilized by a combination of the shaft- and tip resistance.
3. A very stiff soil (or rock) at the base of the pile in which most of the bearing-capacity is mobilized by the tip resistance.

In the Netherlands, the most common situation is illustrated by fig. 2.3.3b. The higher the contribution of the tip resistance, the higher the extend of the plastically deformed zone around the base of the pile, as given in chapter 2.3.3.

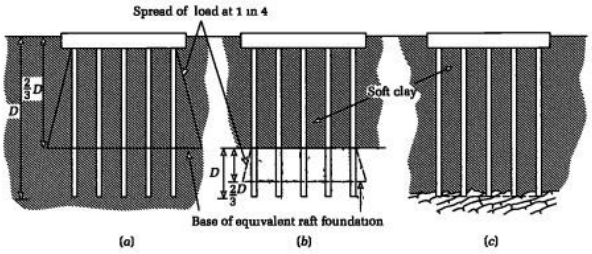

Figure 2.16: The three different types of soil structures influencing the way of end-bearing: a) bearing-capacity from skin resistance b) bearing-capacity from both skin- and foot resistance c) bearing-capacity from foot resistance. Also the equivalent height of a raft foundation is given with D = diameter pile (Tomlinson and Boorman, 1995)

2.3.4. Bearing capacity of piles in groups

Most foundations exist out of pile groups in order to achieve a safe foundation which can carry the load of the structure without creating unacceptable amounts of settlements. Piles within groups can be placed within square, circular or octagonal arrangements as illustrated in fig. 2.17. Pile caps are installed on the heads of the pile groups which may be in direct contact with the top of the soil or on small elevations (Budhu, 2010). Pile caps, as illustrated in fig. 2.17, in touch with the soil carry a part of the load of structure directly to the soil, decreasing the required bearing capacity of the pile groups.

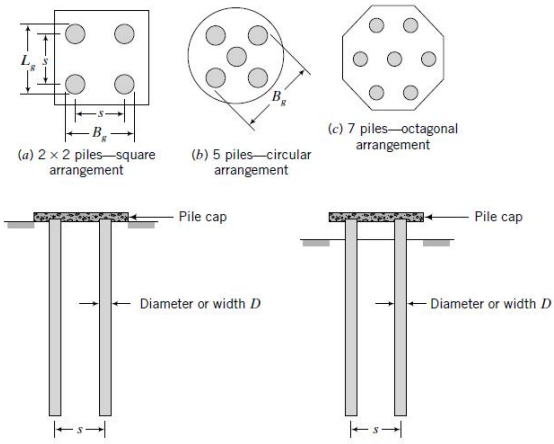

Figure 2.17: Most common types of pile group configurations (Budhu, 2010)

The bearing capacity of piles in groups is determined by an efficiency factor, which expresses the difference in the ultimate bearing capacity of single piles and piles in groups. This is determined by the unique relation of the s/R-ratio (spacing/diameter ratio) of the pile group arrangement and the resulting changes in the strength properties of the soil in which the piles are embedded.

For example in sandy soils, this efficiency factor is determined by the s/R ratio and the relative density of the sand. In loose sands the load on the piles will densify the soil around the piles producing an relatively high efficiency factor. This might be the direct opposite for dense sands (Briaud, 2013), in which strain-softening might occur. In fine-grained soils in general, the piles in the outer region of the groups carry more load than the piles in the center, while this is the direct opposite within coarse-grained soils. All these soil characteristics have an effect on the efficiency factor (Budhu, 2010).
Furthermore, when piles are driven in sandy soils, they produce horizontal stresses allowing to mobilize higher shaft resistance when driven in groups. A single pile driven in sand locks a certain residual point load. When more piles are driven close to that initial pile it releases the locked-in residual point load and decreases its beneficial effects (Briaud, 2013).

Piles in groups do not only fail because of the difference in ultimate bearing capacity between single piles and piles in groups. Another important failure mode is the block failure mode, in this case the block of piles fails as a whole. This type of failure occurs when the pile tips are in a strong layer producing an high ultimate bearing capacity for a single pile but for a group of piles under heavy loading this layer is too thin, as illustrated in fig. 2.18.

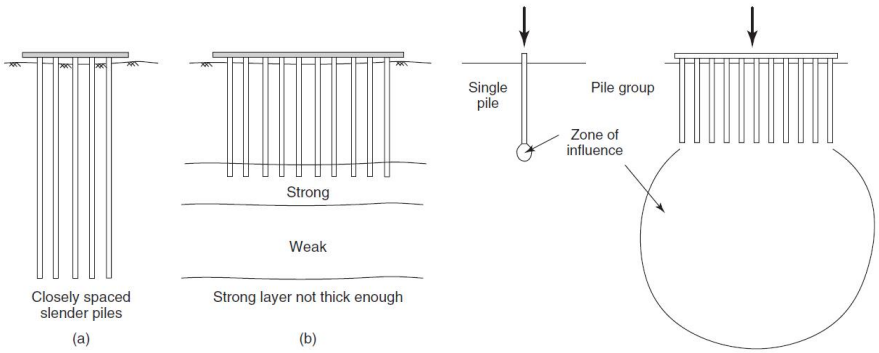

Figure 2.18: Left : a) Group failure due to closely spaced piles. b) Group failure due to a too thin strong (stiff) layer. Right: High extend of the zone of influence due to piles in groups (Briaud, 2013)

2.4. Literature summary

The existing UTES systems come in many different designs, the most common systems used in the Netherlands are ATES (open) and BHE (closed) systems. These systems store excess energy power in the form of heat by means of using a fluid as a heat transferring medium running through vertically drilled boreholes to a depth between 30 - 200m. The open systems use normal ground water for heat convection which is stored in an aquifer at a certain depth in the underground and exist out of one or two wells with a diameter between 0.3m and 1.0m. Closed systems warm up a water-saturated soil volume around multiple boreholes with a varying diameter between 0.1 and 0.3m. The spacing between closed system boreholes varies between 3 - 8m, while for open systems these vary between 50-100m. Open systems are back-filled by an HDPE pipe surrounded by clay and/or gravel. Closed systems are back-filled with thermally-enhanced grout. This grout body might experience shrinkage and expansion.

Boreholes for UTES systems are drilled by straight-flush rotary drilling or reversed-flush rotary drilling techniques. These differ in the way of drilling fluid circulation and due to this, differ in drilling speed. A third drilling technique is pulse-drilling which is problematic for drilling through stiff clay layers and thus less frequently used in the Netherlands. By drilling these vertical circular excavations, the stress state around the soil is redistributed. This stress state changes from an equilibrium condition to a plastic and non-linear zone for a specific extend around the boreholes. Soil parameters, in-situ stresses and borehole casings strongly influence the extends of these zones.

Foundation piles are found in many different shapes and materials. A pile can either be a non-displacement (bored) or displacement pile (driven). By driving a displacement pile, the stresses around the pile shaft and underneath the pile tip are pres-stressed. This causes the bearing capacity of displacement piles to increase. The bearing capacity of piles is mobilized by the tip resistance and shaft resistance of piles, which magnitudes are dominated by the in-situ horizontal and vertical stresses acting on the pile. The determination of bearing capacity magnitude depends on many different factors like soil characteristics and the pile installation method. To determine the bearing capacity of a pile, Cone Penetration Tests are performed and its results included in different existing empirical methods, like the Koppejan method. The bearing capacity of piles in groups differs from that of single piles, which is expressed by means of an empirically determined efficiency factor.

3

Method

This chapter explains the methods that were used in order to solve the main research problem. The problem is visualized and explained by means of the conceptual model which is supported by the hypothesis. The method section starts with a general approach on how the research aim is achieved and by means of which instruments. Secondly, the performed analyzes are explained in more detail. Hereupon the numerical model setup is explained, taking into account the performed simulations. At last, the numerical model is verified by means of an analytical solution and different mesh configurations are checked on accuracy and efficiency.

3.1. Hypothesis and conceptual model

The research problem can be contained in a conceptual model consisting out of two main aspects: a borehole and a pile located close to each other. It was expected that the stress redistribution induced by the drilling of the borehole will decrease the bearing capacity of the pile. The cartoon in fig. 3.1 gives a step-by-step illustration of this process, with a clear scientific explanation of the soil stress changes that occur due to drilling the borehole:

1. The stresses in the soil are in equilibrium and are given in a distribution between a vertical and horizontal stress, as illustrated in fig. 3.1-1b. A pile is present which obtains bearing capacity from shaft- and tip-resistance, dominated by $\sigma_{h=r}$ and σ_v respectively, fig. 3.1-1a.
2. During the excavation of a borehole, the stresses (pressure) inside the borehole decrease due to the loss of support. The equilibrium state of stress is lost and reversible (elastic) deformations occur with a change of stress in the elastic range . These changes will decrease the magnitude of the principal in-situ stresses acting on the pile, as given in fig. 3.1-2a. A decrease in in-situ stresses acting on the pile will probably decrease the bearing capacity of the pile.

   The three principal stresses are given by the vertical, radial and hoop stress given in a vertical cross-section, fig. 3.1-2b. In the elastic zone, the hoop stress increases when approaching the borehole, this is caused by the circular shape of the borehole. The vertical and radial stresses decrease gradually when approaching the borehole wall.

3. Additional stress redistribution causes irreversible (plastic) deformations in a region directly around the borehole, as illustrated in fig. 3.1-3b. This causes a destructive decrease of the principal in-situ stresses in the plastic region. The in-situ stresses acting on the pile will reduce even more. as given in fig. 3.1-3a. These higher stress reliefs will decrease the bearing capacity of the pile even more.
4. The borehole is finalized by back-filling with gravel or grout which has no significant influence on the stress state. With time, however, creep might occur which reduces the deviatoric shear stresses (in the plastic zone) induced by the stress redistribution from step 1-3. The final reduction of the horizontal and vertical stresses acting on the pile have reduced the shaft- and tip resistance, illustrated in 3.1-4a. This causes a loss of bearing capacity. In general, the stress redistribution in the elastic and plastic zone reduces the soil strength and thus the bearing capacity.

The behavior of the soil, like strength, will influence the magnitude and the way of rearrangement of stresses. Next to this, an important factor in this process is the pressure inside the borehole during drilling. All these aspects influence the extend of both the plastic and elastic zone. This extend is an important feature due to the loss of soil strength within these zones. By using the right soil mechanical model for its behavior, these stresses can be plotted against the radial distance from the borehole wall, as performed in the analytical solution by Risnes et al., 1982.

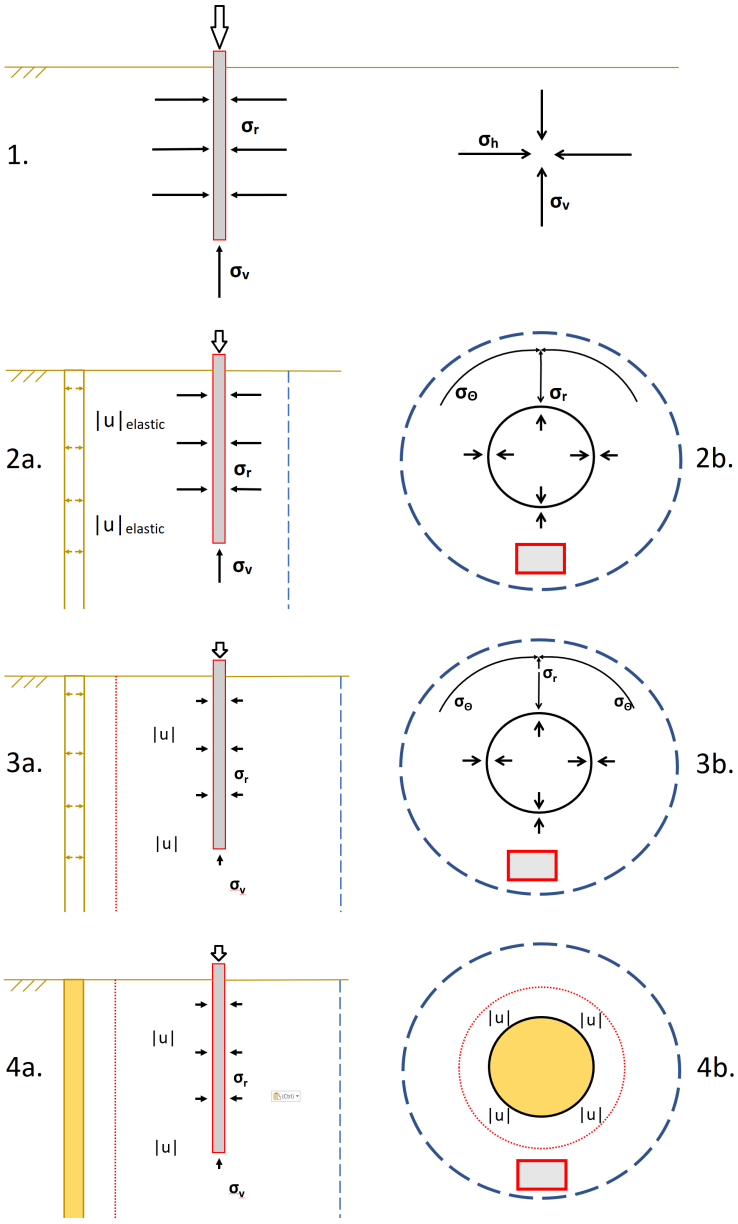

Figure 3.1: Overview of the drilling process of a borehole influencing the bearing capacity of a foundation pile. Blue-dotted line is the outer boundary of the elastic zone. Red-dotted line is the outer boundary of the plastic zone. Fig. 2b, 3b and 4b give a horizontal cross-section of the problem.

3.2. General approach

The aim of this research is to investigate the influence of the installation of ATES and BHE boreholes on the bearing capacity of pile foundations. A numerical model was required which simulates the installation process of a borehole and which includes the features of foundation piles. Next to this, it must contain stress-strain behavior of the soil in which the boreholes and piles are installed. The modelling software PLAXIS was chosen as the appropriate modelling program to simulate required geotechnical features as stated above. PLAXIS is a, Python based, geotechnical modelling software which enables a wide variety of soil behavior, structures, water conditions and numerical features to be implemented in the model. Next to this, the output provides detailed graphs, tables and cross-sections allowing for an user-friendly data analysis.

In order to achieve the main aim, several analyzes were performed: 1) a parametric analysis, 2) a stress analysis and 3) a bearing capacity analysis:

The parametric analysis (explained in chapter 3.3.1) includes sensitivity analyzes on input parameters with varying values that were expected to significantly influence the final results. By performing these sensitivity analyzes, a more quantitative insight in the influence of these parameters on the stress-strain behavior of the soil was obtained.

The stress analysis (explained in chapter 3.3.2) investigates the influence of the borehole drilling process on the stress-strain state around the borehole. In order to investigate this, the main aspects of the drilling process were examined, which include: 1) the drilling fluid pressure, 2) the borehole diameter and 3) possible drilling complications.

The bearing capacity analysis (explained in chapter 3.3.3) investigates the influence of these stress-strain states around drilled boreholes on the bearing capacity of piles. As piles exist in many different forms, the two main types of installation were considered, including a displacement and non-displacement pile. Static pile load tests were simulated in this analysis in order to obtain the bearing capacity of piles.

A 2D-axisymmetric numerical model was used for the first part of the research. To start with, the borehole drilling process was simulated in a simplified conceptual model. This conceptual model includes a single borehole with a drilling fluid pressure to keep the borehole stable and was developed in the 2D-axisymmetric model of PLAXIS. The simulation of the borehole drilling process in this conceptual numerical model was verified by means of an analytical theory in order to be sure that the results were reliable and accurate, as explained in chapter 3.4 and 3.5. After this was achieved successfully, extended 2D-axisymmetric models were built including more realistic simulations. These extended models include: complex soil behavior, adding back-fill materials and boreholes with drilling complications. By means of using these extended 2D-axisymmetric model, results were obtained for the parametric and stress analyzes.

A plane strain 3D model was necessary for the bearing capacity analysis, as both (non-)displacement piles and boreholes were included. Again, a conceptual model was built containing a single borehole with a drilling fluid pressure to keep the borehole stable. Similar to the verification of the 2D model, the results were verified by means of the same analytical solution, explained in chapter 3.4 and 3.5. This model was used for all the simulations contained in the bearing capacity analysis.

3.3. Research analyzes

3.3.1. Parametric analysis

Several key parameters used within the models required extensive investigation before implementation in further research. This included a sensitivity analysis of the following parameters: grout shrinkage and expansion, the Over-Consolidation-Ratio (OCR), Relative Density and the magnitude of drilling complications. The goal of these sensitivity analyzes was to investigate the influence of a variation of values on the stress-strain state of the soil around the boreholes, given in chapter 3.3.1. All drilling processes of the parametric analyzes are drilled with a drilling fluid pressure of $-10.5kPa/m$, as was determined in chapter 5.

Grout shrinkage and expansion

The most important aspect for the completion of the closed systems is the back-fill process of the borehole. The entire borehole is filled with thermally enhanced grout. The grout body might show shrinkage or expansion during the hardening process. This shrinkage and expansion are expressed as volume strains and varied from +10 to -10 vol. percent. The simulation of this in the numerical model is explained in chapter 3.4.3.

Over-Consolidation Ratio

The in-situ far-field principal stresses are another important factor, especially for situations in the Netherlands. Due to over-consolidation, the horizontal in-situ stress can be three times higher than in normally consolidated situations, which is expressed in the over-consolidation ratio. For Dutch sands, this over-consolidation ratio can have values between 1.0 (normally-consolidated) and 4.0 which is highly over-consolidated (Peels and Dijkstra, 2010). So, the OCR was varied from 0 to 4, which is a range of values found for Dutch sands. This can easily be implemented in the numerical model as an input parameter.

Relative Density

The relative density is an important parameters for sand strength and influences its behavior. A magnitude of Relative Density of 30%, 50%, 70% and 90% were chosen. This was done by adjusting the input parameters for the Hardening Soil Small Strain model. These input parameters include the stiffness and strength parameters (E, c', ϕ). which can be directly implemented in the numerical model as input parameters, as explained in chapter 3.4.2. The exact input parameter values are given in appendix B and were determined by means of empirical relationships.

Magnitude of drilling complications

Drilling complications might occur during the drilling process of boreholes. The occurrence of drilling complications is known in practice, however is not studied very comprehensively in literature. This is caused by the limited receptivity of drilling companies, which are not keen on sharing their incompetence. Next to this, the actual measurement of drilling complications are complicated in practice. For this reason a sensitivity analysis is performed on the magnitudes of drilling complications. The volumetric strains, simulating the drilling complication, were -25%, -50% and -75% for a borehole with 0.3m in diameter. These volumetric strains can be expressed as a percentage of excess soil volume loss. This conversion and the simulation in the numerical model are explained in chapter 3.4.3.

3.3.2. Stress analysis

The stress analysis takes into account the influence of the drilling process on the stress-strain state around the borehole. The aspects of the drilling process included in this analysis were: the affect of the drilling fluid pressure, borehole diameter, drilling complications and the introduction of multiple boreholes in the same model. The changes of the extend and magnitude of the stress redistribution by varying these aspects, as given in chapter 5, are of significant importance for the bearing capacity of piles.

Drilling fluid analysis

The drilling fluid pressure keeps the borehole stable during the drilling process, and is seen as an important factor influencing the stress-state around the borehole. The required magnitude of the drilling fluid is determined by: the borehole diameter, borehole depth, soil type and soil behavior. As for this research only one type of soil is used, only the borehole diameters influence the magnitude of the drilling fluid pressure. For every borehole diameter two pressures magnitudes were investigated: 1) the pressure at which the plastic zone was minimized and 2) the lower limit at which the borehole was about to fail. These limit pressures were found for borehole diameters varying from 0.3 to 1.0m.

Borehole diameter

The 'zone of influence' (see chapter) around a borehole is of great significance for this research, as the bearing capacity of piles is highly influenced by changes in in-situ stress state. For the installation location of piles it was necessary to know the extends of these zone of influences. The extends of the zones of influences for varying borehole diameters was investigated. This was done by keeping the soil type (and input parameters) constant and using a low-limit drilling fluid pressure to obtain conservative results. These results gave the amount of stress redistribution and the zone of influence around the borehole wall for boreholes with diameters: 0.3, 0.6, 0.8 and 1.0m. For the 0.3m diameter borehole, the zone of influence was determined with grout shrinkage of $2\ vol.\%$ and without grout shrinkage.

Multiple boreholes

In order to investigate the stress conditions due to the construction of closed systems, several scenarios with different borehole arrays were built. All boreholes for these scenarios have a diameter of 0.3m and a depth of 60m. Next to this, a grout body was included with a shrinkage of $2\ vol.\%$. The amount of boreholes per array were chosen to be 2 and 4. To investigate the effect of this spacing on the soil stress state, a horizontal distance of 2, 3 and 4 meters between the boreholes was chosen for the 2 borehole array. For the four borehole array, a spacing of 2m and 5m were chosen between ever pile. These scenario's are illustrated in appendix C.

Drilling complications

The most interesting and realistic drilling complication was chosen by means of the parametric analysis. Now, the drilling complications were simulated at different depths to investigate the effect on the depth of the pile tip. This was done by means a negative volume strain over a borehole length of 10m. The following scenario's were simulated:

- A total of -50% volumetric strain over a borehole length of 10 meters between a depth of 0 to -10 meters
- A total of -50% volumetric strain over a borehole length of 10 meters between a depth of -15 to -25 meters

- A total of -50% volumetric strain over a borehole length of 10 meters between a depth of -30 and -40 meters

These depths are chosen such that one of the drilling complications occur above, next to and beneath the location of the pile tip at -20m depth. Next to this, all scenario's were investigated for a borehole with a diameter of 0.3m and a diameter of 0.8m. The simulation of these drilling complications in the numerical model are explained in 3.4.3.

3.3.3. Bearing capacity analysis

The bearing capacity analysis investigates the influence of the stress changes on the actual bearing capacity of piles, and is given in chapter 6. The mobilization of the bearing capacity of piles is a complicated process which depends on a lot of variables. The most important variables being: the dimensions, shape and material of the pile. For this research, there is no interest in how these different variables influence the bearing capacity of the piles. That is why the dimensions, shape and material of the pile are kept constant for every calculation. The installation method of the pile, in the contrary, is of interest because it alters the stress state of the soil and thus might influence the effect of the borehole drilling process on the bearing capacity. So, static pile load tests are performed for one type of displacement pile (driven pile) and one type of (non-)displacement pile (wish-in-place pile). Static pile load tests were performed for the following situations: bearing capacity of a pile in unaffected soil, bearing capacity of a pile near a perfectly drilled borehole and a borehole with drilling complications. In addition, the effect of changes in installation phasing were investigated for displacement piles.

As there are many possible combinations of using these different piles, phasing and boreholes multiple scenario's have been chosen that will cover most of the possible combinations.

Bearing capacity of a pile near a perfectly drilled borehole

For this analysis only two borehole diameters were chosen, namely: 0.3m and 0.8m as multiple results are available from previous analyzes. The location of the pile (location A and B) depends on the elastic and plastic regions around the two boreholes. These regions were investigated and given in chapter 5. On this basis, the following two scenario's were considered:

- A 0.3m borehole with a grout shrinkage of $2\ vol.\%$. Static pile load tests were performed at a distance of 0.6m (location A) and 1.0m (location B) from the borehole center. Location A is located at the elastic-plastic boundary while location B is located in the middle of the non-linear elastic zone. The pile tip is located at a depth of -20m and consists of a wished-in-place (non-displacement) pile.
- A 0.8m borehole back-filled with gravel. Static pile load tests were performed at a distance of 0.6m (location A) and 1.0m (location B) from the borehole center. For this borehole size, location A is now located in the middle of the plastic zone while location B is located at the elastic-plastic boundary. The pile tip is located at a depth of -20m and consists of a wished-in-place (non-displacement) pile.

The results from both scenario's are plotted as load-displacement curves in the same graph in order to determine the difference in bearing capacity.

Bearing capacity of a pile near a borehole with a drilling complication

Again, only two borehole diameters were chosen, namely: 0.3m and 0.8m. The magnitude of the drilling complication was determined by means of the sensitivity analysis, given in chapter 4. The location of the pile (location A and B) and the depth of the drilling complications depend on the extends of the stress redistribution, as investigated and given in chapter 5. On this basis, the following two scenario's were considered:

- A 0.3 diameter borehole back-filled with grout and no shrinkage. A drilling complication with a magnitude of 50% volumetric strains was applied between -15 and -25m in depth. Static pile load tests were performed 1.0m and 2.0m away from the borehole center. The pile tip is located at a depth of -20m and consists out of a of a wished-in-place (non-displacement) pile.
- A 0.8 diameter borehole back-filled with gravel. A drilling complication with a magnitude of 50% volumetric strains was applied occurring between -15m and -25m in depth. Static pile load tests were performed 2.0m and 4.0m away from the borehole center. The pile tip is located at a depth of -20m and consists out of of a wished-in-place (non-displacement) pile.

The results from both scenario's are plotted as load-displacement curves in the same graph in order to determine the difference in bearing capacity.

Bearing capacity of a displacement pile near a single borehole

The installation process of displacement piles will influence the stress state around the pile. It is expected that the phasing of the pile installation process relative to the borehole drilling process will influence the eventual bearing capacity. In order to investigate the influence of phasing on the bearing capacity of piles, three situations were chosen:

A. Phasing A: the pile installation process is simulated before the simulation of the borehole drilling process (including possible drilling complications)

B. Phasing B: the simulation borehole drilling process (including possible drilling complications) occur before the simulation of the pile installation process

C. Phasing C: the pile installation process is simulated first. After this, a construction is simulated by loading the pile by half its *Initial bearing capacity*, as given in the results of chapter 6. At last, the borehole drilling process is simulated.

Phasing A and B were performed for a borehole with a 0.8m diameter and a drilling complication ($-50\ vol.\%$) occurring between -15m and -25m depth. A pile-borehole spacing of 2.0m was chosen in order to investigate the influence of phasing under a large stress redistribution.

For phasing C, no drilling complication was applied as this caused a *soil collapse error* or a *severe divergence error* in PLAXIS. For this phasing C, the pile-borehole spacing was varied from 2.0m to 4.0m. A borehole of 0.8m in diameter was used.

In this way, an advice can be given in which of the three scenario's different ways of phasing the installation processes is the most harmless for the bearing capacity. Again, the results are all given in load-displacement curves for the final analyzes.

Influence of soft soil on bearing capacity

All of the above mentioned analyzes contain a soil structure with only sand. In real-life, piles are used for the foundation of constructions when the soil at ground level is not suitable enough. In most of the cases, and especially in the Netherlands, these are soft soils. The

borehole drilling process through soft soil layers is not captured within the analyzes performed in chapter 4 and 5. This means that there is only scarce understanding of the processes and parameters that will influence the borehole drilling process through soft soil instead of through sand, like time-dependent behavior. A Dutch clay type is chosen for this scenario, modelled by a simplified soil model, as explained in chapter 3.4.2. For this scenario, the simulation contains the following:

- A 0.3m borehole back-filled with grout shrinkage of 2 $vol.\%$
- A wished-in-place (non-displacement) pile with tip at -20m depth
- No drilling complication
- A relatively small spacing of 0.6m between the borehole and the pile
- Clay layer between 0 and -15m depth
- Sand layer from -15m depth to lower boundary of model

3.3.4. Real-life case

The extended model and its results were validated by means of their application on a practical case. This practical case was chosen to be the Lisse project, which contains a borehole closely drilled to pile foundation locations. Fugro has performed CPT's before and after the drilling of the boreholes. These CPT results show an significant decrease in cone resistance of the soil around the boreholes. The aim of the validation is to give advice on whether the drilling of the borehole has influenced the bearing capacity of the piles when compared to the initial bearing capacity.

3.4. Numerical model setup

The PLAXIS software from Brinkgreve, 1994 is used in order to perform all the analyzes given in section 3.3. At first, a conceptual model was built which only included the simulation of the drilling process, performed in the 2D and 3D model. This required a specific domain size and boundary conditions. After this, the model was extended by introducing complex soil behavior, back-fill materials and (non-)displacement piles. All of these structural extensions are considered in this section. Next to this, the simulation of some special analyzes are included, like changes in soil volumes and applying static pile load tests. At last, different mesh configurations used for the FEM numerical model are verified by an analytical solution.

3.4.1. Model design

Dimensions and boundary conditions

The numerical model was built as a 2D-axisymmetric model and a plane strain 3D model. The domain size of the models were chosen such that the stress-strain changes due to the borehole drilling process were minimized at the boundaries. The domain differed for the conceptual model (only one borehole) and extended models (> 1 borehole, drilling complications or piles included) but were equal for the 2D and 3D models (the 3D model was chosen such that $x = y$), as given in table 3.1.

Model	Width	Depth
$Conceptual$	$5m$	$-50m$
$Extended$	$30m$	$-60m$

Table 3.1: Domain sizes for the conceptual and extended model

The general boundary conditions that can be applied to PLAXIS models constrain: 1) deformations, 2) dynamics and 3) groundwater flow and precipitation. For all of the developed models in PLAXIS, these boundary conditions are kept at their *default* settings as given in Brinkgreve, 1994 and are given in table 3.2. For the overall water-conditions, the water-table were set at ground level. For the simulation of the drilling process, manually adapted water conditions were used within the boreholes, which are explained in 3.4.3.

Boundary type	Setting
$Deformations$	$Normally-fixed$
$Dynamics$	$Viscous$
$Groundwater-flow$	$Open$
$Precipitation$	$None$

Table 3.2: Default boundary conditions for the conceptual and extended model

Mesh

The PLAXIS model is based on a Finite Element Model (FEM) in which different meshes can be used. Every scenario that is modelled has a specific sensitivity for a mesh type. The three main mesh types were: medium, fine and very-fine, for both the 2D-axisymmetric and 3D plane strain model, shown in fig. 3.2 and fig. 3.3, respectively. All three types of meshes were refined locally where large stress-strain changes would occur. So, this local refinement was done around boreholes and underneath piles. The mesh of the model was converged in such a way that maximum time efficiency and result accuracy were achieved. The accuracy of the model was verified by means of the analytical solution, as given in chapter 3.5.

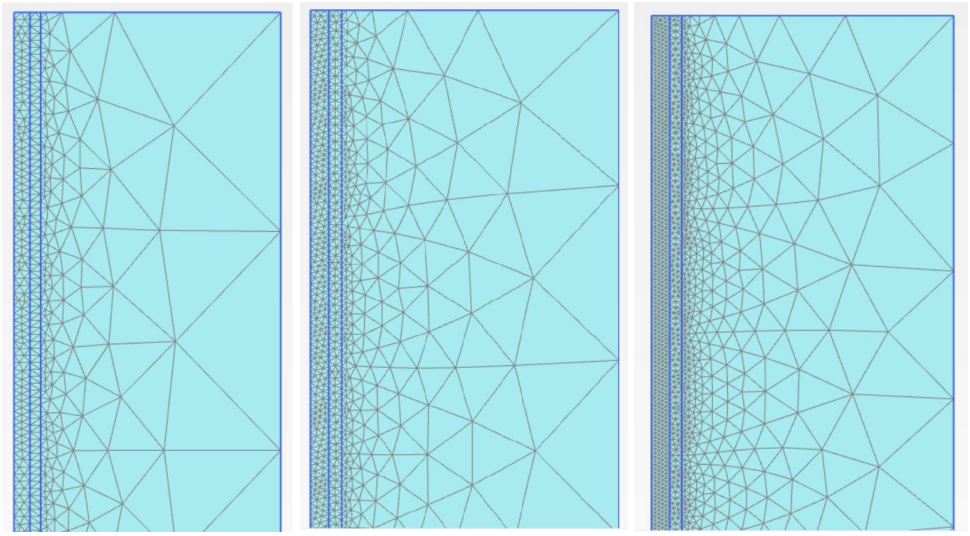

Figure 3.2: Left: 2D-medium mesh, middle: 2D-fine mesh, right: 2D-very fine mesh

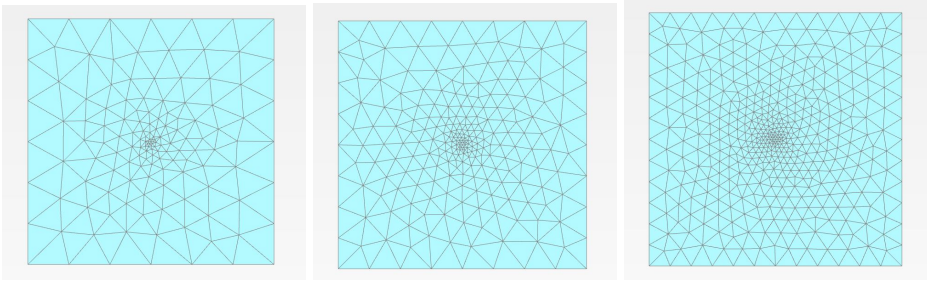

Figure 3.3: Left: medium mesh, middle: fine mesh, right: very fine mesh

3.4.2. Model materials

Soils

The stress-strain changes due to borehole drilling are dominated by the soil behavior. There are numerous different models to describe the behavior of soils numerically. In PLAXIS, the behavior of soils is captured in constitutive soil models, described in Plaxis, 2015. As for the first part of the research only sand is used, only two types of soil models were used. For the last part, a clay layer is introduced and described by a soil model which simplifies the behavior of this clay. All the soil models require input parameters, which were derived from real deposits and obtained from research by Fugro.

For the conceptual part, which was used to verify the PLAXIS model with the analytical model, the Mohr-Coulomb model was used with parameters as given in table 3.3. These input parameters equal those of the analytical solution, as will be discussed in chapter 3.5.

Parameter	Value	Unit
γ_{sat}	20	kN/m^3
γ_{unsat}	18	kN/m^3
E'	$361 * 10^3$	kN/m^2
v	0.3	-
c'	6.5	kN/m^2
ϕ	33	$degree$
ψ	0	$degree$

Table 3.3: Input parameters used for the MC model representing sand in PLAXIS

The goal of the constitutive models, however, is to model the behavior of real sand deposits. This is why the Hardening Soil Small Strain model (HSs model) (Plaxis, 2015) was chosen as the best fit for sand deposits in the Netherlands. This model has strength parameters, c, ϕ and ψ, which are common for sands. Next to this, it allows for plastic strains due to compressive and deviatoric loading which also counts for very small strains (G_0 and $\gamma_0.7$). Also, it has a stress dependent stiffness which is common in thick sand deposits (m). At last, it has the Over Consolidation Ratio (OCR) which determines the initial in-situ stress condition of the sand. This allows for K_0 conditions in which the horizontal stress is higher than the vertical stress. The input parameters used for the extended models are given in table 3.4. To show the significant difference in soil behavior between the Mohr-Coulomb and Hardening Soil Small Strain model, a graph is made showing the difference between both solutions, as given in fig. 3.4.

Parameter	Value	Unit
γ_{sat}	20	kN/m^3
γ_{unsat}	18	kN/m^3
E_{50}	$45 * 10^3$	kN/m^2
E_{oed}	$45 * 10^3$	kN/m^2
E_{ur}	$180 * 10^3$	kN/m^2
$power$	0.5	-
c'	0	kN/m^2
ϕ	33	$degree$
ψ	3	$degree$
$y_{0.7}$	$0.08 * 10^{-3}$	-
G_0	$180 * 10^3$	kN/m^2

Table 3.4: Input parameters used for the HSs model representing sand in PLAXIS

For the simulation of static pile load tests, the Hardening Soil Small Strain model gave numerical errors with extremely small displacements for high loads. This is why for these calculations, the Hardening Soil model (HS model) was chosen in order to overcome the numerical problems. The Hardening Soil model has the exact same parameters as the Hardening Soil Small Strain model but without the G_0 and $\gamma_0.7$ parameters. In order to prove the minimal difference in output, a cross-section is given that compares the the outcome of the models in fig. 3.5.

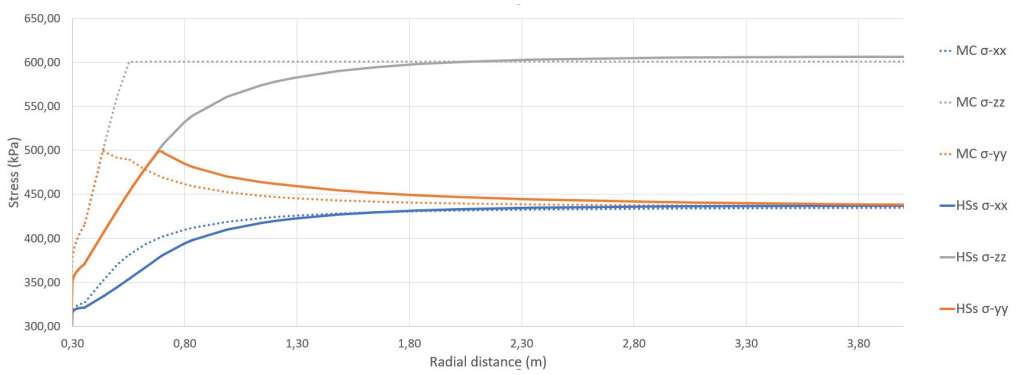

Figure 3.4: Graphs showing the total stress versus the radial distance from the borehole center comparing a solution for the Mohr-Coulomb model and the Hardening Soil Small Strain model

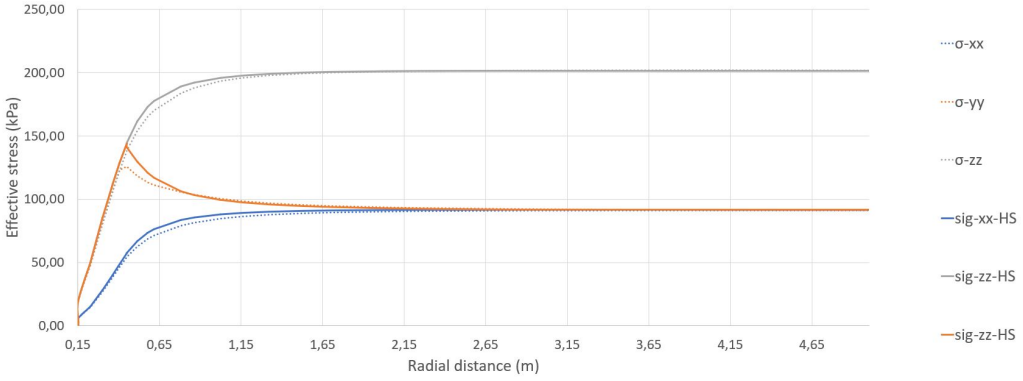

Figure 3.5: Comparison of the stress states after drilling a 0.3m borehole in HS and HSs modelled soil

In the bearing capacity analysis, some calculations were performed including a clay layer. The soil behavior is explained by the HSs model and not by the Soft Soil Model (Plaxis, 2015) because for this research there is no time-dependent behavior included. The input parameters used for the clay layer are given in table 3.5.

Parameter	Value	Unit
γ_{sat}	20	kN/m^3
γ_{unsat}	18	kN/m^3
E_{50}	$45 * 10^3$	kN/m^2
E_{oed}	$45 * 10^3$	kN/m^2
E_{ur}	$180 * 10^3$	kN/m^2
$power$	0.5	-
c'	0	kN/m^2
ϕ	33	$degree$
ψ	3	$degree$
$y_{0.7}$	$0.08 * 10^{-3}$	-
G_0	$180 * 10^3$	kN/m^2

Table 3.5: Input parameters used for the HSs model representing clay in PLAXIS

Back-fill material

For both open and closed systems, different back-fill materials exist. For closed systems, thermally-enhanced grout is used. The exact strength parameters of this material is not known. Despite the ability to use the Concrete Model, it was chosen to use a non-porous linear elastic material in PLAXIS for this grout (Plaxis, 2015). This was assumed because it is not in the scope of this research to include the influence of installing piles on the back-fill materials of UTES boreholes. The input parameters for stiffness and density of the material were obtained from Fugro and rely on practically determined values of grout bodies. The input parameters for the grout body are given in table 3.6.

Parameter	Value	Unit
E	$2 * 10^3$	kN/m^2
c'	0	kN/m^2
ϕ	33	$degree$

Table 3.6: Input parameters for the Linear Elastic model representing the grout body as back-fill material for closed systems

For the open systems, an HDPE pipe is placed in the center of the borehole and the annulus is back-filled with gravel material. The gravel material is strong and very stiff. It was assumed that the effect of the HDPE on the results is negligible. This is why for the simulation, the whole borehole is back-filled with gravel material, represented by the Mohr-Coulomb Model in PLAXIS (Plaxis, 2015). The input parameters for the gravel material are given table 3.7.

Parameter	Value	Unit
E	$50 * 10^3$	kN/m^2
c'	0	kN/m^2
ϕ	45	$degree$

Table 3.7: Input parameters for the Mohr-Coulomb model representing the gravel as back-fill material for open systems

Foundation pile

Next to soil material, a pile is necessary for the bearing capacity analysis and the belonging static pile load tests. For the pile material simulation, a non-porous linear-elastic material (Plaxis, 2015) was used. This is used because the pile has to be extremely stiff material and cannot deform plastically. This was assumed because it is not in the scope of this research to include the effects of the pile material on its bearing capacity. The material parameters used for the pile are given in table 3.8.

Parameter	Value	Unit
γ	25	kN/m^2
E	$30 * 10^6$	kN/m^2
v	0.1	kN/m^2
R_{int}	0.5/0.75	-

Table 3.8: Input parameters for the Linear Elastic model representing a pile

3.4.3. Model simulations

Real-life geotechnical processes, included in the analyzes given in chapter 3.3, are simulated by means of numerical models in PLAXIS. The following simulations of geotechnical processes are explained: borehole drilling process, grout shrinkage and expansion, drilling complications, pile simulation and static pile load tests.

Drilling process

Drilling a borehole can be simplified to the process of excavating a cylindrical segment of soil. In order to keep the excavated part of the borehole stable, a drilling fluid is added. It assumes a perfect removal of soil segments and does not take into account the effects of the mechanical drilling process.
In order to simulate this perfect excavation of soil segments, a step-by-step removal of soil segments is performed. In PLAXIS 2D model, as illustrated in fig. 3.6, the removed soil segment has a width equal to the borehole radius. In the PLAXIS 3D model, as illustrated in fig. 3.7, the boreholes can be simulated completely. As PLAXIS works with calculation phases, every enumeration stands for a calculation phase:

1. Deactivation of first cylindrical soil segment, which length can be chosen arbitrarily. Change the water-conditions in the soil segment from *Global level* to *User-defined* and application of an incremental drilling fluid pressure, as determined in chapter 5.1
2. Deactivation of second cylindrical soil segment and application of an equal incremental drilling fluid pressure

3. Repetition of the previous steps until the required borehole depth is reached
4. Activation of back-fill material (3.4.2) for all borehole segments. Water conditions in all soil segments back from *User-defined* to *Global level*.

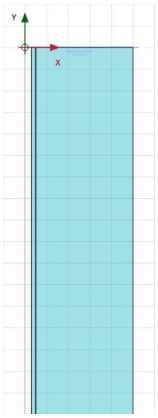

Figure 3.6: The simulation of the drilling process in a 2D-axisymmetric model of a borehole with a 40m depth

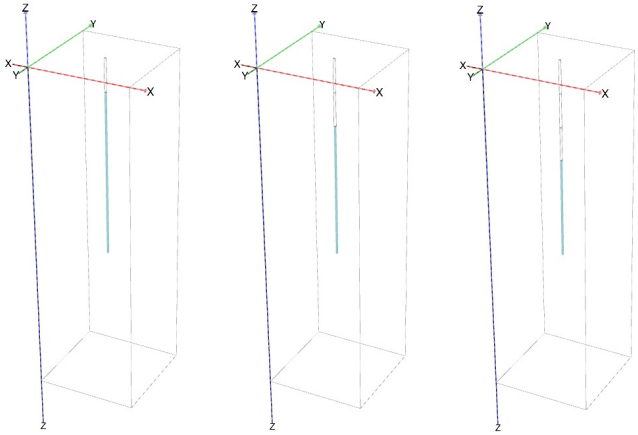

Figure 3.7: The step-by-step drilling process for a 3D model with a borehole depth of 60m and borehole segments of 10m

Drilling complications and grout body volume change

Drilling complications might occur when the drilling process is not performed perfectly. The drilling processes simulated in this research, only include partial collapse or erosion of borehole walls. This type of drilling complication is simulated by means of negative volumetric strains, in x- and y-direction, applied at a soil segment. This is simulated by means of the following PLAXIS calculation phases:

1. Perform the drilling simulation steps as given in chapter 3.4.3
2. During step 4, simulating the back-filling of the borehole, assign a negative volumetric strain with a magnitude as given in table 3.9 to the soil segment with the required depth
3. Apply further simulations, like static pile load tests

The only way to measure drilling complications is by estimating the excess soil volume loss found at the bottom of the borehole between two drilling stages. For simplicity, these excess soil volume losses were expressed in volume percentage of the required excavated borehole volume. In order to simulate these, the volume percentages of soil were computed towards strains, as given in table 3.9. The simulation of grout shrinkage and expansion relies on the

$\varepsilon_{vol.}$ %	$\varepsilon_{x,y}$ %	Excess soil volume %
-25	-12.5	23
-50	-25	43
-75	-37.5	60

Table 3.9: Excess soil volume (%) computed to volume strain (%)

same method, as it simulates soil volume change. The volume strain, in the contrary, was applied over the complete grout body instead over a specified soil volume. Next to this, the volume strains were much smaller and vary between -10 to 10 %.

Simulation of piles

All the simulated piles had a constant circular shape and dimensions with a depth of 20m and a radius of 0.2m.

Non-displacement piles are simulated by giving a soil volume with the dimensions of the pile the Linear Elastic material as given in table 3.8. As the non-displacement piles were wished-in-place, no installation effect was modelled except for the interface between soil and pile, as mentioned in 2.3.1. This shear band was simulated by means of an interface in PLAXIS. This can be given as an strength reducing input parameters (R_{int}) for the interface between the soil and pile materials (Plaxis, 2015). For a wished-in-place pile a realistic strength reducing factor of 0.5 was chosen due to relatively small mobilized shear strengths.

The simulation of a displacement pile had to include rearrangements in the stress state of the soil. This was done according to a method found performed in an earlier study, by Dijkstra et al., 2006. As the methods in this study were performed for a 2D-axisymmetric model and for this research a 3D model is used, it was not possible to perform the best-fit simulation method. However, the following simulation gives a first-order estimation of the stress rearrangements for the simulation of pile driving. This was simulated in PLAXIS by applying the following steps:

1. A horizontal prescribed displacement of 7.5 percent the pile radius is applied at the surface representing the pile shaft.
2. A vertical prescribed displacement of 0.5m in the z-direction is applied at the pile tip.
3. The displacements produced by the prescribed displacements are set to zero, this is done to make sure that only the soil stresses are affected by the installation simulation.
4. The interface strength reduction factor (R_{int}) must be set to 0.75 in order to simulate the shear zone that occurs between soil and pile shaft.
5. The volume representing the pile can be set to the pile material, as given in table 3.8

Static Pile Load Tests

For all calculation containing pile load test simulations, the soil is modelled by an Hardening Soil model instead of an Hardening Soil Small strain model, as explained in chapter 3.4.2. The bearing-capacity of both displacement and non-displacement piles were simulated by means of a static pile load test in PLAXIS by performing the following steps:

1. Introduce a displacement or non-displacement pile in the soil, as given in chapter 3.4.3.
2. Load the pile with a surface load that exceeds the actual load capacity. For simulations containing non-displacement piles, it was set at $6000kN/m^2$, while for simulations containing displacement piles it was set at $40000kN/m^2$.
3. Plastic failure will occur at the tip of the pile and a load-displacement curve can be made.

The ultimate bearing-capacity is the total load value at maximum displacement point (failure point). In this way, the failure mechanisms were derived and a qualitative conclusion on the bearing capacity was drawn.

3.5. Model verification

In this section, the numerical model is verified by means of the an analytical model. Next to this, a mesh analysis for both 2D-axisymmetric and the plane strain 3D model is performed. Different mesh types are checked on accuracy and efficiency.

Analytical model

In order to make sure that the extended models built in PLAXIS give reliable results, the conceptual model was verified by an analytical theory. For this verification, the study on sand stresses around a borehole by Risnes et al., 1982, as described in chapter 2.2.3, was used. This paper provides an analytical solution for the stress state around a borehole with a soil which behaves steady-state, linear-elastic and has a Mohr-Coulomb failure criterion. The formulas used for the analytical solution are given in appendix D.
The input parameters that were used for the analytical solution are given in table 3.10 and simulates a slightly cemented sand, which is contained by the soil parameters S_0, α, v and β. The initial (in-situ) stress states were determined from a K0-calculation in PLAXIS and are due to unit weight, contained in soil stress parameters σ_{r0} and σ_{z0}. In order to keep the 0.6m diameter borehole stable, fluid pressures play an important role. The drilling fluid pressure (σ_{ri}) is chosen a bit higher than the horizontal stress (σ_{r0}) for borehole stability. The fluid pressure at outer boundary (P_0) is the hydrostatic pore pressure in the sand layer. At last, the outer boundary radius (R_0) was chosen such that $R_0 > 10 \times R_i$, which is a rule of thumb used for the zone of influence (Spegelaere M., 2019).

The graph in fig. 3.8, gives the solution for a depth of -30m.

Parameter	Value	Unit	Meaning
S_0	6.5	kN/m^2	cohesive strength
P_0	300	kN/m^2	fluid pressure at outer boundary
R_i	0.6	m	borehole radius
R_0	4	m	radius outer boundary
α	61.5	$degree$	failure angle
v	0.3	–	Poisson's ratio
β	1.0	–	compressibility
σ_{z0}	600	kN/m^2	initial total vertical stress
σ_{r0}	436	kN/m^2	initial total radial stress
σ_{ri}	315	kN/m^2	fluid pressure in borehole

Table 3.10: Input parameters used for the analytical formulas as given in appendix D

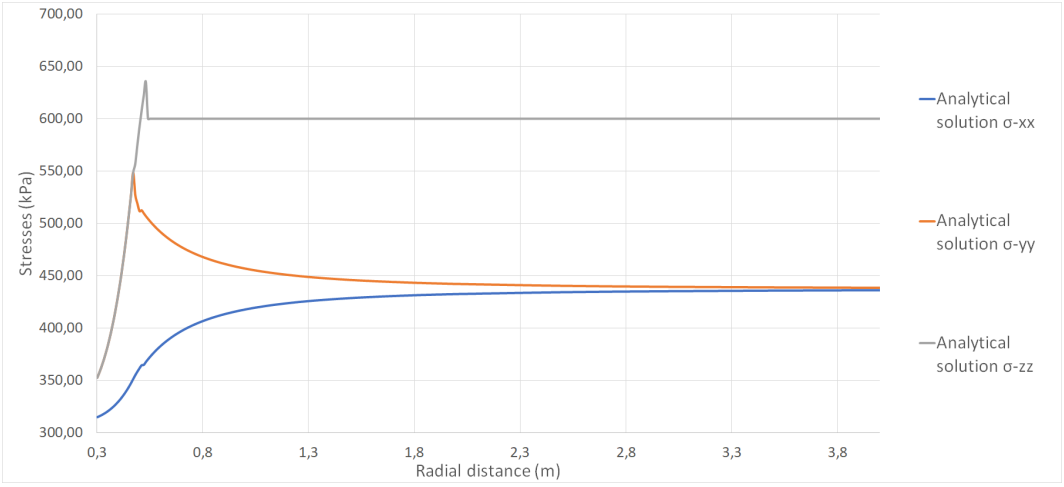

Figure 3.8: The analytical solution for the total stress state around a borehole with a 0.6m diameter at a depth of -30m

Numerical model verification

The conceptual PLAXIS model consists out of one borehole with a 0.6m diameter and a depth of 60m, modelled as given in 3.4.3. The drilling fluid pressure, was set such that at a depth of -30m it was equal to σ_{ri}, as given in table 3.10. Next to this, the soil parameters used in the Mohr-Coulomb model in PLAXIS, as given in table 3.3, were set equal to the analytical input parameters. In this way, all input parameters were set equal and output could be compared.

This calculation was performed using the three different meshes. The radial, hoop and vertical stresses were plotted against radial distance from the borehole center. This was done for both 2D-axisymmetric and 3D-plane strain models. The mesh analysis of the 2D-axisymmetric models are given in fig. 3.9 to 3.11. The mesh analysis for the 3D-plane strain

models are given in fig. 3.12 to 3.14. In this way, the best fit with the analytical solution was chosen by means of an error calculation.

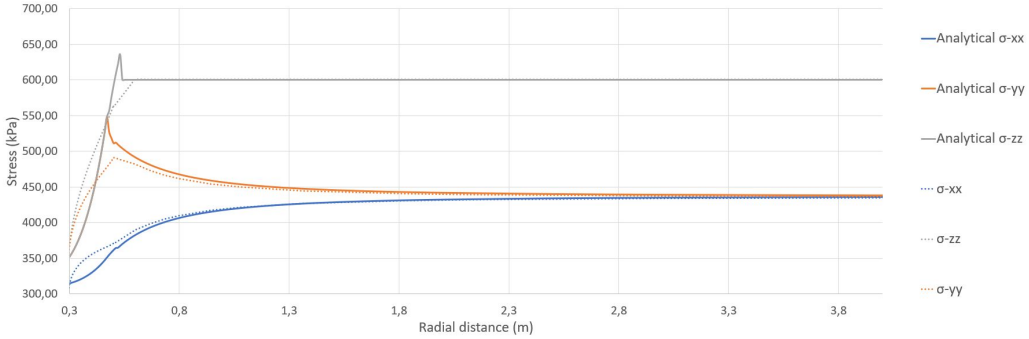

Figure 3.9: Total stress versus radial distance from the borehole center (at x=0m) for a refined medium mesh compared with the analytical solution in a 2D-axisymmetric model

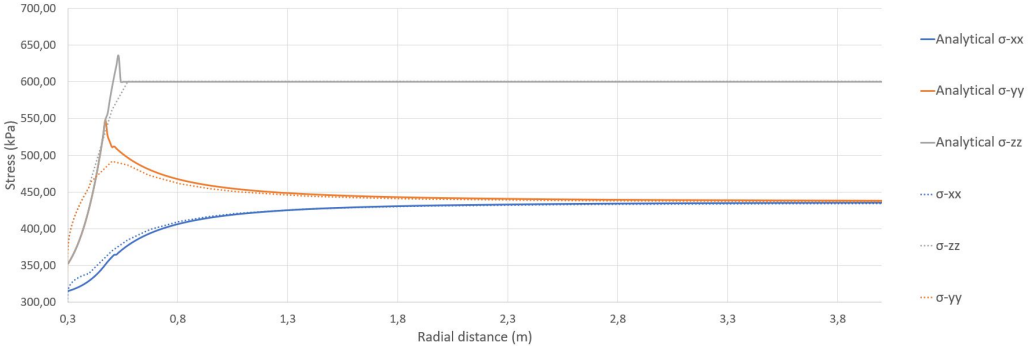

Figure 3.10: Total stress versus radial distance from the borehole center (at x=0m) for a refined fine mesh compared with the analytical solution in a 2D-axisymmetric model

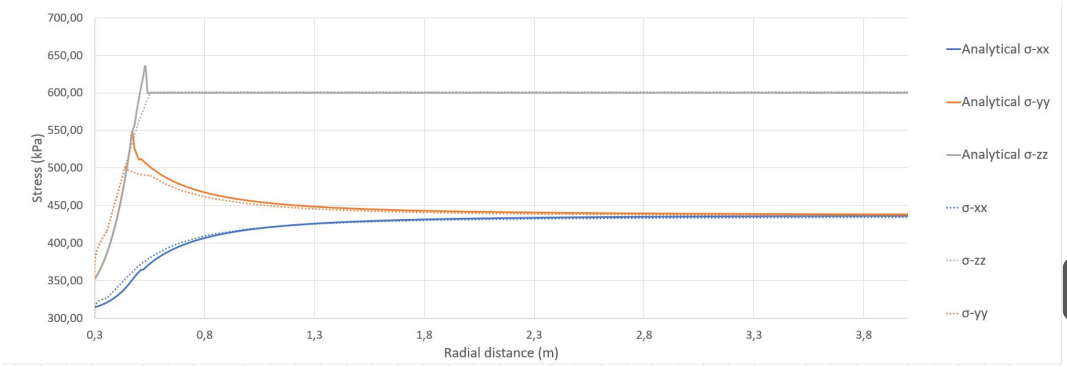

Figure 3.11: Total stress versus radial distance from the borehole center (at x=0m) for a refined very-fine mesh compared with the analytical solution in a 2D-axisymmetric model

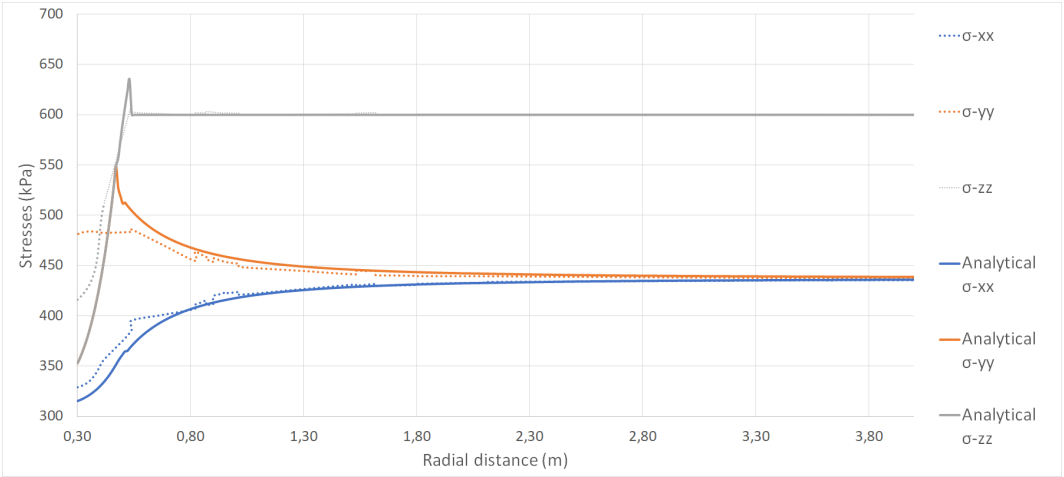

Figure 3.12: Total stress versus radial distance from the borehole center (at x=0m) for a refined medium mesh compared with the analytical solution in a 3D plane strain model

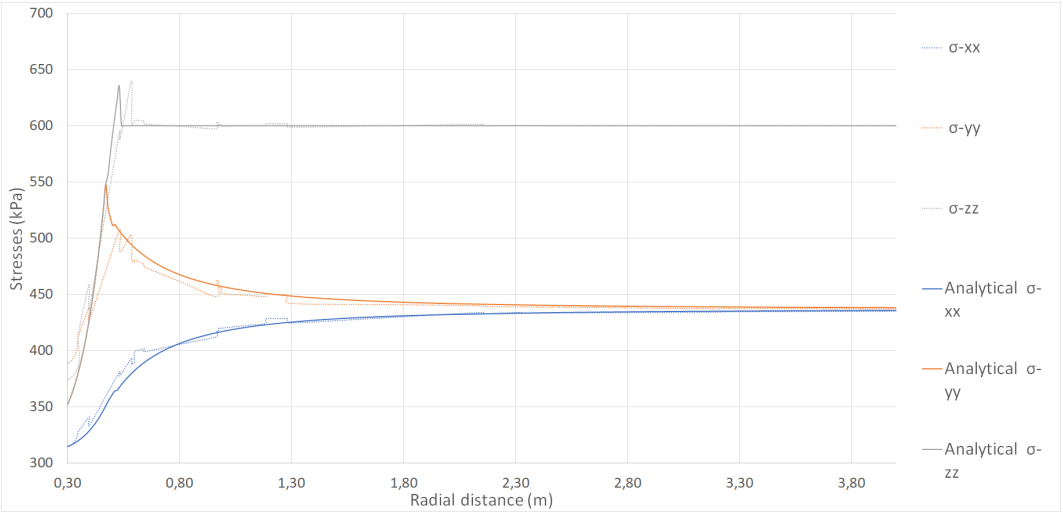

Figure 3.13: Total stress versus radial distance from the borehole center (at x=0m) for a refined fine mesh compared with the analytical solution in a 3D plane strain model

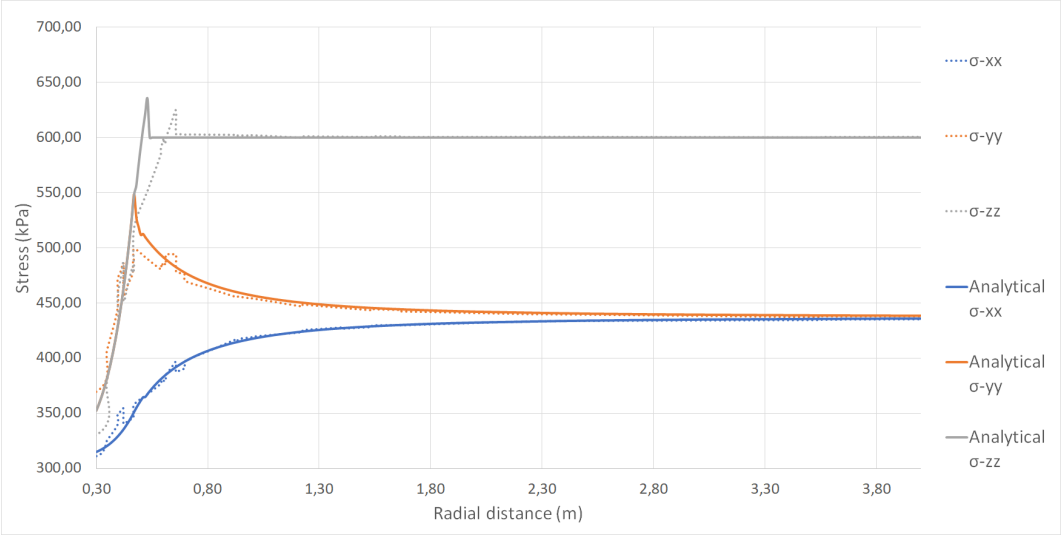

Figure 3.14: Total stress versus radial distance from the borehole center (at x=0m) for a refined very-fine mesh compared with the analytical solution in a 3D plane strain model

The graphs for the 2D-axisymmetric model have more smooth lines, which is due to a better mesh configuration for the circular borehole drilling simulation. The 3D models have way more data points due to which some more local errors exist.
For the 2D graphs it is clear that the solutions get better with finer meshes. However, for the 3D graphs this is less clear, especially between the fine and very-fine mesh. The details

of the 3D mesh analysis show that the most smooth lines exist in the results for the fine and very-fine meshes. For the medium mesh a significant error exist for the hoop stress close to the borehole wall ($x < 0.5m$). In order to get a quantitative insight in the accuracy of the different 3D meshes, an error calculation was performed. The mean deviation from the analytical solution for a depth of -30m in the plastic zone was determined for the three principal stresses separately, as given in table 3.11:

Mesh	Stress	Error	Total error
Medium	σ_{xx}	$18.3kPa$	$154.7kPa$
	σ_{yy}	$77.2kPa$	
	σ_{zz}	$59.2kPa$	
Fine	σ_{xx}	$8.0kPa$	$74.5kPa$
	σ_{yy}	$35.4kPa$	
	σ_{zz}	$31.2kPa$	
Very-fine	σ_{xx}	$6.6kPa$	$59.2kPa$
	σ_{yy}	$29.5kPa$	
	σ_{zz}	$23.3kPa$	

Table 3.11: Error calculation for the three principal stresses for a medium, fine and very-fine mesh

As can be seen from table 3.11, the very fine mesh has the best fit with the analytical solution, and thus is the most accurate mesh to use for the calculations of this research. The difference between the computation times are negligible for this simple conceptual model. For more complex models including more structures and more complex soil models, these computation times may be a reason to use the fine mesh.

4

Impact of borehole installation parameters on stress conditions

In this parameter analysis, the effects of four parameters on the stress state around a borehole are analyzed: grout body shrinkage and expansion, Over-Consolidation Ratio, Relative Density and drilling complication magnitudes. Input values rely on real-life appearances, as explained in chapter 3.3.1.

4.1. Grout shrinkage and expansion

In this section, the influence of grout shrinkage and expansion of the grout body is investigated. The stress states around a 0.3m diameter borehole are considered. The borehole is drilled with a drilling fluid pressure increment of $-10.5kPa/m$. The effective radial (σ'_{xx}), hoop (σ'_{yy}) and vertical (σ'_{zz}) stresses are plotted against the radial distance from the borehole center and given in fig. 4.1 to 4.3. All stress states are taken at a depth of -30m.

The effective radial stress (σ'_{xx}) in fig. 4.1 is more affected by the shrinkage of the grout body than the expansion of it. A shrinkage of -2% shows an effective stress relief of $11kPa$ at a radial distance of 1.0m from the borehole center. The effective stress changes caused by an expansion of $+2\%$ are negligible. For higher shrinkage magnitudes of -10&, stress release can increase up to $41kPa$ at 1.0m distance, which is more than 30% of the initial horizontal stress.

The effective hoop stresses (σ'_{yy}) in fig. 4.2 experience an equal but opposite stress redistribution. The extend of the plastic zone can be analyzed from this graph. The plastic zone is the zone from the borehole wall to the peak of the effective hoop stress.

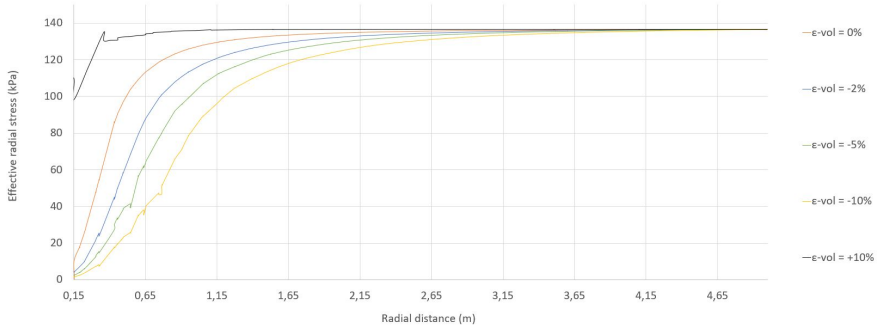

Figure 4.1: The effective radial stress (kPa) versus the radial distance (m) for the sensitivity analysis of the expansion and shrinkage of the grout body, for a borehole with a 0.3m diameter

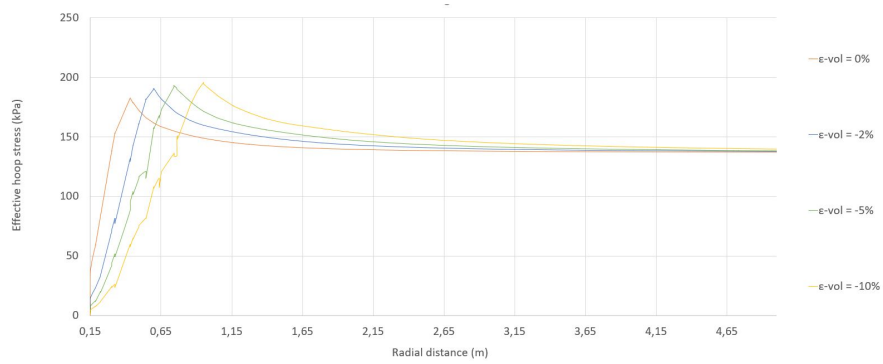

Figure 4.2: The effective hoop stress (kPa) versus the radial distance (m) for the sensitivity analysis of the expansion and shrinkage of the grout body, for a borehole with a 0.3m diameter.

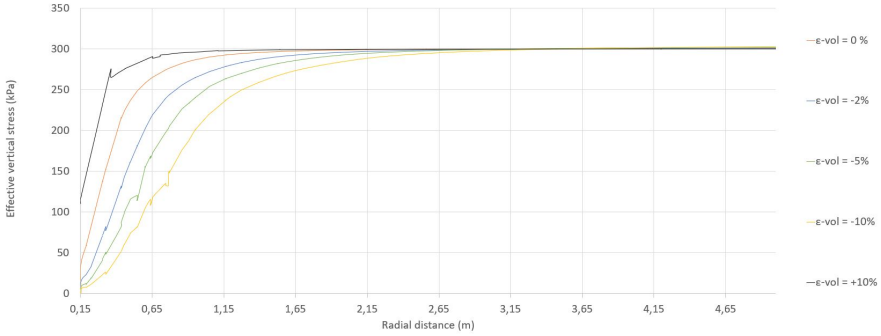

Figure 4.3: The effective vertical stress (kPa) versus the radial distance (m) for the sensitivity analysis of the expansion and shrinkage of the grout body, for a borehole with a 0.3m diameter

The effective vertical stress (σ'_{zz}) in fig. 4.3 is not affected by expansion at all. For shrinkage, on the other hand, it will experience an higher stress relief with increasing volume percentages. The affected radial area does not increase due to higher shrinkage values.

4.2. In-situ stress

In this section, the influence of the OCR on the stress states around a 0.3m diameter borehole is investigated. The borehole is drilled with a drilling fluid pressure increment of $-10.5kPa/m$. The effective radial (σ'_{xx}), hoop (σ'_{yy}) and vertical (σ'_{zz}) stresses are plotted against the radial distance from the borehole center at a depth of -30m and given in fig. 4.4 to 4.6,

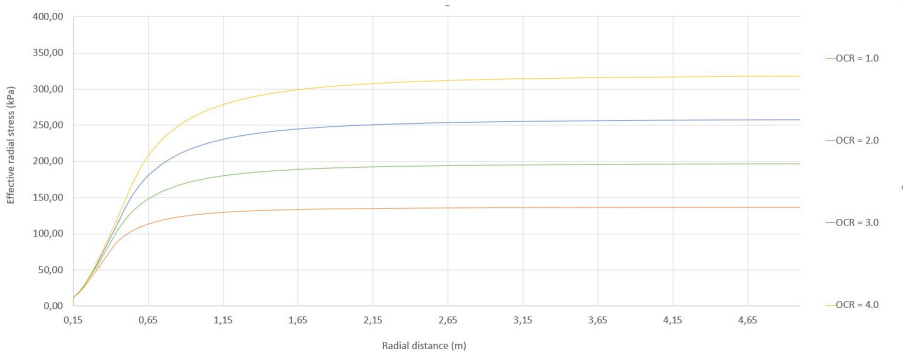

Figure 4.4: The effective radial stress (kPa) versus the radial distance (m) for the sensitivity analysis of the OCR, for a borehole with a 0.3m diameter

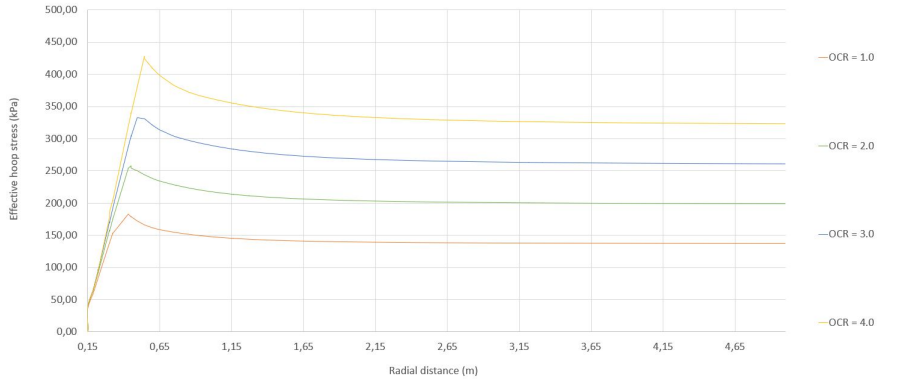

Figure 4.5: The effective hoop stress (kPa) versus the radial distance (m) for the sensitivity analysis of the OCR, for a borehole with a 0.3m diameter

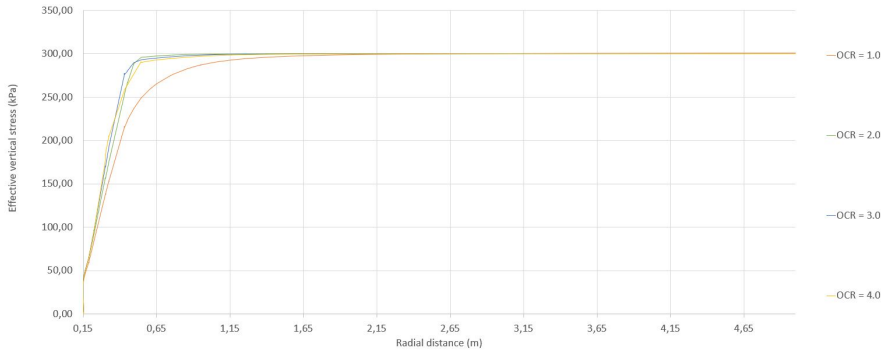

Figure 4.6: The effective vertical stress (kPa) versus the radial distance (m) for the sensitivity analysis of the OCR, for a borehole with a 0.3m diameter

It can be seen that by increasing the OCR from 1.0 to a value of 4.0, the horizontal in-situ stress increases from $136kPa$ to $321kPa$ respectively. For the OCR value of 4.0, the horizontal stress is higher than the vertical stress. The vertical in-situ stress is not influenced by the OCR and has a constant value of $300kPa$.

The effective radial stress (σ'_{xx}) in fig. 4.4 shows stress relief for all OCR values when approaching the borehole wall. The radial zone of influence increases with increasing OCR values. The zone of influence are 0.85m, 1.4m, 1.66m and 1.85m for an OCR of 1.0, 2.0, 3.0 and 4.0 respectively.

The effective hoop stress (σ'_{yy}) in fig. 4.5 shows an equal but opposite behavior. It can be seen that the extend of the plastic zone increases for higher OCR values.

The effective vertical stress (σ'_{zz}) in fig. 4.6 shows no relief up to a point 25 cm from the borehole wall for an OCR > 1.0. For an OCR of 1.0 the relief of the vertical stress starts starts at a higher horizontal distance form the borehole wall.

4.3. Relative Density

In this section, the influence of the RD on the stress states around a 0.3m diameter borehole is investigated. The borehole is drilled with a drilling fluid pressure increment of $-10.5kPa/m$. The effective radial (σ'_{xx}), hoop (σ'_{yy}) and vertical (σ'_{zz}) stresses are plotted against the radial distance from the borehole center at a depth of -30m and given in fig.4.7 to 4.9.

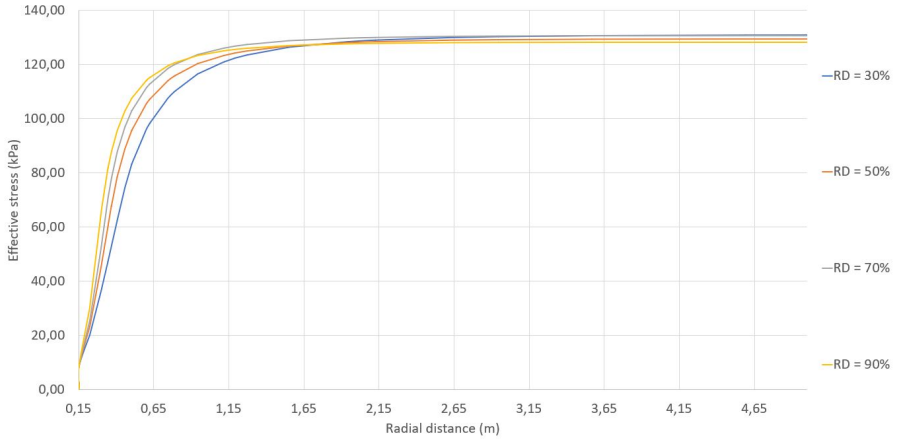

Figure 4.7: The effective radial stress versus the radial distance for the sensitivity analysis of the Relative Density, for a borehole with a 0.3m diameter

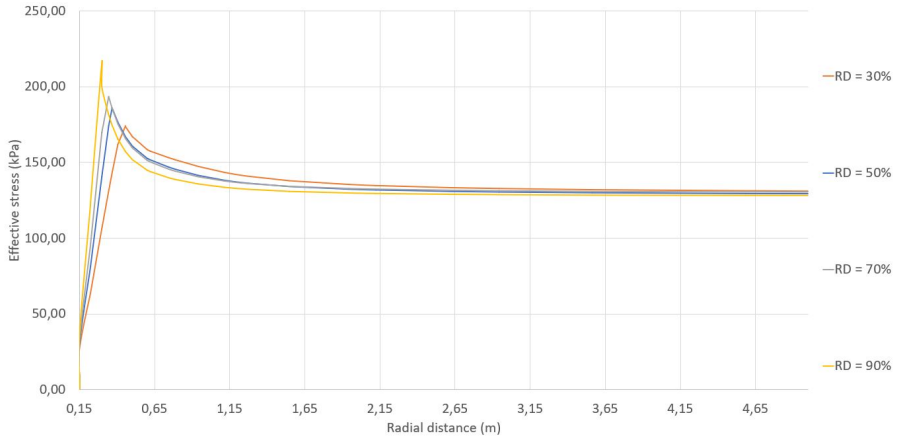

Figure 4.8: The effective hoop stress versus the radial distance for the sensitivity analysis of the Relative Density, for a borehole with a 0.3m diameter

The effective radial stress (σ'_{xx}) in fig. 4.7 shows an higher stress relief for lower Relative Density values. At a radial distance of 0.65m from the borehole center, the 30% RD curve shows a stress value of $100kPa$ while the 90% RD curve shows a stress value of $180kPa$.

The effective hoop stress (σ'_{yy}) in fig. 4.8 shows an higher peak value for higher Relative Density values. The extend of the plastic zone is larger for high RD values. This means that the stresses at the elastic-plastic boundary are higher for higher RD values.

The effective vertical stress (σ'_{zz}) in fig. 4.9 shows an equal relationship with Relative Density as the radial stress. Again, the stress values at a distance of 0.65m from the borehole center are higher for higher RD values.

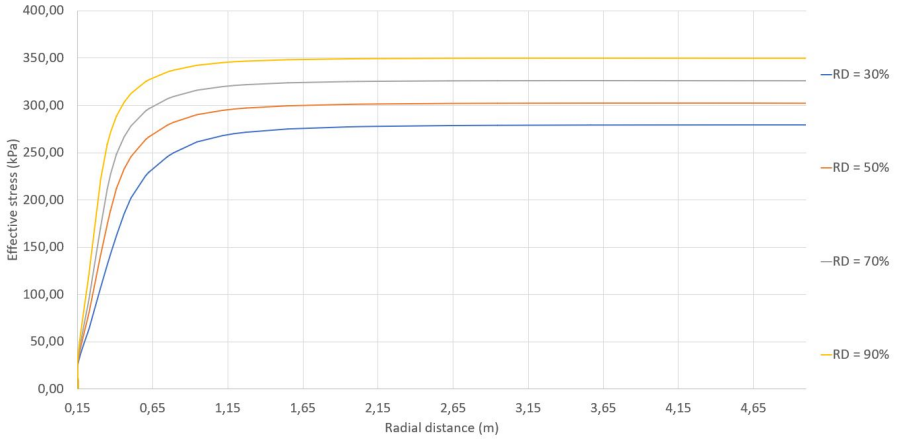

Figure 4.9: The effective vertical stress versus the radial distance for the sensitivity analysis of the Relative Density, for a borehole with a 0.3m diameter

4.4. Drilling complication

In this section, the influence of different magnitudes of drilling complications on the stress state is investigated. The borehole is drilled with a drilling fluid pressure increment of $-10.5kPa/m$. The effective radial (σ'_{xx}), hoop (σ'_{yy}) and vertical (σ'_{zz}) stresses are plotted against the radial distance from the borehole center at a depth of -30m and given in fig. 4.10.

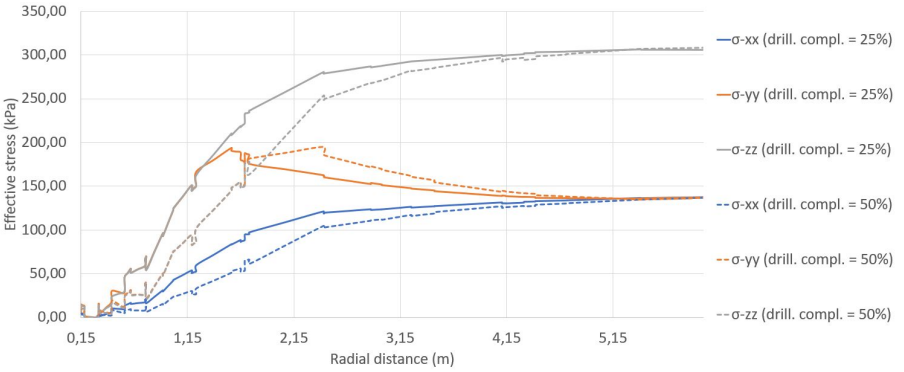

Figure 4.10: The effective vertical stress versus the radial distance for the sensitivity analysis on drilling complications, for a borehole with a 0.3m diameter

As can be seen from fig. 4.10, there is significant increase in the extend of the zone of influence when drilling complications are simulated. The extend of the plastic zone increases from $0.4m$ to $1.5m$ and $2.5m$ for a drilling complication with -25 $vol.\%$ strains and -50 $vol.\%$ strains respectively. For a drilling complication with -75 $vol.\%$ strains, the PLAXIS gave an instability and a borehole collapse error. The plastic zone was extended by such

a magnitude, that no effective stresses were present in the soil to keep it stable. This is why for further research it was chosen to simulate drilling complication with the maximum magnitude possible in simulations, namely $-50\ vol.\%$ strains.

4.5. Summary

For increasing shrinkage, the extend of the plastic zone increases significantly. The plastic zone increases from 0.15m for 0 percent shrinkage to 0.68m for -10 percent shrinkage. Next to this, it will increase the non-linear zone around the borehole wall. For expansion, it will only cause a decrease in stress redistribution for very high volume percentages. The extend of the plastic zone is not affected by expansion of the grout body.

The OCR will determine the extend of the zone of influence for the hoop and radial stresses. This zone will increase with increasing OCR values. For the vertical stress this zone of influence will decrease with higher OCR values. This is due to the decrease in deviatoric stresses in the plastic zone.

For higher Relative Density values hoop stresses show higher peaks at the elastic-plastic boundary due to higher stiffness of the soil. Overall stress redistribution behaves more overexcited with higher soil stiffness. A higher RD will decrease the extend of the zone of influence and the stress reliefs, which has to do with the strength of the soil. A decrease in strength (and in RD) will cause a decrease in the extend of the plastic zone.

The extends of the zone of influence increases extremely when drilling complications occur. For drilling complications with a magnitude of $-75\ vol.\%$ strains, the soil body collapses due to a serious loss of effective stresses in the soil. For this reason, the maximum possible magnitude of drilling complication was chosen for further research with a value of $-50\ vol.\%$ in strains. This is equal to an excess soil volume loss of 43%.

5

Impact of installing UTES boreholes on stress conditions

To understand the influence of the drilling process of boreholes on the bearing capacity of piles, it is important to analyze its effect on the soil stress state. In this chapter, results of this investigation are given. First, the drilling fluid analysis is performed as this is the major aspect effecting soil stress conditions around the boreholes. Next, the influence of the borehole diameter on the stress state around perfectly drilled boreholes are investigated. After all, drilling processes including a drilling complication is considered.

5.1. Drilling fluid pressure analysis

The drilling fluid pressure in boreholes has an upper and lower limit. The upper limit is the pressure at which a borehole burst-out will occur, which is not interesting for this analysis. The most desired drilling fluid pressure in the borehole at a certain depth is equal to that of the total horizontal stress at that depth in the soil and is diameter independent. The lower limit is the drilling fluid pressure at which the borehole wall is about to become unstable at which borehole collapse occurs.

For the soil type that is chosen, as given in table 3.4, the total horizontal stress at a depth of -30m is equal to $435kPa$. In order to obtain an equal counter-pressure from inside the borehole, an optimal drilling fluid pressure increment of $14.5kPa/m$ is required (such that $14.5 \times 30 = 435kPa$). In practice, however, such a constant pressure is unrealistic. The lower-limit for each borehole diameter is found by lowering this pressure increment from $14.5kPa/m$ until a borehole collapse occurs.

As an example, fig. 5.1 shows the stress-state for a drilling simulation with lower-limit drilling fluid pressure ($-10.28kPa/m$) and the desired drilling fluid pressure of $14.5kPa/m$ for a borehole with a diameter of 0.3m.

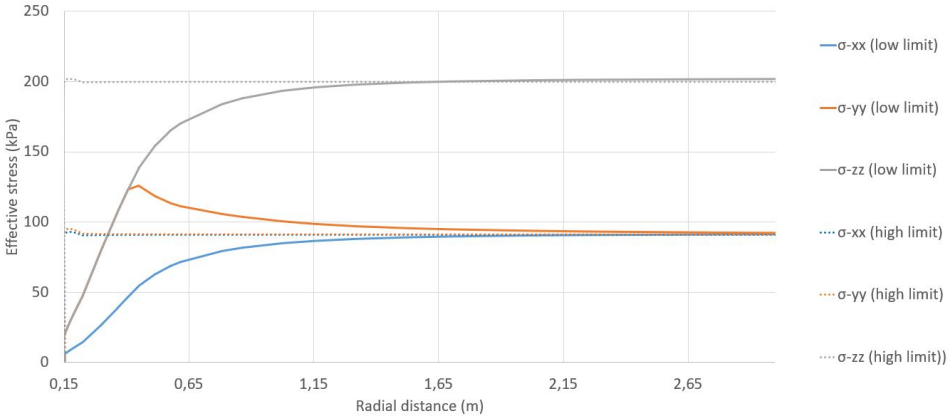

Figure 5.1: Stress state around the borehole for drilling at low and high limit drilling fluid pressures

It can be seen that the stress redistribution of the drilling with the lower-limit is significantly higher than that with the optimal drilling fluid pressure. The stress state around the borehole is highly dependent on the drilling fluid pressure during drilling and the plastic zone around the borehole can be completely minimized for the results in this model. For this research the changes in stress state are of interest, which are only caused for lower-limit drilling pressures. This way of drilling, however, produces very fragile and unstable boreholes. This is why for further research, it is chosen to increase the drilling fluid pressure increment by $-0.5kPa/m$ for all simulations.

An overview of the lower limits of drilling fluid pressure increments for boreholes with varying diameters are given in table 5.1:

Diameter (m)	Lower Limit (kPa/m)
0.3	10.28
0.4	10.34
0.8	10.35
1.0	10.36

Table 5.1: The lower limit of the drilling fluid pressures for boreholes with varying diameter

The required pressure is constant for all different boreholes as it depends on the horizontal stress at a certain depth which is determined by the unit weight of the soil. In the contrary, the lower limit pressure shows a non-linear relationship with the borehole diameter. The larger the borehole diameter, the less additional drilling fluid pressure has to be added. It can be seen that increasing the diameter from 0.3 to 0.4m, a pressure increment of $0.06kPa/m$ has to be added. While for an increase from 0.8 to 1.0m, it only needs $0.01kPa/m$. These are extremely small differences and it is doubtful whether this is not a numerical problem caused by mesh dependency.

5.2. Stress state around perfectly drilled boreholes

After the determination of the lower-limit and required drilling fluid pressures, the stress states for boreholes with varying diameter can be investigated. First, the stress state of single boreholes with a diameter varying from 0.3 to 1.0m are provided. After this, the stress state around arrays of two boreholes and four boreholes are given.

Stress states for single boreholes with varying diameter

Fig. 5.2 to 5.5 gives the effective stresses versus the radial distance from the borehole center for single boreholes with varying diameter. The cross-sections are taken at a depth of 20m, because this is the pile tip depth used for the bearing capacity analysis.

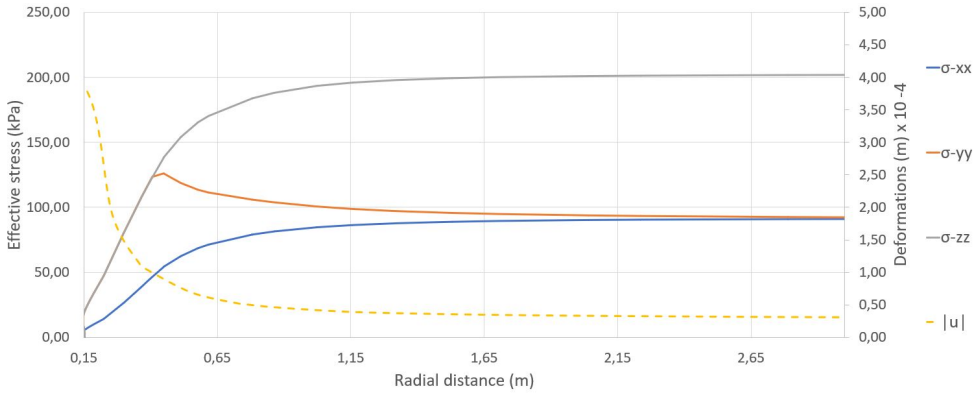

Figure 5.2: The effective stress state for a borehole with a diameter of 0.3m at a depth of 20m with total deformations |u| versus the radial distance from the borehole center

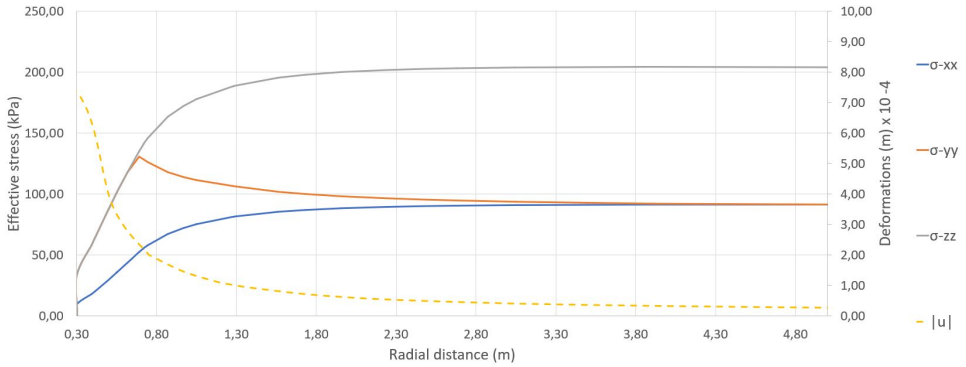

Figure 5.3: The effective stress state for a borehole with a diameter of 0.6m at a depth of 20m with total deformations |u| versus the radial distance from the borehole center

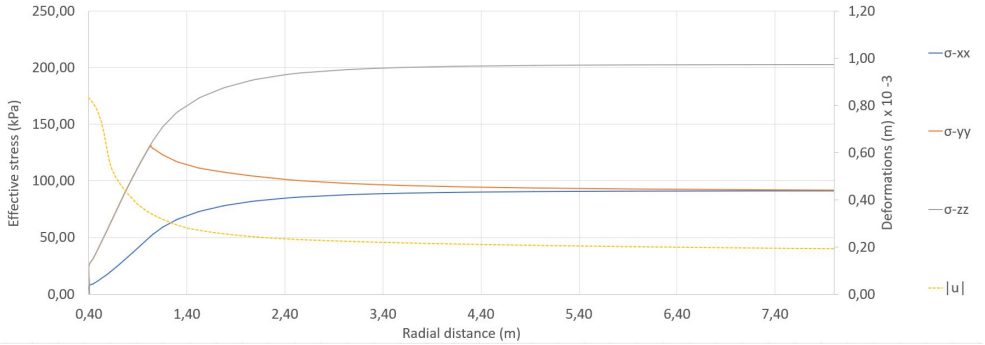

Figure 5.4: The effective stress state for a borehole with a diameter of 0.8m at a depth of 20m with total deformations |u| versus the radial distance from the borehole center

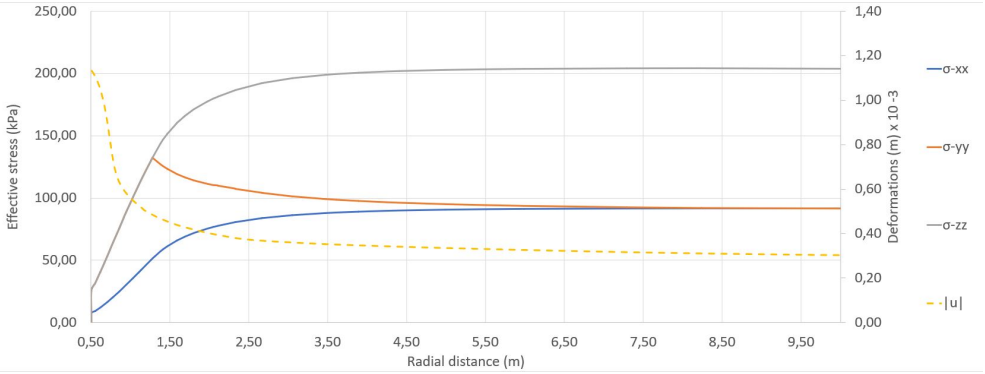

Figure 5.5: The effective stress state for a borehole with a diameter of 1.0m at a depth of 20m with total deformations |u| versus the radial distance from the borehole center

The magnitudes of the stress redistribution are equal for all borehole diameters. The hoop stresses all reach a more or less maximum value of $130kPa$ at the plastic-elastic boundary. Next to this, the vertical and radial stresses decrease when approaching the borehole wall.

The radial zone of influence around the boreholes, however, is influenced by the borehole diameter. As can be seen in fig. 5.2 to 5.5, there is difference between the zone of influence of the vertical stress and horizontal stress. This zone of influence is defined as the radial extend around the borehole in which less than 95% of the initial in-situ stress is present. The zone of influence per borehole diameter is given for the horizontal and vertical stresses separately in table 5.2.

Diameter (m)	Zone of influence σ_h (m)	Zone of influence σ_v (m)
0.3	1.2	1.0
0.3 (grout)	1.7	1.45
0.6	1.7	1.5
0.8	2.7	2.3
1.0	3.2	2.8

Table 5.2: The zones of influence around the boreholes with varying diameters for the horizontal and vertical stress separately at a depth of -20m. The 0.3 (grout) stands for the case in which the grout body has experienced a shrinkage of $-2vol.\%$

For the 1.0 diameter borehole, the stress redistribution is significant for a radial distance of only 3 meters around the borehole. For the boreholes with a diameter of 0.3, the zone of influence only becomes significant when there is shrinkage of the grout body. This means that for perfectly drilled boreholes, the bearing capacity analysis has to be performed very close to the boreholes (<3.0m) in order to investigate the influence of the stress redistribution on the bearing capacity of the piles.

Stress states for a two borehole array

Fig. 5.6 shows the effective vertical stress versus the depth at location (x, y) = (15, 15) which is in the middle of the two boreholes. The stress states at this location for varying borehole spacing is given and compared to the initial stress state.

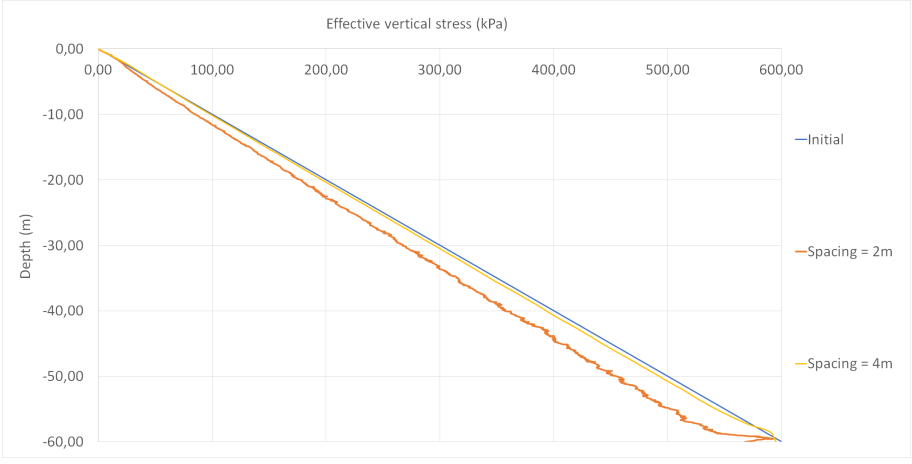

Figure 5.6: Graph showing the vertical stress versus depth at location (x, y) = (15, 15) in between two 0.3 diameter boreholes

There is a significant vertical stress relief for a spacing of 2m. The vertical stress relief at the same location for a borehole spacing of 4m is almost negligible. The horizontal stresses in x-direction and horizontal stresses in y-direction experience an equal but opposite stress

redistribution, these graphs are given in appendix E.

For a spacing of 2 meters between the boreholes, the vertical stress redistribution is noticeably higher than with situations performed with larger spacing. This is due to the intersection of the non-linear stress zones of both boreholes. A minimum spacing of 5 meters between the borehole and the pile location is necessary in order to obtain initial stress conditions at the location in the middle of those. For boreholes with higher diameters, this spacing is higher due to the higher extend of the non-linear zone.

Stress states for a four borehole array

Fig. 5.7 provides the effective vertical stress versus depth at the location x,y = (10;10) in the middle of four boreholes. The spacing this location and the borehole is 2m.

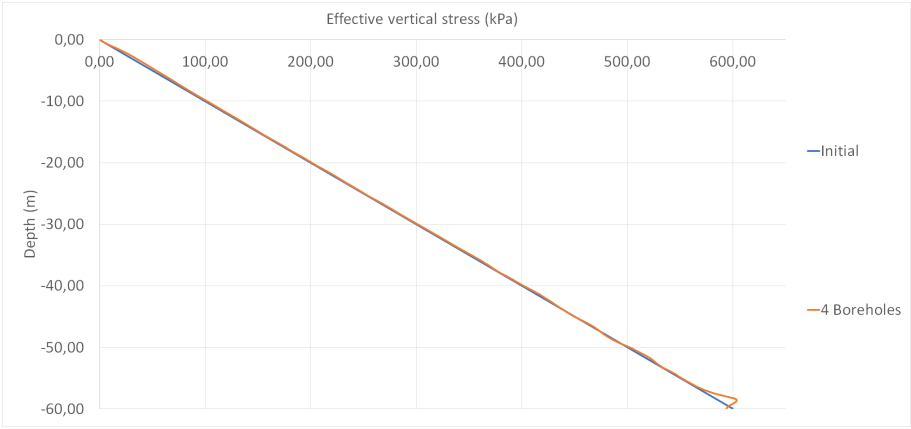

Figure 5.7: Graph showing the vertical stress versus depth at location (x, y) = (10, 10) in the middle of four 0.3 diameter boreholes

The effective vertical stress does not experience any stress relief. This also counts for the horizontal stress in x- and y-direction, for which the graph is provided in appendix E.

Fig. 5.8 gives the effective vertical stress versus the depth in the middle of two boreholes in a four borehole array configuration. The spacing between the two boreholes is a little more than 2 meters. In the graph this is compared with the situation in which a two borehole configuration is used.

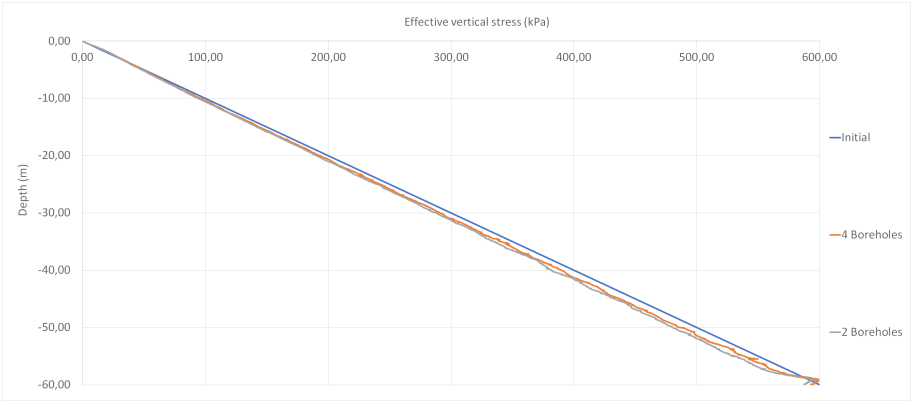

Figure 5.8: Graph showing the effective vertical stress versus the depth in between two boreholes for a two borehole array and a four borehole array

It is clear that there is a small stress relief of 6% the initial stress at 40m depth for the two borehole configuration. The configuration with four boreholes has a slightly smaller stress relief.

5.3. Drilling complications

Fig. 5.9 to 5.10 give the effective vertical stress relief due to a drilling complication at different depths for a 0.3m and 0.8m diameter borehole, as explained in chapter 3.3.

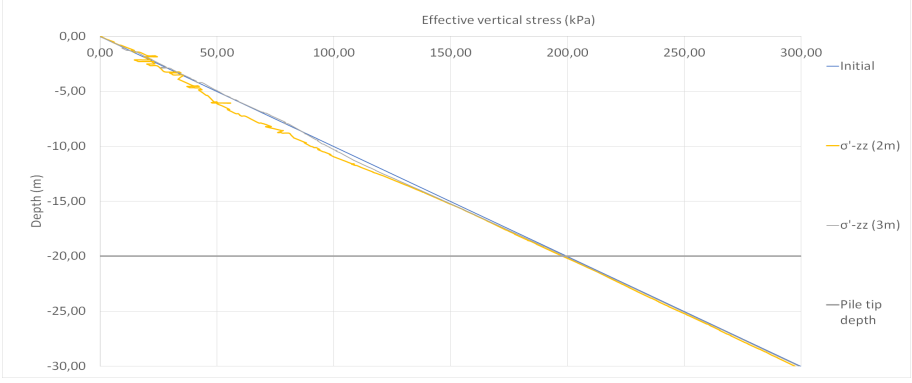

Figure 5.9: Graph showing the effective vertical stress versus depth for a borehole with a diameter of 0.3m and an excess loss of soil volume between 0 - 10 meter depth with varying distances from borehole center

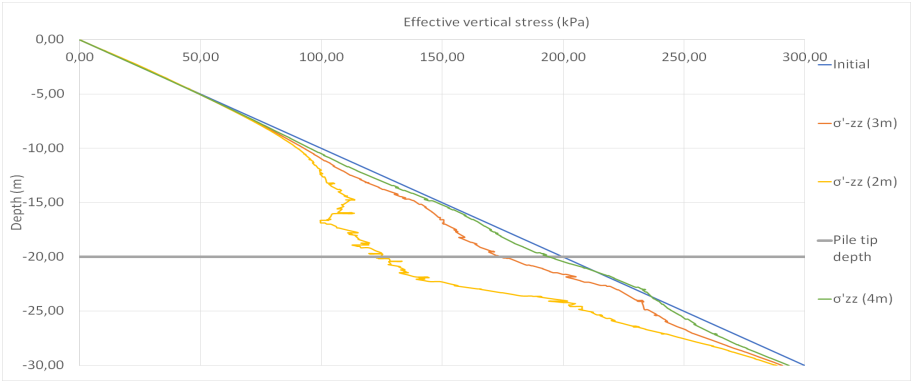

Figure 5.10: Graph showing the effective vertical stress versus depth for a borehole with a diameter of 0.3m and an excess loss of soil volume between 15-20 meter depth with varying distances from borehole center

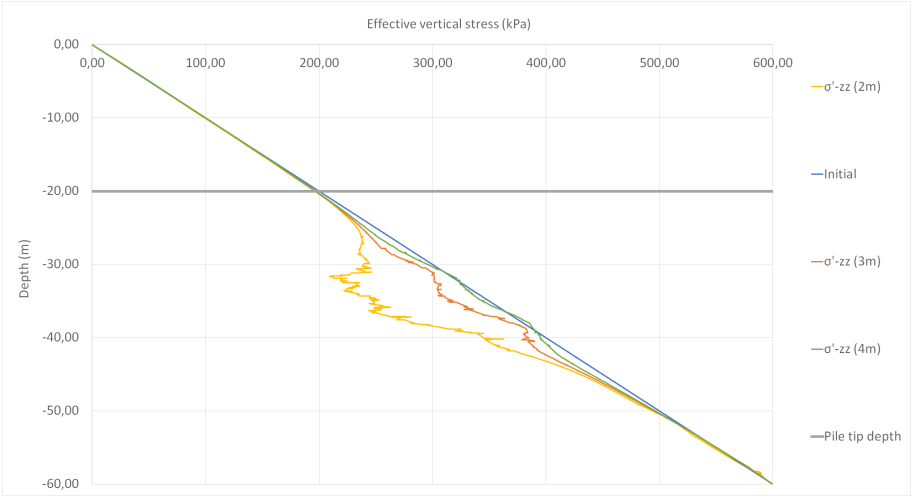

Figure 5.11: Graph showing the effective vertical stress versus depth for a borehole with a diameter of 0.3m and an excess loss of soil volume between 30-40 meter depth with varying distances from borehole center

For 0.3m diameter boreholes, the zone of influence due to the drilling complication is 4 meters from the borehole center. For locations closer to the borehole center (2 meters distance), the vertical effective stress will experience the highest stress relief at the pile tip for drilling complications occurring between 15-25m. For deeper or more shallow drilling complications, the stress relief at the pile tip is negligible.

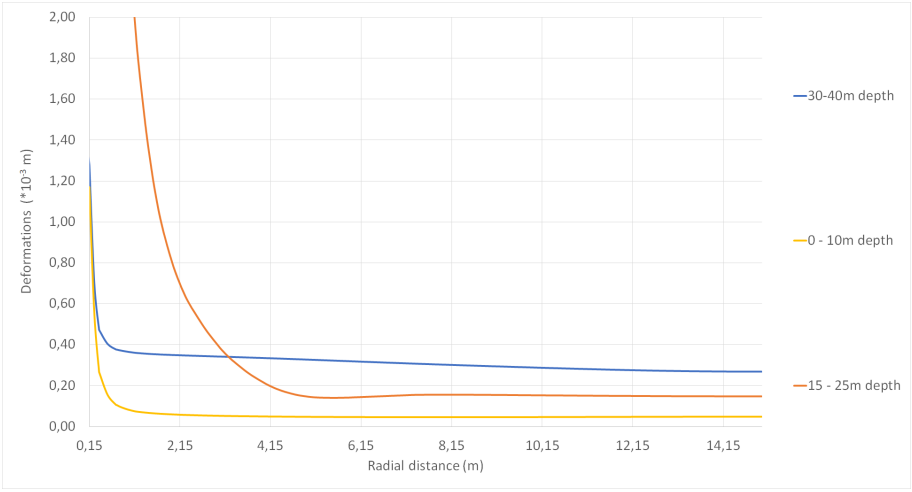

Figure 5.12: Graph showing the total deformations |u| versus the radial distance from the borehole center at the pile tip depth of 20m for drilling complications occurring at different depths. For a borehole with a 0.3m diameter.

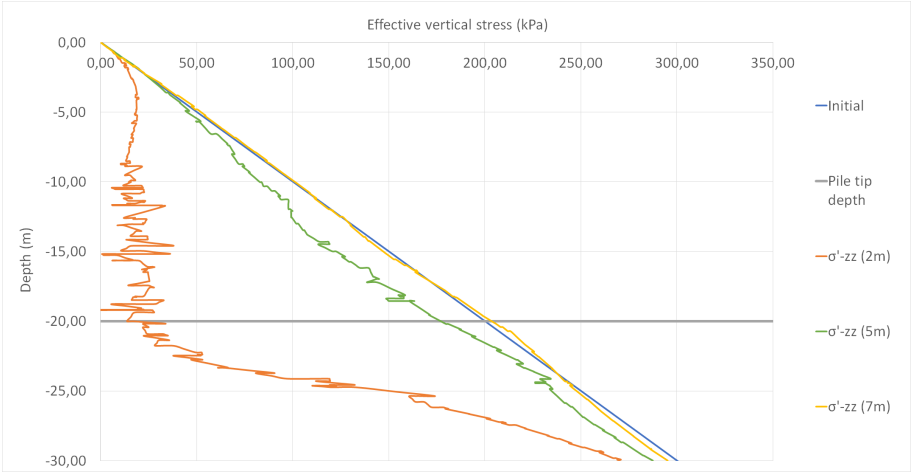

Figure 5.13: Graph showing the effective vertical stress versus depth for a borehole with a diameter of 0.8m and an excess loss of soil volume between 15-25 meter depth with varying distances from borehole center

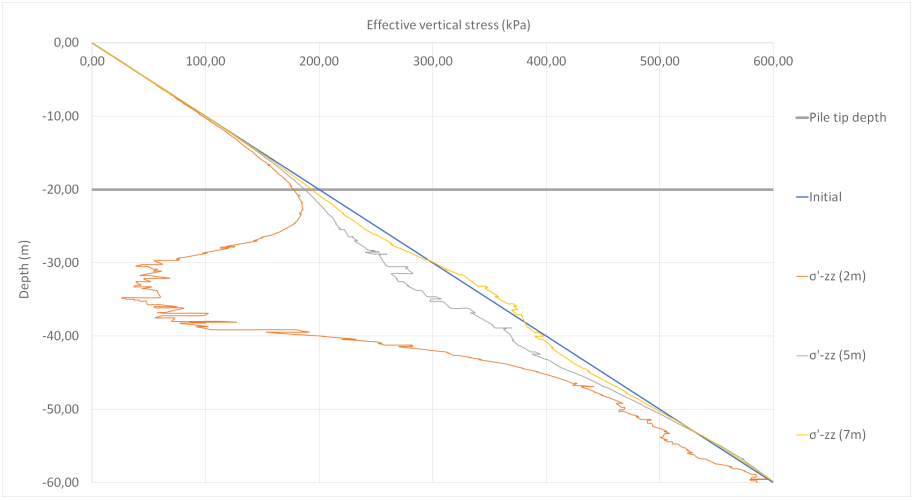

Figure 5.14: Graph showing the effective vertical stress versus depth for a borehole with a diameter of 0.8m and an excess loss of soil volume between 30-40 meter depth with varying distances from borehole center

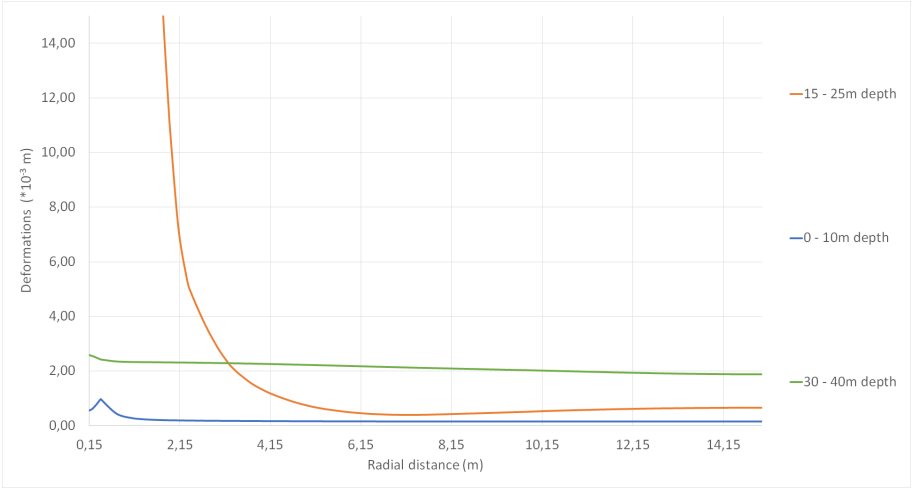

Figure 5.15: Graph showing the total deformations |u| versus the radial distance from the borehole center at the pile tip depth of 20m for drilling complications occurring at different depths. With a borehole with a 0.8m diameter.

For larger borehole diameter, with more excess soil volume loss, the stress redistribution is more serious. The zone of influence is more or less 7 meters away from the borehole center. The stress relief is very high at a distance of 2m away form the borehole center. At this distance, the stress relief at the pile tip is extremely high for the drilling complication occurring between -15m and -25m and is negligible when occurring between -30 and -40m.

It is noticeable that for a horizontal stress redistribution happening more than 2m away from the borehole center, a relief of radial stress is compensated by an increase in hoop stress. This means that it will not effect the shaft resistance of the pile and thus bearing capacity in this region depends only on vertical effective stresses.

For drilling complications occurring at a depth of 30-40m, the deformations at the depth of the pile tip (-20m) are highest and have an almost constant value of 0.02m. For the drilling complications occur at more shallow depths, these deformations are less than 0.01m.

5.4. Summary

The drilling fluid pressure in the borehole during drilling has significant influence on the stress state around the boreholes. A required drilling fluid pressure can be calculated from soil dependent in-situ horizontal stresses. For the soil used in this research, an increment of $-14.5kPa/m$ was required to minimize the zone of influence around the borehole. The lower-limit is the minimum drilling fluid pressure necessary to keep the borehole stable during drilling. The pressure increments need to be raised with $0.08kPa/m$ for an increase in diameter from 0.3m to 1.0m. These might be caused by mesh dependency as magnitudes are very small. All drilling processes executed in this research are performed at a drilling fluid pressure increment $0.5kPa/m$ higher than their lower-limit in order to be conservative.

As soil and drilling fluid pressure is kept constant, stress states around different borehole diameter can be analyzed. The stress states around the boreholes with varying diameters are almost identical except for the zone of influence and deformations. The peak of the hoop stress points out the elastic-plastic boundary and lies at $130kPa$ for all borehole diameters. The deformations increase in the plastic zone and are negligible outside the plastic zone. A zone of influence is found for the vertical and horizontal stress and is given in table 5.2.

Stress states in between two boreholes will not interfere with each other when the spacing is $> 4m$. In the middle of four boreholes, the spacing between the middle and all boreholes need to be $> 2m$.

Drilling complications occurring will initiate extreme stress reliefs close to the borehole. For drilling complications occurring at shallow depths ($< 15m$), these stress reliefs are small. For drilling complications occurring deeper ($> 15m$), the stress reliefs are extremely high close to the borehole. The zone of influence for an 22% excess soil volume loss can reach up to 4m for 0.3m diameter boreholes and up to 7m for 0.8m diameter boreholes. At a depth of the pile tip (20m), the far-field deformations are highest for drilling complications at a large depth. For a pile located $< 4m$ away from the borehole, a drilling complication occurring between 15-25m depth has highest deformations.

6

Impact of installing UTES boreholes on bearing capacity of piles

In the previous chapter, the influence of installing UTES boreholes on the stress conditions was investigated. In this chapter, calculations are performed concerning the influence of the stress states on the bearing capacity of piles. Due to the complexity of the bearing capacity of piles, this is done by means of pile load test simulations. The results of these pile load tests are provided as load-displacement curves. First, the bearing capacity of the pile in a soil with no boreholes is determined by means of an analytical solution and a pile load test simulation in 2D and 3D models. After this, the effect of spacing between pile and borehole on the bearing capacity is analyzed for perfectly drilled boreholes and a borehole with a drilling complication. Finally, the effect of: 1) using driven (displacement) piles instead of wished-in-place (non-displacement) piles and 2) varying installation phasing on bearing capacity is investigated.

6.1. Bearing capacity of a pile in unaffected soil

In order to compare the change in bearing capacity due to change in in-situ stress states, an initial value of the bearing capacity is obtained. This initial value is the bearing capacity of a single pile with a specified depth and dimension in unaffected soil. All parameters rely on those of the HS-model as given in chapter 3.4.3. At first, a first-order estimate was made by performing an analytical calculation. After this, the initial bearing capacity is determined by means of simulating a static pile load test in an axisymmetric 2D model and a plane strain 3D model. In addition, different meshes were checked on accuracy for further research.

Analytical solution

For the analytical solution, the method of Véric is used for the tip resistance, as given in appendix A. The formula (2.5) is used for this analytical approach with the input parameter values given in table 6.1. These input parameters are obtained from the HSs-model given in table 3.4. The shaft resistance was obtained by using formula (2.8).

Parameter	Value	Unit
ϕ	33	$degrees$
K_0	0.4554	-
N_q	14	-
q	200	kN/m^2
L	20	m
B	0.4	m

Table 6.1: Input parameters for the analytical calculation of the bearing capacity of a pile with a depth of -20m and a width of 0.5m

This analytical solution gives a tip resistance of $1588kN$ and a total shaft resistance of $2261kN$. The analytical solution gives a total bearing capacity of $3849kN$.

2D and 3D model

A 2D-axisymmetric model was built, as explained in chapter 3.4.3, to obtain quick and coherent results and perform a mesh sensitivity analysis. This analysis was performed for different mesh types, which are given in appendix F. The same static pile load test with equal input parameters was performed for these different mesh types and the result is given in fig. 6.2. In order to check which of the load-displacement curves are the most realistic, the failure pattern was studied for every mesh. The failure pattern was expressed best around the pile tip of the finest mesh and is given in fig. 6.1.

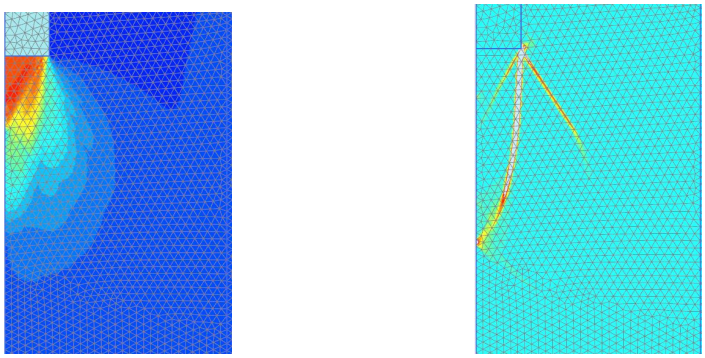

Figure 6.1: Mobilized shear strains (left) and incremental shear strains (right) at pile tip of finest mesh model

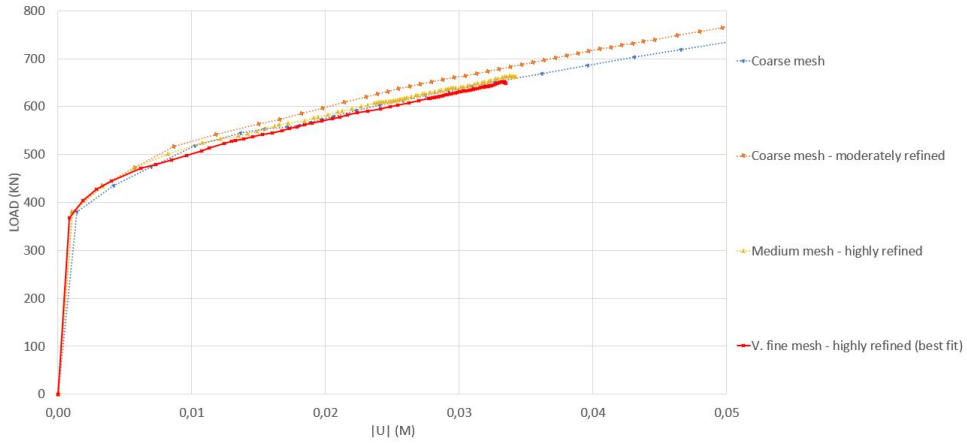

Figure 6.2: The 2D-axisymmetric load-displacement curves for different types of meshes

For further calculations with static pile load tests including boreholes, the model was extended to 3D. In order to obtain the exact same load-displacement curves as in the 2D-axisymmetric model, very-fine locally refined meshes were required. This 3D very-fine mesh type had very high computation times (> 16 hours). For time efficiency, a coarser mesh was tested and compared with the 2D-axisymmetric model. As given in fig. 6.3, the results of this coarser mesh have an acceptable deviation from the 2D results with a value less than 10%. This is an acceptable deviation and thus this coarser mesh will be used for further calculations in 3D models.

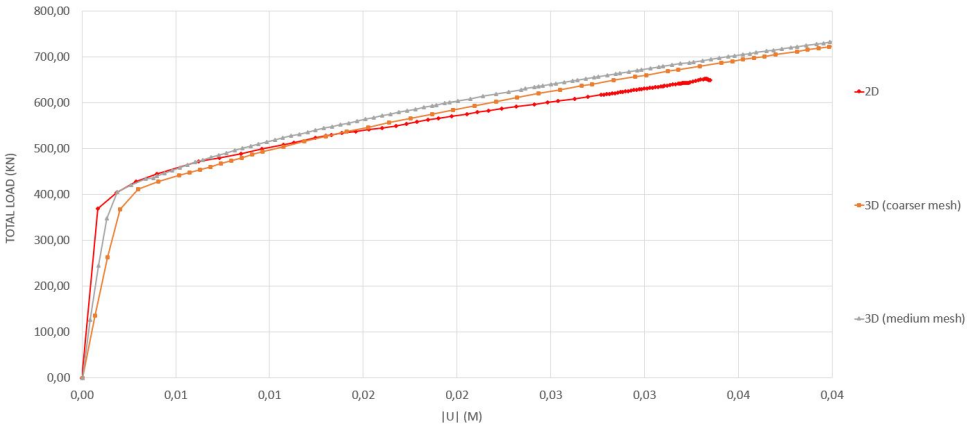

Figure 6.3: Comparison between the 2D and 3D load-displacement curves

As can be seen from the load-displacement curve in fig. 6.3, the 2D model gives a bearing capacity of $630kN$ while the 3D model with a coarse mesh gives a bearing capacity of $660kN$. Every different type of calculation in this chapter has its an identical mesh. For this reason, the initial bearing capacity is calculated separately for every calculation type to raise accuracy in comparisons. As a reference, the 3D load-displacement curve as given in fig. 6.3 is illustrated as *Reference curve* for all given results.

The difference between the analytical and numerical models can be explained by the type of installation for the numerical model. The results given in fig. 6.3 give the bearing capacity of a wished-in-place pile, while the analytical model takes into account a different type of pile installation.

6.2. Bearing capacity of a pile near a single borehole

In this section the influence of a perfectly drilled borehole on the bearing capacity of a pile is investigated. This is done by performing the same static pile load tests at two different distances from the borehole center. These distances are based on the elastic and plastic zones from the stress states given in chapter 5.2.

For the 0.3m diameter closed borehole, location A is at the elastic-plastic boundary and location B is in the middle of the non-linear elastic region. These pile locations were: 0.6m (location A) and 1.0m (location B) away from the borehole center. The effective stress difference ($\Delta\sigma_{xx,yy,zz}$) from the initial values, due to the borehole drilling process, are given in fig. 6.4 and fig. 6.5.

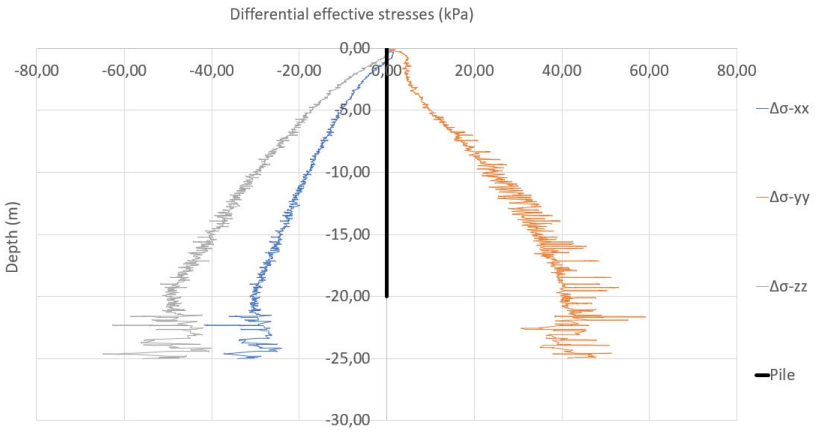

Figure 6.4: Changes of in-situ stresses from initial values at location A (0.6m) due to borehole drilling of a 0.3m diameter borehole

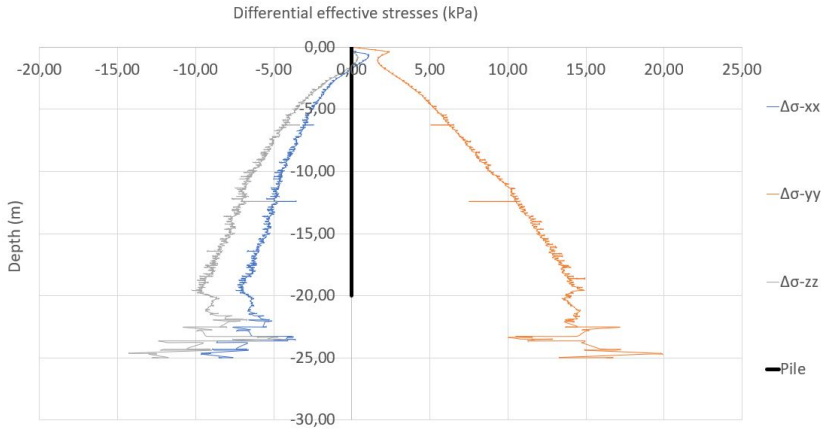

Figure 6.5: Changes of in-situ stresses from initial values at location B (1.0m) due to borehole drilling of a 0.3m diameter borehole

In order to investigate what influence these stress differences given in fig. 6.4 and fig. 6.5 have on the bearing capacity of piles, the load-displacement curves are compared and given in fig. 6.6.

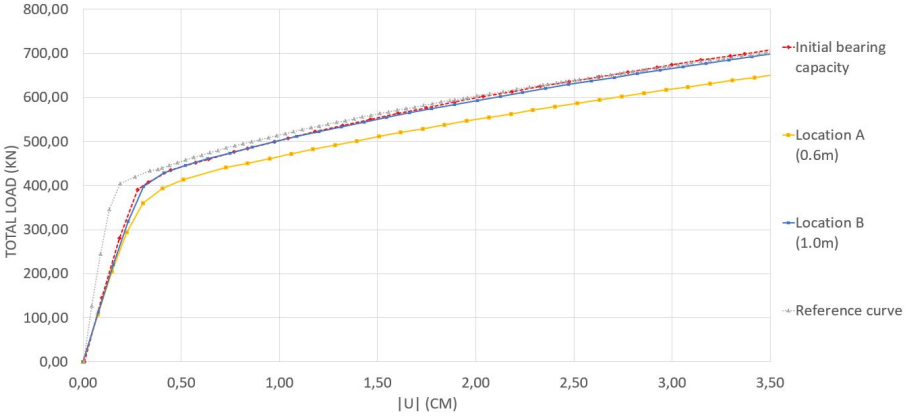

Figure 6.6: Load-displacement curve of a pile located at location A and B near a single 0.3m diameter borehole

The load-displacement curves show that the bearing capacity at location A will decrease with 52 kN (= 7 percent of initial). At location B this decrease is only 7 kN, which is a negligible amount. The part with high increments of load for displacements are due to the mobilized shaft resistance of the pile. It can be seen that the shaft resistance of the pile at location A is mobilized completely at a lower load. Next to this, the loss of bearing capacity increases with higher loads and displacements for the pile at location A.

6.3. Influence of drilling complications on bearing capacity

Next to a perfect drilling process, which is assumed for the results given in chapter 6.2, drilling complications might occur. These drilling complications are simulated for two scenario's as explained in chapter 3.3.3.

For the 0.3m diameter borehole, location A and location B are located 1.0m and 2.0m away from the borehole center. The effective stress differences ($\Delta\sigma_{xx,yy,zz}$) from the initial values, due to the drilling complication, are given in fig. 6.7 and fig. 6.8.

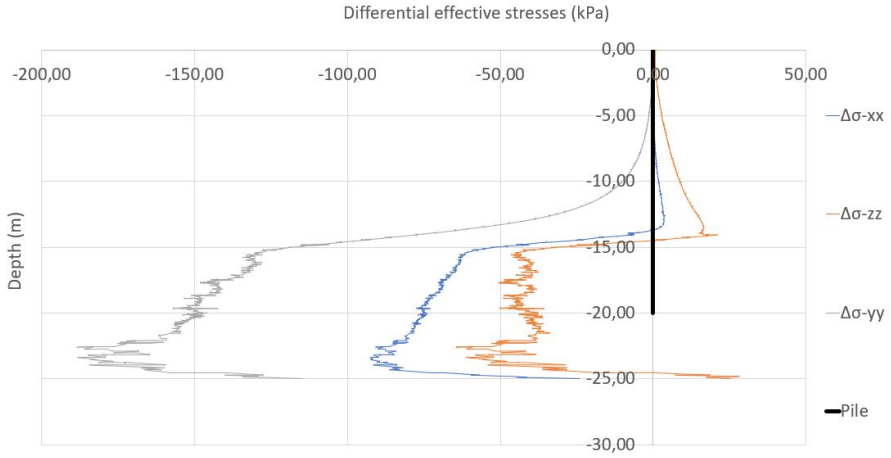

Figure 6.7: Changes of in-situ stresses from initial values at location A (1.0m) due to borehole drilling of a 0.3m diameter borehole

A significant stress change has occurred due to the drilling complication, as illustrated in fig. 6.7. The small spacing between the pile and the borehole has caused a significant decrease in stresses for all three principal stress directions. A substantial vertical effective stress decrease has occurred at the pile tip of $-150kPa$.

A larger spacing between the pile and the borehole is illustrated in fig. 6.8. For this spacing, the radial stress decreases while the hoop stress increases, but with a different magnitude. The vertical stress still decrease, but with significantly lower magnitudes, which has a maximum of $-55kPa$ at the pile tip.

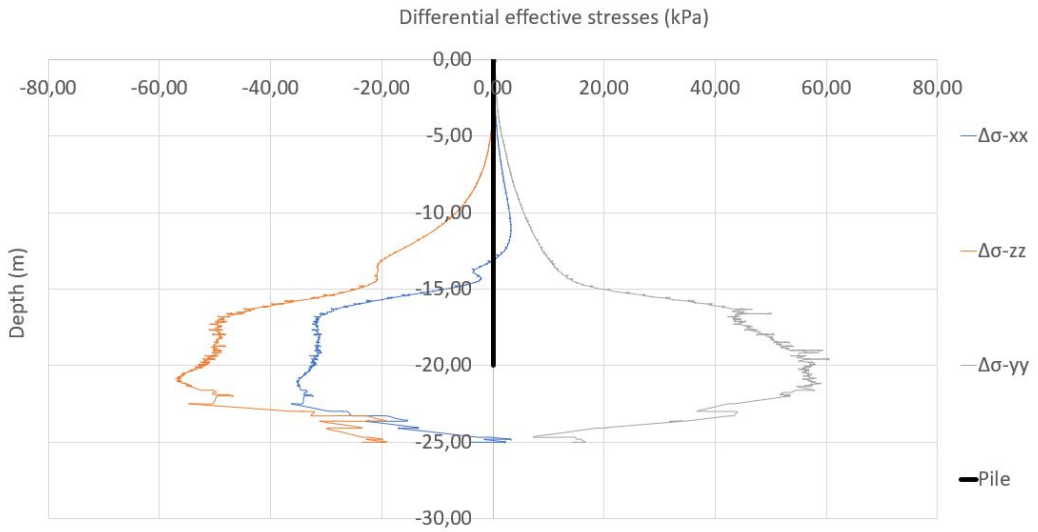

Figure 6.8: Changes of in-situ stresses from initial values at location B (2.0m) due to borehole drilling of a 0.3m diameter borehole

In order to investigate what influence these stress differences given in fig. 6.7 and fig. 6.8 have on the bearing capacity of piles, the load-displacement curves are compared and given in fig. 6.9.

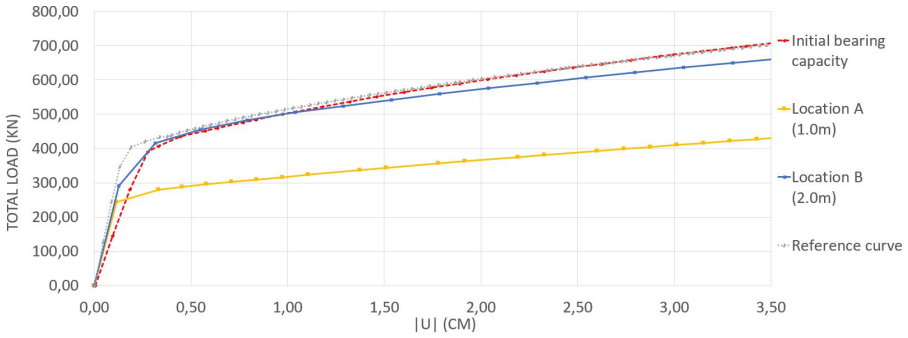

Figure 6.9: Load-displacement curve of the pile for drilling complications between -15m and -25m for 0.3m diameter borehole

For a relatively large spacing (location B) the stress changes of the hoop and radial stresses are opposite and will compensate each other, the bearing capacity is mainly determined by the decrease in the effective vertical stress at the pile tip. A decrease of $50kPa$ in effective vertical stress will cause a decrease of only $35kN$ in bearing capacity.
A small spacing for location A in the plastic zone, will cause all stresses around the pile tip to

decrease, which has a more harmful effect on the bearing capacity. No compensation of the radial stress decrease by the increase in hoop stress occurs. Next to this, the magnitudes of stress decrease are significantly higher. An effective vertical stress decrease of $-150kPa$ will now cause a decrease of $265kN$.

For the 0.8m diameter borehole, location A and location B are located 1.0m and 4.0m away from the borehole center. The effective stress differences ($\Delta\sigma_{xx,yy,zz}$) from the initial values, due to the drilling complication, are given in fig. 6.10 and fig. 6.11.

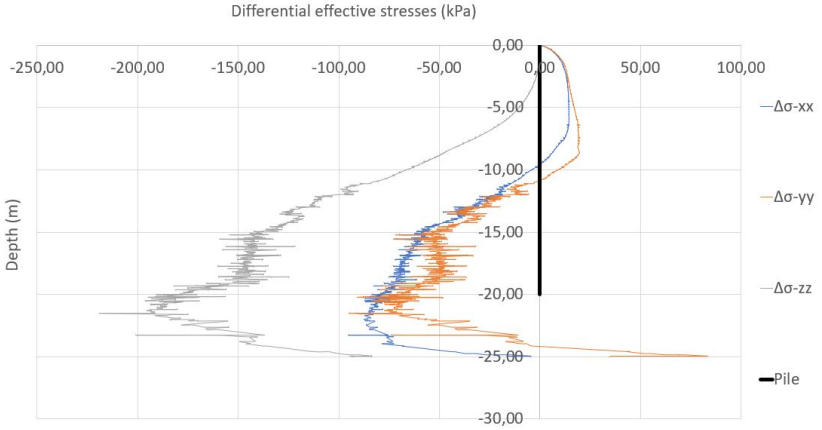

Figure 6.10: Changes of in-situ stresses from initial values at location A (1.0m) due to borehole drilling of a 0.8m diameter borehole

Similar to the 0.3m diameter borehole, a small spacing of only 1.0m will cause extremely high stress decrease, even for the hoop stresses which normally increase. In order to obtain equal stress redistribution to fig. 6.11, the spacing between borehole and pile has to be 2.0m more for 0.8m diameter borehole.

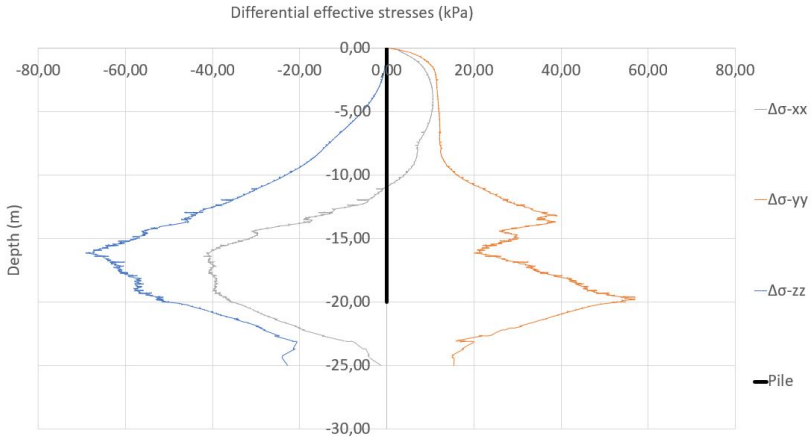

Figure 6.11: Changes of in-situ stresses from initial values at location B (4.0m) due to borehole drilling of a 0.8m diameter borehole

In order to investigate what influence these stress differences given in fig. 6.10 and fig. 6.11 have on the bearing capacity of piles, the load-displacement curves are compared and given in fig. 6.12.

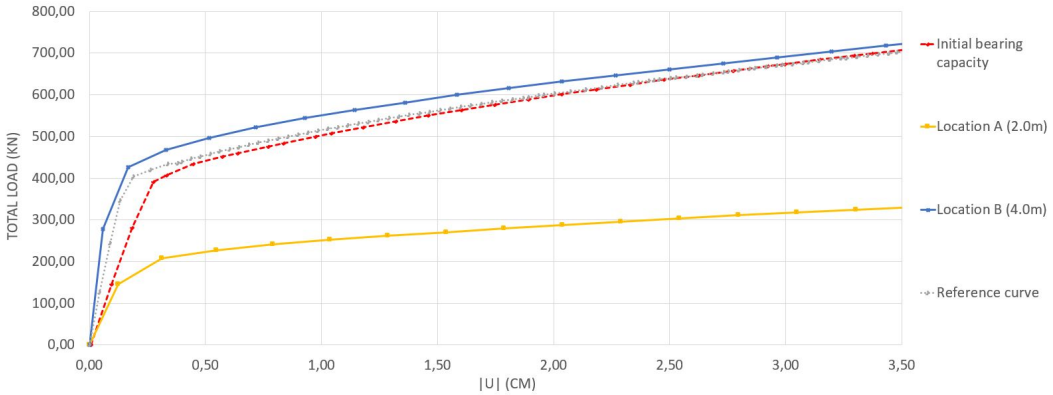

Figure 6.12: Load-displacement curve of the pile for drilling complications between -15m and -25m for 0.8m diameter borehole

Again the small spacing causes a serious decrease in effective vertical stress which decreases the tip resistance of the pile. Next to this, the decrease in radial stress is not compensated for by an increase in hoop stress, which was is seen in fig. 6.11. This causes less mobilized shaft resistance. A combination of the decreases in resistances will cause a total decrease in bearing capacity of $355kN$.

For a distance of 4m between the pile and borehole center, an effective stress decrease of $-50kPa$ causes no change in bearing capacity and thus will contain its initial bearing capacity magnitude. However, the mobilization of the shaft resistance differs from all other curves, which can be explained by the deviating hoop stress around the pile.

6.4. Bearing capacity of a displacement pile near a single borehole with a drilling complication

The type of installation in previous results have been a non-displacing way (wished-in-place). The displacement piles are simulated by means of the method explained in chapter 3.4.3. In this section, the stress changes around and underneath the pile due to the installation process will be visualized first, as given in fig. 6.13. Hereafter different scenario's are considered for the analysis, as described in chapter 3.3.3. These scenarios consider the effects of installing a displacement pile for several types of phasing.

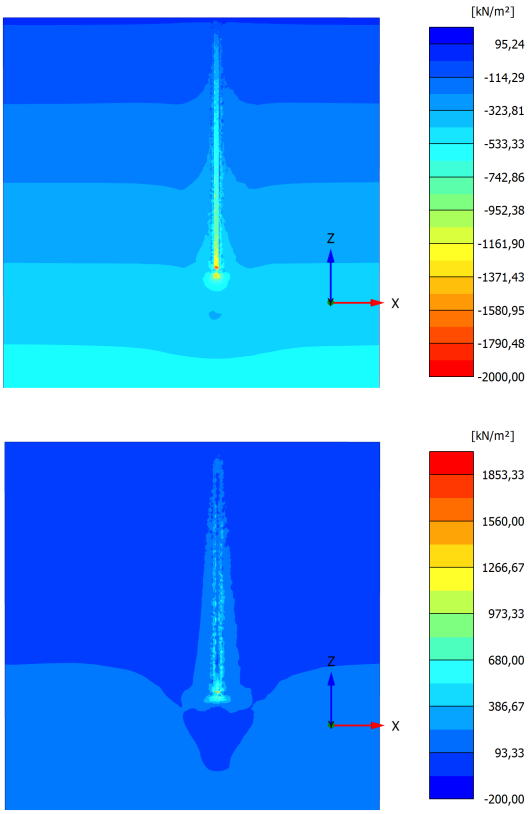

Figure 6.13: Upper: total mean stress (p). Lower: deviatoric stress (q)

Boreholes with drilling complications result in very high stress releases, as was seen in fig. 6.10. In the following results, the effect of phasing and use of displacement piles is investigated as explained in chapter 3.3.3. Situation A and B are contained in load-displacement curves given in fig. 6.14.

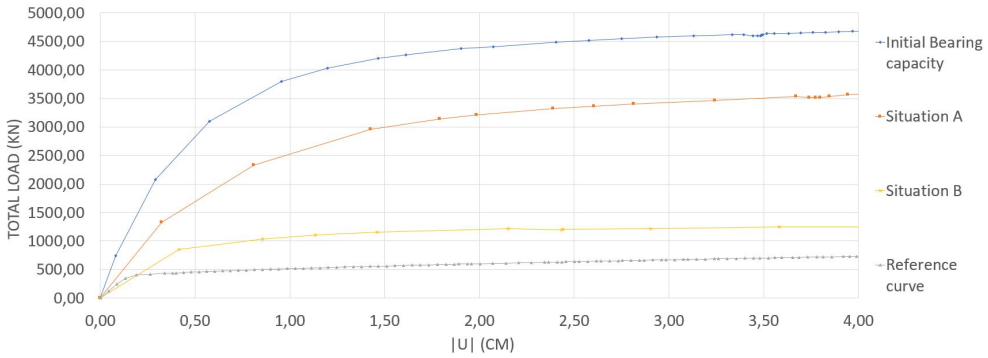

Figure 6.14: Load-displacement curve of a displacement pile in situations A and B

It can be seen that the initial bearing capacity of a displacement pile is significantly higher than for a non-displacement pile with a bearing capacity of $4600kN$ and $660kN$ respectively.

It is clear that the phasing in situation B is the most harmful for the bearing capacity of a displacement pile. The displacement pile in situation B experiences bearing capacity loss of $3360kN$. For a situation A, which has the same phasing as for the results in chapter 6.4. The bearing capacity for a displacement pile in situation A experiences a loss of $1140kN$, which is 25% of the initial bearing capacity. In comparison the bearing capacity losses for non-displacement piles, displacement piles are more sensible to changes in stress states.

Next to situation A and B, static pile load tests were performed for displacement piles in situations C1 and C2. During the realisation of phasing C in scenario's with drilling complications no calculation maintained stable during loading. Soil collapse or severe divergence of the pile occurred. This means that situation C is the most sensitive for stress changes when compared with situation A and B.

The load-displacement curves for situations C1 and C2 are given in fig. 6.15.

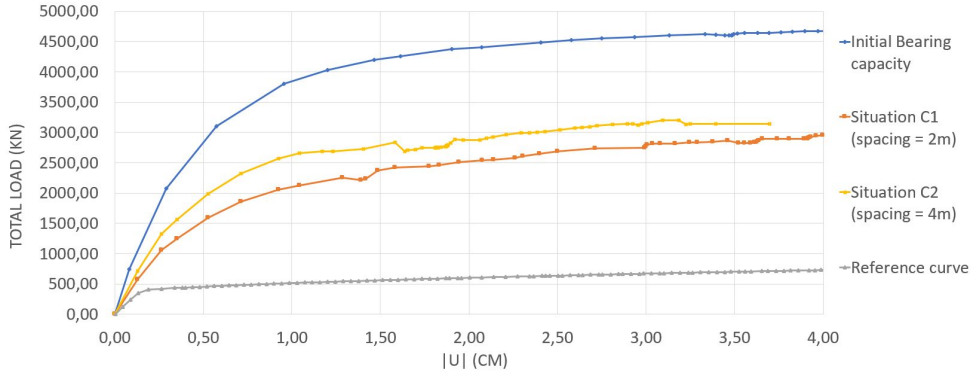

Figure 6.15: Load-displacement curve of a displacement pile in situations C1 and C2

It can be seen that even when placing the pile at a distance of 4m away (situation C2) from the borehole with no drilling complication, there is still serious loss of bearing capacity. This means that the spacing between an existing building founded on driven piles and a 0.8m diameter borehole has to be significantly larger than 4m.

6

6.5. Bearing capacity of a pile in a soft soil layer

Foundation piles in practice are used to built on soft soils, with the pile tip situated in stiff sand layers. This is why a situation is considered as described in chapter 3.3.3, with a soft soil (clay) layer from 0 to -15m depth.

The effective stress differences ($\Delta\sigma_{xx,yy,zz}$) from the initial values, due to the drilling process in this soft soil situation, are given in fig. 6.16.

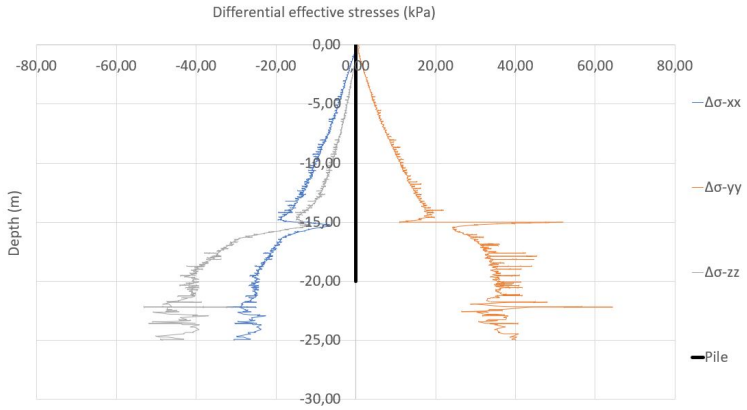

Figure 6.16: Changes of in-situ stresses from initial values in soft soil due to borehole drilling of a 0.3m diameter borehole

The stress changes due to the drilling of the borehole through soft soil differs from the situation with only sand, as given in fig. 6.4. The magnitudes of stress changes are smaller in the clay layer, when compared to sand. A clear boundary can be recognized at -15m depth, in which clay turns into sand. The configuration of stress redistribution, on the other hand, does not differ from the stress redistribution in sand. Around the tip situated in the sand layer, the stress redistribution and magnitudes are equal to that in fig. 6.4.

In order to investigate what influence the stress redistribution in the clay layer has on the bearing capacity of the pile, the load-displacement curves are given in fig. 6.17.

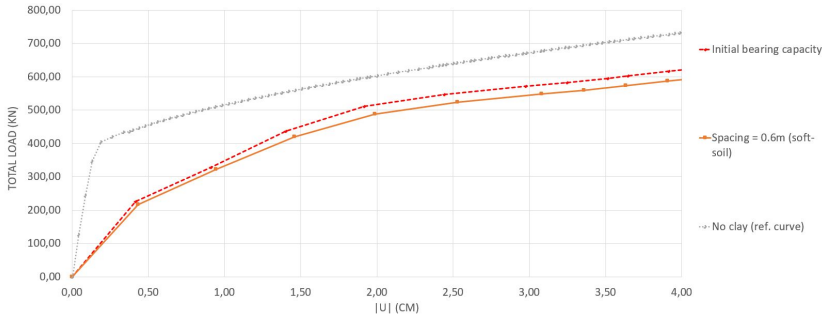

Figure 6.17: Load-displacement curve of a pile in a soft soil situation for a 0.3m diameter borehole

The load-displacement curve differs a lot from the reference curve which is caused by another way of mobilizing shaft resistance. Different magnitudes of in-situ effective stresses in the clay layer cause lower bearing capacity than for a pile in only sand. When compared to the initial bearing capacity, the difference is almost negligible. As can be seen in fig. 6.16, the stress differences due to the drilling process are very small in the clay layer, with magnitudes around $15kPa$. This will cause a negligible decrease in the shaft resistance.
The decrease in bearing capacity for the soft soil situation is $47kN$, while for the situation with only sand it is $41kN$. This means that adding a soft soil layer will not influence the decrease in bearing capacity due to the drilling process.

6.6. Summary

For boreholes which are perfectly drilled, the stress redistribution magnitudes around the boreholes are small, with a small zone of influence. For this case, piles need to be placed very close to a borehole (0.6-1.0m) in order to be located in this zone of influence. For a pile located at the elastic-plastic boundary or somewhere in the non-linear elastic zone, the decrease in radial stress is compensated by an increase in hoop stress. This compensation of horizontal stresses leads to an unaltered shaft resistance. The effective vertical stress, however, decreases with only $50kPa$ which will cause the bearing capacity to decrease by only $35kN$. So, for non-displacement piles located outside the plastic zone, the loss of bearing capacity has negligible values.

When drilling complications occur between -15m and -25m, the magnitude of stress redistribution increases. The extend of the zone of influence, due to the drilling complication, will increase with increasing borehole diameter. The extend reaching a distance of 2.0m for a 0.3m diameter borehole and 4.0m for a 0.8m diameter borehole. For piles located at these distances from the borehole, the bearing capacity maintains its initial value.
For piles located within the plastic zone, both radial and hoop stresses decrease with the same magnitude. The vertical stress decreases with an even higher magnitude. This decrease in effective vertical stress reaches a magnitude of $150kPa$ for a 0.3m diameter and up to $200kPa$ for a 0.8m diameter. The sum of both horizontal and vertical stress decrease causes a decrease in shaft resistance and a significant decrease in tip resistance. For a borehole to pile spacing of 1.0m, this entails a decrease in bearing capacity of $265kN$ and $357kN$ for 0.3m and 0.8m diameter boreholes respectively.

The change from a wished-in-place (non-displacement) pile to a driven (displacement) pile will increase the bearing capacity significantly, with a magnitude of more than $3940kN$. For the exact same simulation, the percentage of bearing capacity loss was higher for the displacement pile than for the non-displacement pile. This means that displacement piles are more susceptible for in-situ stress changes due to drilling processes. Furthermore, situation B is more harmful for the bearing capacity than situation A. This means that installing a displacement pile before drilling the borehole is the safest installation phasing.
Next to phasing A and B, phasing C was investigated. Two situations (C1 and C2) were considered, differing in borehole-pile spacing. In general, phasing C is more susceptible for borehole drilling processes than phasing A and B. Next to this, a large borehole-pile spacing (significantly more than 4m) is necessary for the pile to obtain its initial bearing capacity.

The drilling process of a borehole through a soft soil layer will cause a smaller magnitude of stress redistribution than in sand. For the exact same spacing, installation type and phasing the bearing capacity for this situation and the situation with only sand is equal. This means that adding a soft soil layer will not influence the effect of the borehole drilling process on the bearing capacity. The loss of $47kN$ in bearing capacity is due to the stress redistribution in the sand layer rather than in the clay layer.

7

Case study: Lisse ATES project

7.1. Introduction

In this chapter, a real-life case study in investigated in order to validate the model results given in previous chapters. The case study is from a project in Lisse, which is a village in the Netherlands close to Amsterdam and Haarlem. This means that it is located in a typical Dutch polder with an interesting soil stratigraphy. The case consists out of a mono-well ATES (open) system which is to be installed close to foundation piles. This case is considered relevant and interesting due to the following aspects:

- The well is drilled at a distance of 3.5m from the closest foundation pile to the borehole wall, which is a very close spacing.
- The well is drilled with plain groundwater, with no additives (e.g. bentonites) that might increase borehole stability.
- CPT-data is available before and after the drilling process of the well.
- Displacement piles are to be installed after the installation of the ATES well.

The aim of this case study is to investigate the influence of the drilling of this well on the stress state of the surrounding soil and the bearing capacity of the surrounding piles. In addition, an advice is given on: 1) the potential hazards and where these are most likely to occur and 2) how to prevent these hazards from occurring.

7.2. Method

As stated above, there are numerous reasons to closely investigate the case study. In order to start investigating, an overview must be provided on the setting of the case.

A mono-well is installed with a diameter and drilling bit of 0.8m, this means that the borehole diameter will most likely be higher, but not much if drilling is performed correctly. For the calculations, the borehole diameter is assumed to be 0.8m over its complete length because earlier results have already been given on boreholes with an equal diameter.

Three displacements piles are to be installed by means of the driving method. These piles are squares with dimensions of $400mm \times 400mm$ and a depth of 20m. As square piles produce simulation problems due to the inability to include interface, the piles are assumed to be circular piles. It is not expected that this assumption influences any of the advice and allows for an easy model building process in PLAXIS. A complete overview of the situation is given in fig. 7.1 with the center-to-center spacing between closest pile and borehole included.

The soil stratigraphy at Lisse is simple, with a series of sand, peat and clays, which is typical for Dutch soils. The pile are driven to a depth of 20m, where the second sand layer is present. As was seen in the results from chapter 6.5, the stress changes due to borehole drilling in the bearing sand layer are not influenced by the introduction of a clay layer on top of the sand layer. For this case, the interest lays in the bearing capacity of the sand and that is why the complete soil stratigraphy is modelled as sand with equal input parameters as given in table 3.4.

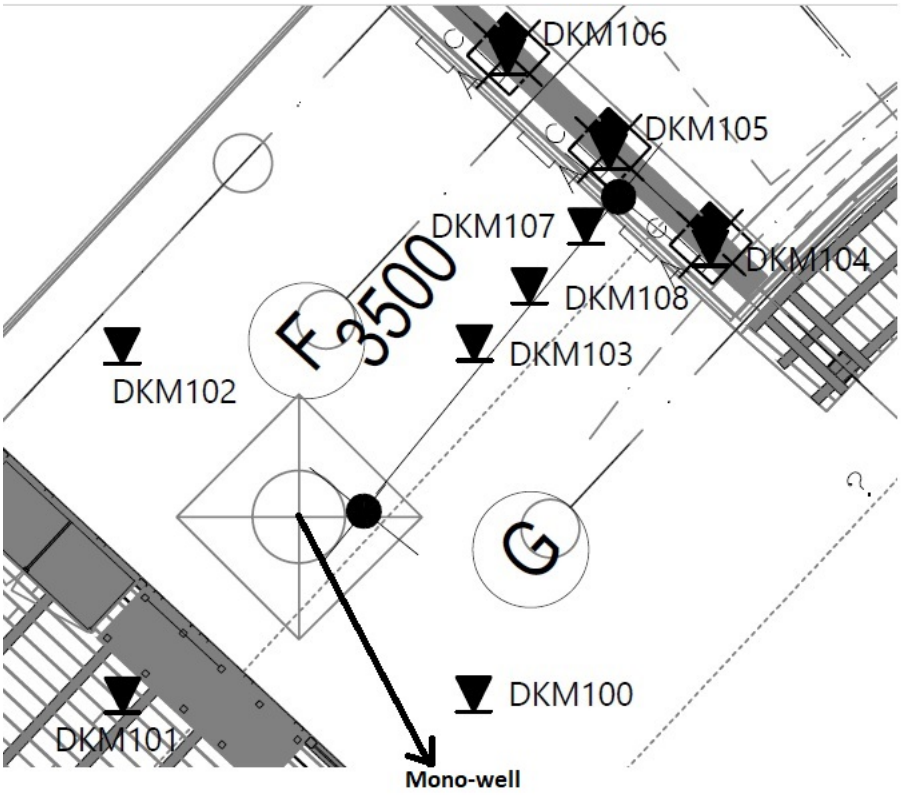

Figure 7.1: Schematic overview of the situation in Lisse with the location of the mono-well, piles and taken CPT's (Hogervorst and Hoefsloot, 2020)

7.3. Results

Zone of influence of perfect drilling process

For the 0.8m borehole, the stress-states in the surrounding soil after drilling are provided in fig. 7.2. As the distance between the pile and borehole is known, an advice can be given.

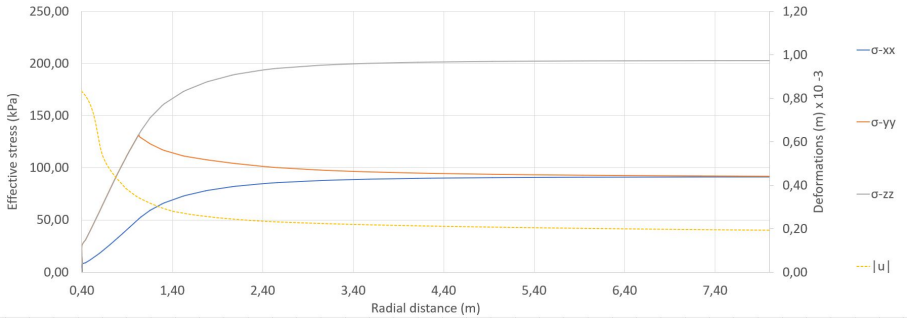

Figure 7.2: The effective stress state for a borehole with a diameter of 0.8m at a depth of 20m with total deformations |u| versus the radial distance from the borehole center

This analysis is for a perfect drilling process, in which no complications have occurred. When looking at these results, the pile distance of 3.9m from the center of the borehole, is outside the zone of influence. This means that the bearing capacity of the pile is not affected by the installation of the mono-well. The pile will maintain its initial bearing capacity. In order to conclude this, the degree of perfection of the drilling process must be known. There is no information provided by the drilling master that there were any visible drilling complications or borehole collapses. This lack of information means that there is no guarantee that there were no drilling complications and thus more investigation on this is required.

CPT data

In order to investigate possible drilling complications around the borehole, CPT data is used for an first estimate. This is because the in-situ stress state can be linked directly to cone resistance. An in-situ stress decrease will influence the experienced cone resistance and its pathway to the required depth. The CPT's have been taken before and after the drilling process of the well. There are two interesting CPT's taken after the drilling process that show deviations from the CPT-data taken before the drilling process. These deviations have occurred over the length of the sand layer (-18 to -25m) in which the piles are to be installed. The deviations were found in DKM-103 and DKM-108. The locations with respect to the well and pile can be found in fig. 7.1 and are 1.8m and 2.25m from the well for DKM103 and DKM108 respectively.

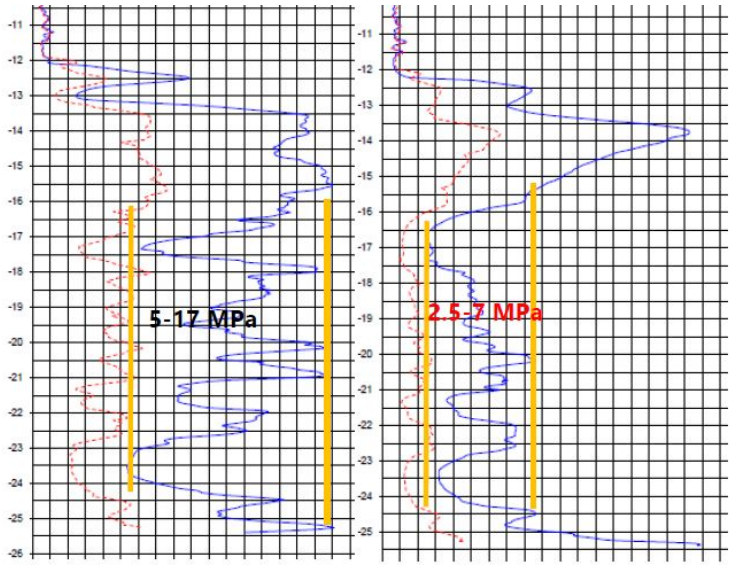

Figure 7.3: Cone resistance of DKM108 (right) compared with cone resistance of DKM107 (left)

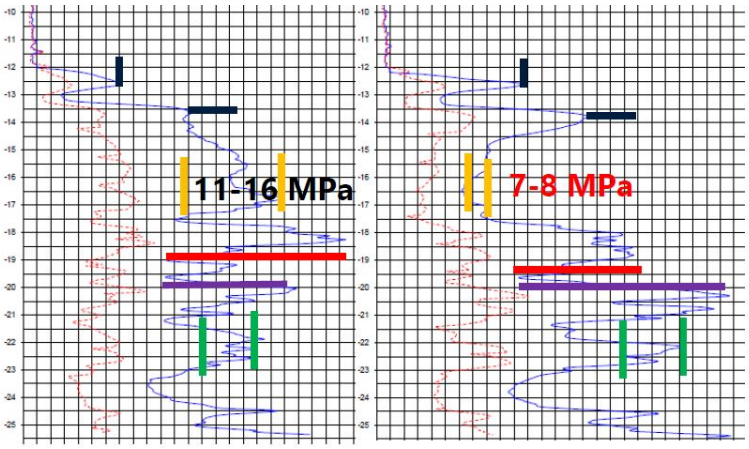

Figure 7.4: Cone resistance of DKM103 (right) compared with cone resistance of DKM102 (left) (Hogervorst and Hoefsloot, 2020)

As can be seen in fig. 7.3 and fig. 7.4, a bisection of the cone resistance has occurred over the length of the sand layer. The CPT data from DKM103 and 108 are compared with corresponding CPT data in order to visualize the lost cone resistances.

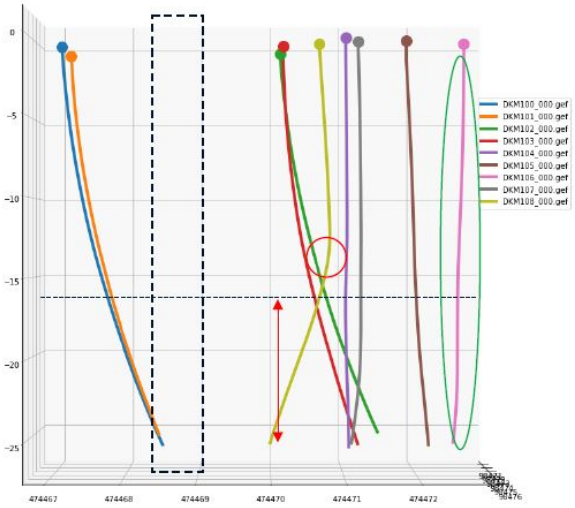

Figure 7.5: Skew angles of the CPT's seen from west (left) to east (right) (Hogervorst and Hoefsloot, 2020)

Next to a decrease in cone resistance, there is another way of determining changes in-situ stress states from CPT's. This is done by looking at the relative skew angles of the driven pathways to a certain depth, as given in fig. 7.5 and fig. 7.6.

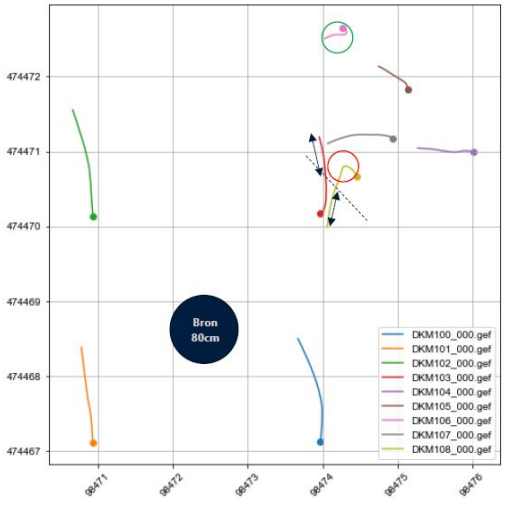

Figure 7.6: Skew angles of the CPT's upper view

It is clear that all CPT's have a skew angle in their pathways, which is usual for natural soils. The skew angle of DKM108, however, needs more attention. A very sharp angle in found in the pathway of DKM108 in which it experiences a change in direction of 270 degrees, visualized in fig. 7.5. After this abrupt change in direction, it continues following the same path towards the borehole, visualized in fig. 7.6. So this means that a strong resisting force has been subdued by the cone, indicating a strong deviation in stress state. This indicates a weak zone located close to the borehole probably caused by the borehole installation.

There are three more CPT's taken at an almost equal distance (180cm) from the borehole wall; DKM100, DKM101 and DKM102, as given in fig. 7.1. The results from these CPT's do not show the same deviation in cone resistance or the same distinguishable skew angle as DKM108. This, in combination with the axisymmetric results given in fig. 7.2, it must be a local weak zone at the location of DKM103 and DKM108.
On basis of 19 additional CPT's taken within the project area before the drilling of the borehole, it must be stated that there is a significant chance that the weak zone has a natural cause. In fig. 7.7, there are three more CPT results that represent a similar deviation pattern of the cone resistance and were taken far outside of the possible zone of influence of the drilling process.

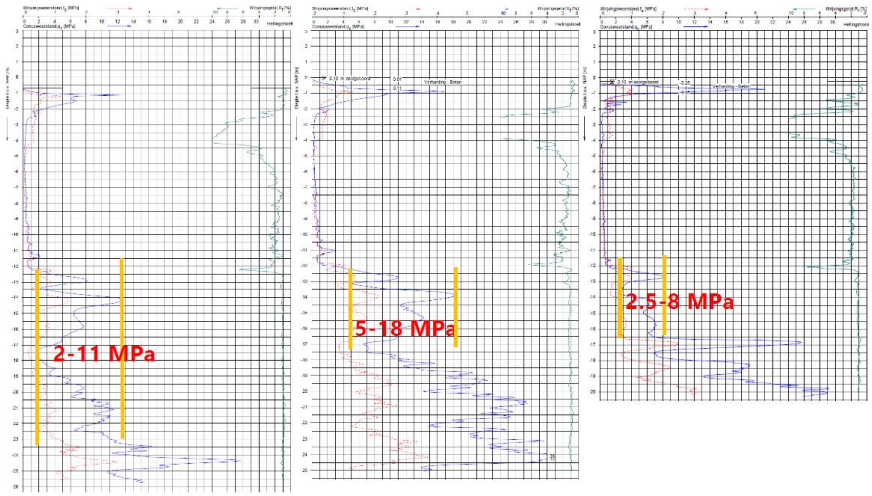

Figure 7.7: Three more CPT results taken at the Lisse project area (Hogervorst and Hoefsloot, 2020)

A PLAXIS model is built to investigate the extend and magnitudes of a weak zone caused by the drilling process instead of natural causes. No information was provided from which the degree of perfection of the drilling processes can be deducted. This is why the partial borehole collapse or erosion can be of any magnitude. The cone resistance data from DKM108 and DKM103 show a strong decrease between a depth of -15 and -25m. This is why it is very feasible that the partial collapse or erosion has occurred over the same borehole length. This is investigated in PLAXIS by applying three different degrees of excess soil volume losses. Volumetric strains of 10%, 20% and 30% were applied in the direction of DKM103 and DKM108 between -15m and -25m borehole depth. These results are compared

with the cone resistances of DKM103 and DKM108. It is assumed that a bisection of the cone resistance is equal to a bisection of the vertical effective stress , which is based on empirical theories by Baldi (Cabal and K.L., 2015).

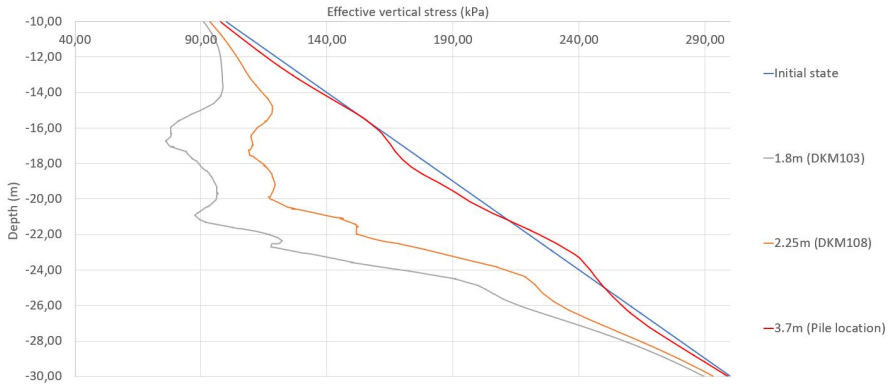

Figure 7.8: The vertical effective stress relief by 15 percent volume loss between -15m and -25m depth for the borehole in Lisse

The amount of excess soil volume that was lost due to a possible drilling complication (erosion or partial collapse) determines the vertical effective stress at the locations of DKM103 and DKM108. The PLAXIS simulation with a volume strain of 15 percent gives a bisection of the effective vertical stress at the location of DKM103 and DKM108, given in fig. 7.8. This simulation might explain the stress in-situ cone resistances found by the DKM103 and DKM108. Next to the vertical effective stresses found at the CPT locations, it was also plotted at the pile location, 3.7m from borehole wall. The vertical effective stress relief at the pile tip (-20m depth) is more or less $20kPa$. This means that a possible weak zone affecting the stress states at the locations of DKM103 and DKM108 has minimal influence on the stress states at the pile location.

7.4. Advice

The research done on this project on the basis of various CPT's and PLAXIS simulation gives a reliable amount of evidence to advice on further construction works. The following has been concluded based on the evidence given in chapter 7.3:

- A perfect drilling process of the borehole will have a zone of influence that will not effect the in-situ stress state at the pile location.
- A local weak zone is present located between and -15m and -25m stretching out towards the location of DKM103, DKM108 and the location of the pile
- The weak zone might have a natural cause, based on three more CPT's with equal cone resistance deviation patterns.
- A weak zone induced by the drilling process can cause significant weakness and stress redistribution at the location of the location of DKM103 and DKM108, however will have only minimum influence at the location of the pile ($\Delta\sigma_{zz} = -20kPa$).

Based on the results given above, the weak zone at the location of DKM103 and DKM108 will not cause a decrease in bearing capacity of the piles. All the CPT's taken at the pile locations give expected results with normal cone resistances. Even when the weak zone is caused by a drilling complication, it has not extended far enough to cause bearing capacity decrease at the pile locations. In addition to this, the piles are driven and will function as displacement piles. This way of installing will increase stiffness at the pile tip, which will easily amend the 20 kPa decrease in vertical effective stress.

8

Discussion

8.1. Parametric analysis

Shrinkage of the grout body causes a serious increase in the zone of influence for both horizontal and vertical stresses. Next to this, the horizontal stresses experience an higher stress redistribution. The vertical stresses experience an higher stress relief, which decreases the bearing capacity of piles. Next to this, an increase in the zone of influence will increase the risky zone for pile locations.
The magnitudes of the grout shrinkage and expansion were chosen arbitrarily. In practice, no clear evidence exists for large volumetric shrinkage magnitudes. This is why for further research a magnitude of -2% shrinkage was applied to the grout body, to be conservative for further calculations. There is a lot of variation in the choice for back-fill materials for closed systems, as there are many aspects influencing efficiency. They vary in: thermal conductivity, permeability, strength and workability and exist out of conventional or modern natural or chemical substances (Javadi et al., 2018). When new materials are used as back-fill grout, a test on the amount of shrinkage is useful as large shrinkage will influence the stress states around the boreholes.

High OCR values, in general, will decrease the vertical stress relief and increase the horizontal stress relief. For piles that obtain their bearing capacity from end-bearing at the pile tip, a higher OCR value is probably favoured due to lower stress reliefs. On the other hand, stress redistribution of the horizontal stresses (hoop and radial) increases with higher OCR values and might influence the mobilized shaft resistance of a pile.
For this analysis, the OCR was varied for one type of soil stiffness and strength. In practice, highly over-consolidated soils will have high stiffness and high strength, influencing the results. In this thesis, only the ratio between horizontal stress and vertical stress with a constant stiffness and strength was considered. Furthermore, the effective in-situ stresses are very high, which are susceptible for vibrations and deformations during installation of piles (Peels and Dijkstra, 2010).
Naturally, highly over-consolidated deposits only exist in the northern part of the Netherlands. This is why for practical applications the OCR is not very significant and needs more detailed investigation.

The higher the Relative Density of sand, the stronger the sand behaves. Stronger and stiffer sands show less stress relief and a smaller zone of influence. The amount of stress redistribution at a specific location within this zone of influence is higher for lower Relative Densities. So, the stress state around the borehole is favorably influenced by stiffer and stronger sands in relation to the bearing capacity of piles.

8.2. Stress analysis

It is clear that by using the right drilling fluid pressure, which is required to equal the total horizontal stress at a certain depth, the stress redistribution around the borehole can be minimized. This means that using a drilling fluid pressure at the lower-limit will increase the zone of influence and stress reliefs around the borehole. The decision to drill at lower-limit pressures has given conservative results.
Drilling companies, in the contrary, will never drill at lower-limit pressures. And it is hard to keep the pressure constant at all times due to heterogeneity of the soil and mechanical issues. This is why the conservative results will always give a criterion for the possible stress redistribution during drilling at low-limit pressures. The simulation of the drilling fluid pressures in PLAXIS, however, is not in accordance with reality. Pressure increments were used, with higher densities than water, producing unrealistic hydrostatic pressures. This might simulate a drilling fluid pressure with additives allowing for heavier unit weights. So, by increasing the pressure increment, the model simulates a heavier drilling fluid due to more additives. Next to this, the plastering effect of drilling mud additives is not contained in the model. Small amounts of clay or bentonite will cause a layer cake on the inner borehole wall decreasing the risk of circulation control loss. Next to this, state of the art additives exists,which allows for drilling through very difficult soil layer, like shale (Bloys et al., 1994)

The variation of the stress magnitudes in the plastic and elastic regions are equal for all borehole diameters and depend only on the initial stress state. The radial extends of these plastic and elastic regions, in the contrary, are diameter dependent. This means that a relationship between the borehole diameter and the extend of the redistributed stress region can be developed. For this zone of influence the following rule of thumb can be applied:

$$ZOI = BH - diameter \times 4 \tag{8.1}$$

In which ZOI is the zone of influence (95 percent of initial effective stress value at a specific depth) and $BH - diameter$ the excavated borehole diameter. This relationship is based on many assumptions and involves many constraints. The relationship only holds:

- For single boreholes with diameters between 0.3m and 1.0m
- When no shrinkage of the grout body occurred
- For perfectly drilled boreholes with no drilling complications
- For sand characteristics as given in table 3.4

This equation is based on results from the model, which are based on many assumptions. Next to this, the constraints for which the rule of thumb is applicable are hard to abide in practice.

The assumptions that were made in the model can influence the results on which the relationship in equation (8.1) is based. First of all the drilling process is modelled as a perfect

excavation of the borehole segments. No effect of the mechanical drilling process are included and might increase the plastic zone around the borehole. Mechanical drilling will cause an inconsistent borehole diameter over its whole length. The provoked deviations in borehole diameter, however, are relatively small and thus will only minimally influence the zone of influence given in the results.
Secondly, the back-fill process simulations in the model are simplified. The material behavior is based on simple soil models, like the linear elastic and Mohr-Coulomb models. The exact behavior of back-fill grout and gravel in the soil can be described by more constitutive models. Especially the hardening process of the grout in the soil body over time can have large influence on borehole stability and stress states. As there is significant time between the completion of the drilling process and the back-filling process, the time-dependent behavior of the soil influences the borehole stability significantly. In this time, swelling of clay layers might occur. Next to this, partial collapse of the borehole might occur.
Furthermore, there is a complex soil stratigraphy with naturally occurring sands. These sands will not be as homogeneous as simulated in the model. Biological or human remains may have a large effect. Next to this, the transition between soft soils and sands or gravels are not as distinct as modelled. Many circulation problems occur at these soil boundaries due to abrupt changes in horizontal in-situ stresses.
The accuracy of the drilling processes in practice is not examined in such extend to secure the above mentioned constraints with certainty. Especially the occurrence of drilling complications can easily reject this rule of thumb. The occurrence of drilling complications and its effects is discussed later in this chapter.

Despite that the relationship only holds for the above mentioned constraints and relies on results based on many assumptions, conservative results were used. The drilling fluid pressure during the drilling process was set at the lower limit. In practice, it is aspired never to reach the lower limit. Next to this, the relationship is based on the horizontal stresses instead of the vertical stresses. This leads to conservative results because the zone of influence is larger for horizontal stresses than for vertical stresses. Earlier studies state that the zone of influence extends to a distance of 10 times the borehole diameter (Spegelaere M., 2019). For perfectly drilled boreholes, this relationship is excessively conservative and will tend more to equation (8.1).

For closely spaced borehole arrays, that exist for some closed systems (BTES), the non-linear elastic zones can interfere. This means that stress redistribution in the area of interference might be higher than in the non-linear elastic zone around single boreholes. The additional stress redistribution, however, is negligibly small and will not influence the bearing capacity of piles. A spacing of 2m between boreholes used for closed systems (diameter <0.3m) is enough to eliminate interference.

A drilling complication in x- and y-direction with a total ε_{vol} of 50% will cause serious stress reliefs around the boreholes. Next to this, the zone of influence of these stress reliefs can extend up to 7m. There is a plastic zone around the borehole segment of the drilling complication which can extend up to several meters. These plastic zones are denoted by relatively large deformations. In these plastic zones, both vertical and horizontal stresses show extremely high reliefs. In the non-linear elastic zone, with relatively small deformations, the reliefs in radial stresses are compensated by an increase in hoop stresses. For the bearing capacity of piles, drilling complication occurring at the depth of the pile tip will influence the in-situ stresses acting on the pile the most. Next to this, drilling complications occurring at

shallow depths will have small influences on these in-situ stresses.

The simulations of drilling complications in the model were exactly into x- and y-direction with known magnitude. This might simulate erosion of the borehole wall with a known loss of soil and a consistent dimension. In real-life, drilling complications can be cracks or holes with unknown direction and magnitude. The only measurements that can be done in real-life to detect drilling complications is by measuring the excavated soil per meter depth. The exact direction of stress relief, however, will be unsure. The boreholes for UTES systems are often drilled close to pile foundations. From the results it it can be deduced that drilling complications are a key factor in bearing capacity loss. This is why a study focusing on drilling complications is necessary. A better understanding of which drilling complications occur in what type of soil is required. Many of the studies on borehole stability in literature focus on highly consolidated sediments or rock masses, like the studies by Press et al., 1993 and Haimson and Kovacich, 2003. Instead of this, methods for modelling drilling complications and the influence on the stress state in shallow sediments need to be developed. As PLAXIS is FEM based and does not allow large strains to occur, other numerical models need to be used, for example a Discrete Element Method. Now, drilling complications can only be detected when performing Cone Penetration Tests in the surrounding soil.

8.3. Bearing capacity analysis

The results for a perfectly drilled borehole gave small stress changes at the pile location, when the constraints and assumptions discussed in chapter 8.2 are fully met.
For a non-displacemet pile in the non-linear elastic zone, the loss of bearing capacity was negligible. This minimal loss can be explained by a constant effective horizontal stress ($\sigma_{xx,yy}$) acting on the pile. The loss of radial stresses were compensated by an increase in tangential stresses, keeping the shaft resistance unaltered. In addition, the relief of effective vertical stresses were relatively small, keeping the bearing capacity unamended. This is because a non-displacement pile obtains most of its bearing capacity from shaft resistance.
For non-displacement piles in the plastic zone, where both tangential stresses will drastically decrease in magnitude, loss of bearing capacity will be more severe. It is, however, very unlikely that piles will be placed in this very small plastic zone due to the possibility of other hazards to occur. During pile loading, obliqueness can occur when the pile tip is willing to drag towards the weaker zone. Next to this, the grout and gravel may deform plastically due to high pile loads causing excessive stresses around the pile tip. At last, a wished-in-place pile that is installed in real-life will be bored, whereupon it is filled with reinforced concrete. During this installation process small plastic and elastic zones will occur around the pile shaft (due to soil excavation). The in-situ stress condition may change from a K value of 1.5 to 1.1 after installation (Moor, 1994). In the PLAXIS simulations these installation effects are not modelled and might influence the eventual bearing capacity and soil behavior around the pile. For further research, the installation effects of bored piles need to be included and simulated.

For the boreholes with a drilling complication, the above mentioned relationship between stress release and bearing capacity is confirmed. For large spacing between pile and borehole, small vertical effective stress releases occur, leading to negligible or minimal loss of bearing capacity. Smaller spacing situations, with piles located in the plastic zone, show rigorous releases in horizontal and vertical effective stresses, leading to dangerous losses in bearing capacity of more than half its initial value.
The overall uncertainties of drilling complications were discussed in chapter 8.2 and are ap-

plicable for these results as well. In addition to these, the depth of occurrence and its harmful effect on the bearing capacity is an important factor. For the given results, the drilling complication occurred at the pile tip depth. Drilling complications above the pile tip may have less harmful effects, as only the effective horizontal stresses will influence the shaft resistance as given by Han et al., 2017, Lehane and White, 2005 and Loukidis and Salgado, 2008. So, decreases in effective vertical stress will not influence the shaft resistance. Generally, as the pile is located outside the plastic zone, the shaft resistance will not decrease due to unamended effective horizontal stresses.
The depth of drilling complications in practice, as was discussed in chapter 2.2.4, is most likely to occur due to drilling fluid circulation problems. Piles are usually drilled through soft soil layer with 25% of the pile length in the sand layer, which means the boundary between the soft soil and sand is at a depth of 75% the pile length. This boundary is where it is most likely for circulation problems to occur due to over or under estimating the necessary fluid pressure. As this is relatively close to the pile tip, it is crucial for the drilling company to drill with additional caution. Next to this, the exact depth of this boundary has to be investigated before the drilling process.

For displacement piles, the overall bearing capacity is significantly higher than for non-displacement piles. In the simulation results, the bearing capacity of the displacement pile (driven) in unaffected soil is $4600kN$ while for a non-displacement pile (bored) it is only $680kN$. The effect of a borehole with a drilling complication on the bearing capacity of a non-displacement pile was significant, decreasing it by more than 50%. This non-displacement pile was installed and loaded after the drilling process (phasing B). For a displacement pile with the same phasing (phasing B), the loss of bearing capacity is more than 70%. A displacement pile is more susceptible for high stress releases than a non-displacement pile. This difference might be explained by the substantial loss of in-situ stress and strength of the soil before pile installation, making it impossible to increase stresses around the pile tip during driving. This lower degree of pre-stressed soil is the cause for the relatively high loss of bearing capacity. So, a displacement pile is more susceptible for changes in the stress state than a non-displacement pile.
Phasing A and B, simulated a scenario's in which the pile was unloaded during borehole drilling and thus the foundation was still under construction. Phasing C, in the contrary, the pile was loaded during borehole drilling, simulating an existing buildings founded on displacement piles. Phasing C is most susceptible for the borehole drilling process. Pile failure will occur for very small drilling complications and thus this phasing is most harmful with respect to the bearing capacity. Phasing A is more harmful than phasing B. For further construction works, it is best to first install the pile without loading it after which the boreholes can be drilled.
The simulation of the displacement piles was a first-order estimation and does not completely simulate the effects of driving piles, further implementation of installation effects can be done when using 2D axisymmetric models or Material Point Methods, like described in Dijkstra et al., 2006 and Phuong et al., 2016. For a 3D FEM model, such simulations are unexplored and need more investigation. Next to this, there are several degrees of soil displacement during pile installation. For this research, only the two extremes were considered while there are many more installation types in between both, that are of interest for practical knowledge.

9

Conclusion and recommendations

In this chapter a conclusion will be drawn on the results obtained in this research. First, the main research question will be answered. After this, the sub-questions are answered to obtain a more detailed insight in the conclusions. At last, recommendations will be given which can be used for further research or more practical issues.

9.1. Conclusion

The chapters with the results from this research are sub-divided into four main parts and focus on: key parameters, stress states, bearing capacity and a case study. The results from these four chapters will give an answer to the research questions as given in chapter 1.

What is the influence of installing UTES boreholes on the bearing capacity of piles?

The drilling of boreholes will influence a 'zone of influence' around the borehole. The extend of the zone of influence is affected by the borehole diameter, soil properties and above all the drilling process. A minimum borehole-pile spacing of 6m is necessary to minimize the risk of bearing capacity loss. When locating piles at closer spacing, a successful drilling process without any complications is indispensable. Within the zone of influence, a stress redistribution will occur, containing a non-linear elastic zone and a plastic zone. Piles that are placed within this plastic zone experience a severe loss of bearing capacity. For piles within the non-linear elastic zone a negligible loss of bearing capacity occurs. Displacement piles are more susceptible to effective stress losses than non-displacement piles. For minimum bearing capacity loss of displacement piles, they need to be driven first, then the borehole can be drilled after which the pile can be loaded. Pre-loaded (driven) piles of existing buildings are extremely vulnerable for in-situ stress changes and require relatively large borehole-pile spacing.

9.1.1. Influence of key parameters

What is the influence of drilling boreholes for UTES systems on the stress-strain state and strength of soils and how is this influenced by Over-Consolidation Ratio?

A variation of Over-Consolidation Ratio's have given different results for the effective tangential stresses (σ'_{xx} and σ'_{yy}) and the effective vertical stress (σ'_{zz}). The results indicate that for the tangential stresses, an increase in OCR will increase the zone of influence and the extend of the plastic zone. Next to this, the stress relief increments are higher for sands with higher OCR. For the vertical stress, a higher OCR means a decrease of the zone of influence.

What is the influence of drilling boreholes for UTES systems on the stress-strain state and strength of soils and how is this influenced by Relative Density?

The Relative Density of a sand determines its strength parameters. An increase in the Relative Density of sand means a smaller zone of influence and a smaller extend of the plastic zone, due to the higher strength of the sand. For the horizontal stresses, it also means that the elastic stress redistribution will be concentrated at the plastic-elastic boundaries.

What is the influence of drilling boreholes for UTES systems on the stress-strain state and strength of soils and how is this influenced by shrinkage or expansion of grout bodies?

During the hardening process of grout material, it might experience shrinkage. The results denotes that even small amounts of shrinkage (2 volume percentage), will increase the zone of influence and the magnitude of stress redistribution significantly. For thermally-enhanced grouts, which are usual for closed systems, no such shrinkage has been experienced in practice. However, as the systems are still unexplored, other types of grout may be used as back-fill material. Grout material experiencing shrinkage will most likely increase stress redistribution and is suggested to be less suitable as back-fill material for UTES boreholes.

9.1.2. Influence of UTES boreholes on stress state

What is the influence of drilling boreholes for UTES systems on the stress-strain state and strength of soils and how is this influenced by borehole diameters?

For a perfectly drilled borehole (no drilling complications), an increase in borehole diameter will increase in the zone of influence. A conditional rule of thumb can be deducted from the results in this research. This rule of thumb on the zone of influence is given by:

$$ZOI = BH - diameter \times 4 \tag{9.1}$$

In which ZOI the zone of influence (less than 95% of initial effective stress value at a specific depth) and $BH - diameter$ the excavated borehole diameter.
The relationship is very conditional and only holds for the following constraints:

- For single boreholes with diameters between 0.3m and 1.0m
- When no shrinkage of the grout body
- For perfectly drilled boreholes with no drilling complications

- For sand characteristics as given in table 3.4

What is the influence of drilling boreholes for ATES and BHE systems on the stress-strain state and strength of soils and how is this influenced by the drilling process?

The drilling process itself has serious effect on the stress states around boreholes. There are two main aspects of the drilling process which have high influence: 1) the drilling fluid pressure and 2) the degree of perfection of drilling. The drilling fluid pressure inside the borehole must always equal the value of the total horizontal stress acting on the borehole wall. In this way, the zone of influence can be minimized to negligible extends. A small plastic zone will always be present directly around the borehole wall. Losses of excess soil volumes due to drilling complications will cause severe reliefs of in-situ stresses around the borehole. Both tangential and vertical stresses are affected in the directions of at which excess volume loss occurred. The extend of the severe stress reliefs, however, is not extremely large. In relatively strong sands as used in simulations for this research, the capability of stress recovery in radial direction is large.

9.1.3. Influence of UTES boreholes on bearing capacity

What is the influence of the installation of ATES and BHE systems on the bearing capacity of piles and how is this influenced by drilling complications?

Only the tip resistance will by effected by the borehole drilling process for piles in the non-linear elastic zone. This causes a negligible loss of bearing capacity. In the plastic zone, both tangential and vertical stresses will have high reliefs, causing high bearing capacity loss. It is not advised to place piles in this region.
For boreholes with drilling complications, the plastic and non-linear elastic zones have large extend in horizontal direction. The stress relief in the plastic zone is significantly higher than with perfectly drilled boreholes, increasing the loss of bearing capacity.

What is the influence of the installation of ATES and BHE systems on the bearing capacity of piles and how is this influenced by the installation type of piles?

The results show that the bearing capacity of displacement piles is higher than that of non-displacement piles. In addition to this displacement piles as simulated in this model, are more susceptible for changes in in-situ stress state and are highly influenced by the phasing of installation processes. Especially piles loaded by half the ultimate bearing capacity fail or diverge due to borehole drilling processes. In general, it is advantageous for the bearing capacity of a pile to install it before drilling the borehole.

Can the extended models developed in this research be validated with a practical case in the Netherlands ?

The Lisse Project included the exact same problems as were treated in this research. The developed PLAXIS model works for boreholes drilled in sandy soils. The model can give the zone of influence for the drilled borehole in different types of sand (which is an essential aspect in practice). Next to this, the model can predict the changes in stress states for an loss of excess soil volume due to drilling complications. At last, load-displacement curves

can be produced and changes in the bearing capacity of piles can be calculated due to stress changes in the soil. As the model runs on several assumptions, it always has to be combined with CPT's or other project specific data. By the combinations of these two a more reliable and precise advice can be given on the problem.

9.2. Recommendations for practical use

There are several general recommendations for practical use that can be endowed from the conclusion of this research:

- New types of grouts for closed systems require investigation on shrinkage behavior as this can significantly increase the extend of the zone of influence around boreholes
- Borehole stability must be secured at all times when drilling at a depth around the pile tip (over a length of 5m below and 5m above the pile tip)
- For small horizontal borehole-pile spacing (<6m), the use of non-displacement piles is preferred over displacement piles
- The most favourable phasing for displacement pile installation is: 1) pile driving, 2) borehole drilling and 3) pile loading
- Existing foundations are extremely susceptible for borehole drilling processes and require relatively large borehole-pile spacing.

As borehole stability is very important for specific sections of the borehole length. The following measures can be undertaken to increase stability in this area:

- When passing this borehole section and leaving it at night, make sure to check the depth of the borehole when starting to drill in the morning.
- Keep track of the drilling fluid pressures and inflow-outflow equilibrium at this section of the borehole
- With very high uncertainties about borehole stability in this section of the borehole, use a casing (although vibrations can aggravate the problem)
- Make use of drilling fluid additives to secure the borehole stability at this section of the borehole minimally (especially for closed system borehole for which these additives will not influence the efficiency of the heat exchange system)

The degree of perfection of boreholes is very unsure and complete borehole stability during the drilling process is hard to confirm. Especially for projects with small borehole-pile spacing this becomes of high significance. A higher degree of certainty can be obtained by performing Cone Penetration Tests before and after the borehole drilling process. Based on this research, the following recommendations can be given for pre-post Cone Penetration Tests:

- Take multiple CPT's into the direction of the pile(s), with one CPT at the location of the pile
- Perform CPT's up to a minimal depth of 5m underneath the pile tip
- The bearing sand layer is of highest interest because it is most susceptible to drilling complications
- For a known depth of a drilling complication, take several CPT's around the borehole to identify its direction. After this, take CPT's into the direction of the drilling complication to identify its extend

9.3. Recommendations for further research

There are several recommendations for further and extended research on this subject, especially when modelling with PLAXIS. The assumptions that have been made during modelling need better simulations and further investigation. Next to this, there are several subjects that have not been covered in this thesis that might be of interest.

Soils

Most of the research has been performed with a very simplified soil structure. These soil structures consist out of sand completely. The stress states around a borehole in soft soils, however, has hardly been investigated. Piles are mostly driven though clay in order to reach a sand deposit, the stress changes in this clay layer may influence the shaft resistance of piles. Furthermore, soft soils exhibit complex behavior, like time-dependent creep and swelling processes. At last, hydrological processes are not included. The water level can be beneath ground level or fluctuating over time. Next to this, consolidation processes due to changes in pore pressures are not considered in this research.

Drilling process

Next to this, the simulation of drilling complications was very limited. Further research on the causes, magnitudes and dimensions of drilling complications is necessary. Scans of borehole walls after drilling processes may be an option. In this way, the simulation of drilling complications can be performed with higher accuracy and with results showing the consequences on stress-states and deformations. The modelling in PLAXIS will be hard, however, due to limited strain. The effects of drilling complications can be modelled by means of other numerical methods, like the Discrete Element Method. Next to this, only the stress redistribution due to excavating soil was considered for this research. The effects of the mechanical part of the drilling process is not included and can be included by further simulation of the drilling process.

Piles

There are many different types of pile installation, influencing soil stress conditions. For this research, a full-non-displacement pile and a full-displacement pile have been chosen. The simulation of the full-displacement pile was only a first order estimate and can be improved. Next to this, different installation types might be of interest due to different stress rearrangement around the piles.

A

Appendix

A.1. Analytical bearing capacity

Tip resistance by Vesic

$$p_{tip} = \eta q(N_q - 1)d_q \tag{A.1}$$

$$\eta = (1 + 2K_0)/3 \tag{A.2}$$

$$d_q = 1 + 2tan\phi(1 - sin\phi)^2 tan^{-1}(L/B) \tag{A.3}$$

Tip resistance by Brinch-Hansen

$$p_{tip} = i_c s_c c N_c + i_q s_q q N_q + i_\gamma s_\gamma \frac{1}{2}\gamma B N_\gamma \tag{A.4}$$

$$s_c = 1 + 0.2\frac{L}{B} \tag{A.5a}$$

$$s_q = 1 + \frac{L}{B}sin\phi \tag{A.5b}$$

$$s_\gamma = 1 - 0.3\frac{L}{B} \tag{A.5c}$$

Shaft resistance

$$q_{shaft,neg} = K_0 * \sigma'_v * tan\delta \tag{A.6}$$

A

ϕ	N_c	N_q	N_γ
0	5.142	1.000	0.000
1	5.379	1.094	0.003
2	5.632	1.197	0.014
3	5.900	1.309	0.032
4	6.185	1.433	0.060
5	6.489	1.568	0.099
6	6.813	1.716	0.151
7	7.158	1.879	0.216
8	7.527	2.058	0.297
9	7.922	2.255	0.397
10	8.345	2.471	0.519
11	8.798	2.710	0.665
12	9.285	2.974	0.839
13	9.807	3.264	1.045
14	10.370	3.586	1.289
15	10.977	3.941	1.576
16	11.631	4.335	1.913
17	12.338	4.772	2.307
18	13.104	5.258	2.767
19	13.934	5.798	3.304
20	14.835	6.399	3.930

ϕ	N_c	N_q	N_γ
20	14.835	6.399	3.930
21	15.815	7.071	4.661
22	16.833	7.821	5.512
23	18.049	8.661	6.504
24	19.324	9.603	7.661
25	20.721	10.662	9.011
26	22.254	11.854	10.558
27	23.942	13.199	12.432
28	25.803	14.720	14.590
29	27.860	16.443	17.121
30	30.140	18.401	20.093
31	32.671	20.631	23.591
32	35.490	23.177	27.715
33	38.638	26.092	32.590
34	42.164	29.440	38.366
35	46.124	33.296	45.228
36	50.586	37.753	53.404
37	55.630	42.920	63.178
38	61.352	48.933	74.899
39	67.867	55.957	89.007
40	75.313	64.195	106.054

Figure A.1: Bearing capacity correction factors (Verruijt, 2010)

Pile Material	δ
Steel	0.67 ϕ to 0.83 ϕ
Concrete	0.90 ϕ to 1.0 ϕ
Timber	0.80 ϕ to 1.0 ϕ

Figure A.2: Delta values for shaft resistance (USACE, 1977)

B

Appendix

B.1. Input parameters used for Relative Density variation

Parameter	Value	Unit
γ_{unsat}	16.2	kN/m^3
γ_{sat}	19.2	kN/m^3
E_{50}	$18 * 10^3$	kN/m^2
E_{oed}	$18 * 10^3$	kN/m^2
E_{ur}	$80.4 * 10^3$	kN/m^2
power	0.606	-
c′	0	kN/m^2
ϕ	31.75	degree
ψ	1.75	degree
$\gamma_{0.7}$	$0.17 * 10^-3$	-
G_0	$80.4 * 10^3$	kN/m^2

Table B.1: Input parameters used for the HSs model for a Relative Density of 30 percent

B

Parameter	Value	Unit
γ_{unsat}	17	kN/m^3
γ_{sat}	20	kN/m^3
E_{50}	$30 * 10^3$	kN/m^2
E_{oed}	$30 * 10^3$	kN/m^2
E_{ur}	$90 * 10^3$	kN/m^2
power	0.544	-
c′	0	kN/m^2
ϕ	34.25	degree
ψ	4.25	degree
$y_{0.7}$	$0.15 * 10^-3$	-
G_0	$94 * 10^3$	kN/m^2

Table B.2: Input parameters used for the HSs model for a Relative Density of 50 percent

Parameter	Value	Unit
γ_{unsat}	17.8	kN/m^3
γ_{sat}	20.8	kN/m^3
E_{50}	$42 * 10^3$	kN/m^2
E_{oed}	$42 * 10^3$	kN/m^2
E_{ur}	$126 * 10^3$	kN/m^2
power	0.481	-
c′	0	kN/m^2
ϕ	36.75	degree
ψ	6.75	degree
$y_{0.7}$	$0.13 * 10^-3$	-
G_0	$107.6 * 10^3$	kN/m^2

Table B.3: Input parameters used for the HSs model for a Relative Density of 70 percent

Parameter	Value	Unit
γ_{unsat}	18.6	kN/m^3
γ_{sat}	21.6	kN/m^3
E_{50}	$54 * 10^3$	kN/m^2
E_{oed}	$54 * 10^3$	kN/m^2
E_{ur}	$162 * 10^3$	kN/m^2
power	0.419	-
c′	0	kN/m^2
ϕ	39.25	degree
ψ	9.25	degree
$y_{0.7}$	$0.11 * 10^-3$	-
G_0	$121.2 * 10^3$	kN/m^2

Table B.4: Input parameters used for the HSs model for a Relative Density of 90 percent

C

Appendix

C.1. Overview of scenario for multiple boreholes

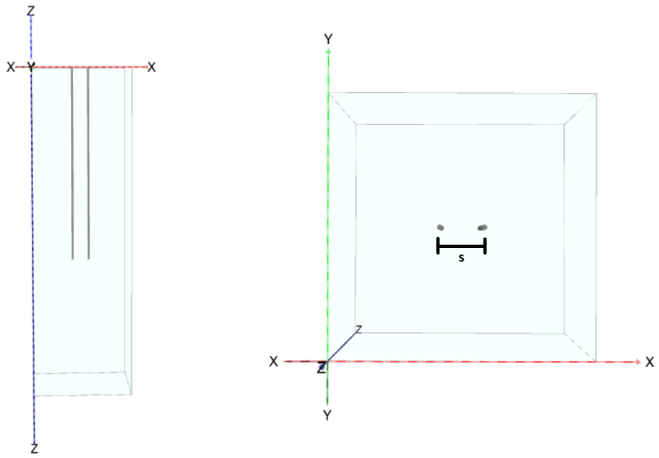

Figure C.1: Overview of scenario for two boreholes. Spacing is varied from 2 to 5 meters point to point. Possible location of the pile location is in the center of the domain (x, y) = (15, 15)

C

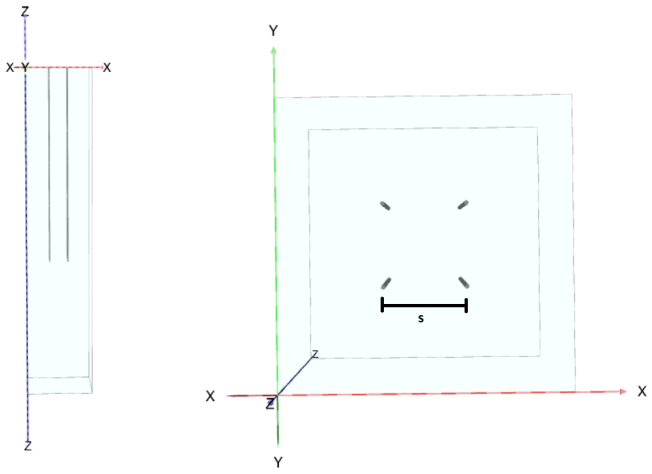

Figure C.2: Overview of scenario for four boreholes. Spacing is varied from 2 to 5 meters point to point. Possible location of the pile location is in the center of the domain (x, y) = (10, 10)

D

Appendix

D.1. Formulas used for the analytical solution

$$\sigma_r = \sigma_{ro} + (\sigma_{ro} - \sigma_{ri}) \frac{R_i^2}{R_o^2 - R_i^2} \left[1 - \left(\frac{R_o}{r} \right)^2 \right]$$
$$- (P_o - P_i) \frac{1-2\upsilon}{2(1-\upsilon)} \beta \left\{ \frac{R_i^2}{R_o^2 - R_i^2} \right.$$
$$\left. \cdot \left[1 - \left(\frac{R_o}{r} \right)^2 \right] + \frac{\ln(R_o/r)}{\ln(R_o/R_i)} \right\}. \quad \ldots\ldots\ldots (1)$$

$$\sigma_\theta = \sigma_{ro} + (\sigma_{ro} - \sigma_{ri}) \frac{R_i^2}{R_o^2 - R_i^2} \left[1 + \left(\frac{R_o}{r} \right)^2 \right]$$
$$- (P_o - P_i) \frac{1-2\upsilon}{2(1-\upsilon)} \beta \left\{ \frac{R_i^2}{R_o^2 - R_i^2} \right.$$
$$\left. \cdot \left[1 + \left(\frac{R_o}{r} \right)^2 \right] + \frac{1}{\ln(R_o/R_i)} [\ln(R_o/r) - 1] \right\}.$$
$$\ldots\ldots\ldots\ldots\ldots\ldots\ldots (2)$$

$$\sigma_z = \sigma_{zo} + 2\upsilon(\sigma_{ro} - \sigma_{ri}) \frac{R_i^2}{R_o^2 - R_i^2} - (P_o - P_i)$$
$$\cdot \frac{1-2\upsilon}{2(1-\upsilon)} \beta \left\{ \upsilon \frac{2R_i^2}{R_o^2 - R_i^2} + \frac{2}{\ln(R_o/R_i)} \right.$$
$$\left. \cdot [\ln(R_o/r) - \frac{\upsilon}{2}] \right\}. \quad \ldots\ldots\ldots\ldots\ldots\ldots (3)$$

Figure D.1: Analytical formulas for the elastic part of the solution for the three principal stresses

For $R_i < r < R_b$,

$$\sigma_r = P_o + \frac{1}{t} 2S_o \tan\alpha \left[\left(\frac{r}{R_i} \right)^t - 1 \right]. \quad \ldots\ldots\ldots (31)$$

For $R_b < r < R_c$,

$$\begin{aligned}
\sigma_r = P_o + \frac{1}{t} 2S_o \tan\alpha \Bigg\{ & \left[\left(\frac{\gamma + t + 1}{2\gamma} \right) \left(\frac{R_b}{R_i} \right)^t \right. \\
& \left. - \frac{\gamma + 1}{2\gamma} \right] \left(\frac{r}{R_b} \right)^{\gamma - 1} + \left[\left(\frac{\gamma - t - 1}{2\gamma} \right) \left(\frac{R_b}{R_i} \right)^t \right. \\
& \left. - \frac{\gamma - 1}{2\gamma} \right] \left(\frac{r}{R_b} \right)^{-\gamma - 1} \Bigg\} - \frac{1}{\tan^2\alpha - 2\upsilon} \\
& \cdot \left[(1 - 2\upsilon)(1 - \beta) P_o + 2S_o \tan\alpha - \frac{(1 + \upsilon)(1 - 2\upsilon)}{1 - \upsilon} \right. \\
& \left. \cdot (\sigma_{zo} - \beta P_o) \right] \left[1 - \left(\frac{\gamma + 1}{2\gamma} \right) \left(\frac{r}{R_b} \right)^{\gamma - 1} \right. \\
& \left. - \left(\frac{\gamma - 1}{2\gamma} \right) \left(\frac{r}{R_b} \right)^{-\gamma - 1} \right]. \quad \ldots\ldots\ldots\ldots (32)
\end{aligned}$$

For $R_i < r < R_b$,

$$\sigma_\theta = \sigma_z = P_o + \frac{1}{t} 2S_o \tan\alpha \left[(t + 1) \left(\frac{r}{R_i} \right)^t - 1 \right].$$

$$\ldots\ldots\ldots\ldots\ldots\ldots\ldots\ldots (33)$$

Figure D.2: Analytical formulas for the plastic part of the solution for the three principal stresses

For $R_b < r < R_c$,

$$\sigma_\theta = P_o + \frac{1}{t} 2S_o \tan\alpha \left\{ \left[\left(\frac{\gamma+t+1}{2} \right) \left(\frac{R_b}{R_i} \right)^t - \frac{\gamma+1}{2} \right] \left(\frac{r}{R_b} \right)^{\gamma-1} - \left[\left(\frac{\gamma-t-1}{2} \right) \left(\frac{R_b}{R_i} \right)^t - \frac{\gamma-1}{2} \right] \left(\frac{r}{R_b} \right)^{-\gamma-1} \right\} - \frac{1}{\tan^2\alpha - 2\upsilon} \cdot \left[(1-2\upsilon)(1-\beta)P_o + 2S_o \tan\alpha - \frac{(1+\upsilon)(1-2\upsilon)}{1-\upsilon} \cdot (\sigma_{zo} - \beta P_o) \right] \left[1 - \left(\frac{\gamma+1}{2} \right) \left(\frac{r}{R_b} \right)^{\gamma-1} + \left(\frac{\gamma-1}{2} \right) \left(\frac{r}{R_b} \right)^{-\gamma-1} \right] . \quad \ldots\ldots\ldots\ldots (34)$$

For $R_b < r < R_c$,

$$\sigma_z = P_o + 2S_o \tan\alpha + \frac{t+1}{t} 2S_o \tan\alpha \left\{ \left[\left(\frac{\gamma+t+1}{2\gamma} \right) \cdot \left(\frac{R_b}{R_i} \right)^t - \frac{\gamma+1}{2\gamma} \right] \left(\frac{r}{R_b} \right)^{\gamma-1} + \left[\left(\frac{\gamma-t-1}{2\gamma} \right) \cdot \left(\frac{R_b}{R_i} \right)^t - \frac{\gamma-1}{2\gamma} \right] \left(\frac{r}{R_b} \right)^{-\gamma-1} \right\} - \frac{t+1}{\tan^2\alpha - 2\upsilon} \cdot \left[(1-2\upsilon)(1-\beta)P_o + 2S_o \tan\alpha - \frac{(1+\upsilon)(1-2\upsilon)}{1-\upsilon} \cdot (\sigma_{zo} - \beta P_o) \right] \left[1 - \left(\frac{\gamma+1}{2\gamma} \right) \left(\frac{r}{R_b} \right)^{\gamma-1} - \left(\frac{\gamma-1}{2\gamma} \right) \left(\frac{r}{R_b} \right)^{-\gamma-1} \right] . \quad \ldots\ldots\ldots\ldots (35)$$

Figure D.3: Analytical formulas for the plastic part of the solution for the three principal stresses

E

Appendix

E.1. Two boreholes with varying spacing

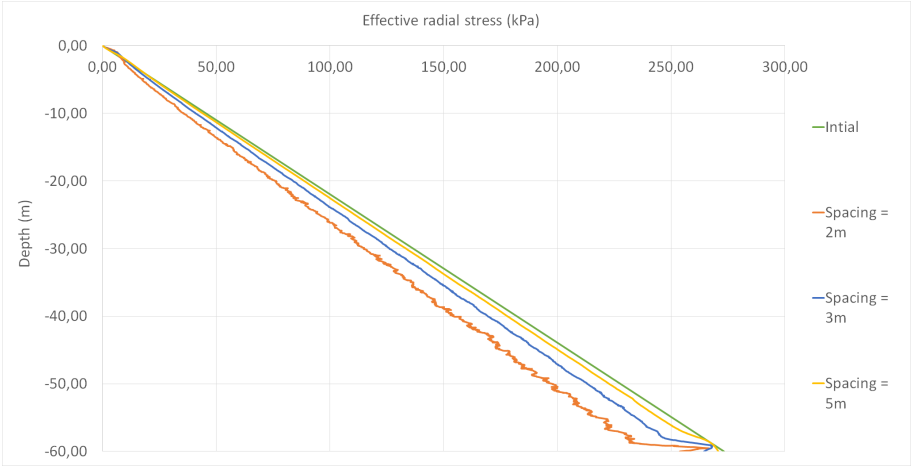

Figure E.1: Graph with the effective radial stress versus the depth for two boreholes with a varying spacing from 2m to 5m

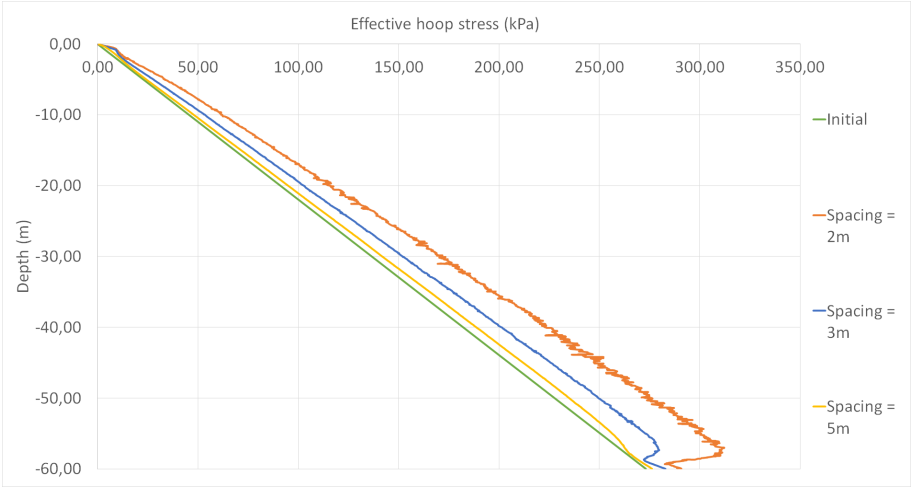

Figure E.2: Graph with the effective hoop stress versus the depth for two boreholes with a varying spacing from 2m to 5m

E.2. Four boreholes with varying spacing

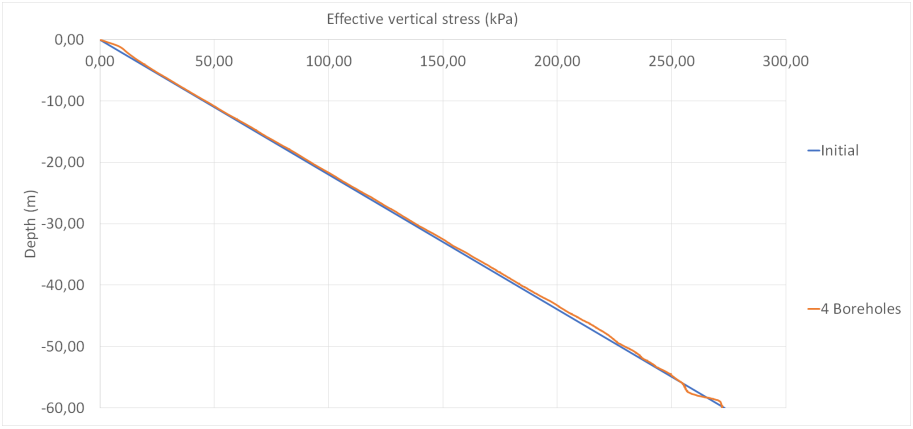

Figure E.3: Graph with the effective radial stress versus the depth in the middle of an four borehole configuration

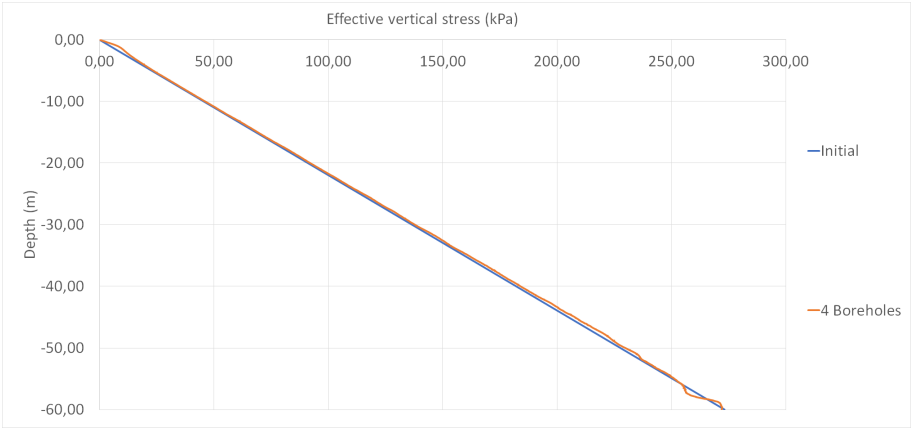

Figure E.4: Graph with the effective hoop stress versus the depth in the middle of an four borehole configuration

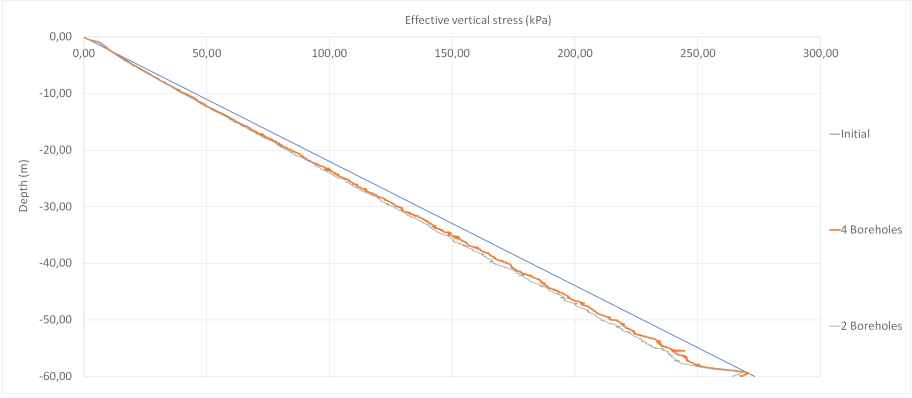

Figure E.5: Graph with the effective radial stress versus the depth between two boreholes in an four borehole configuration

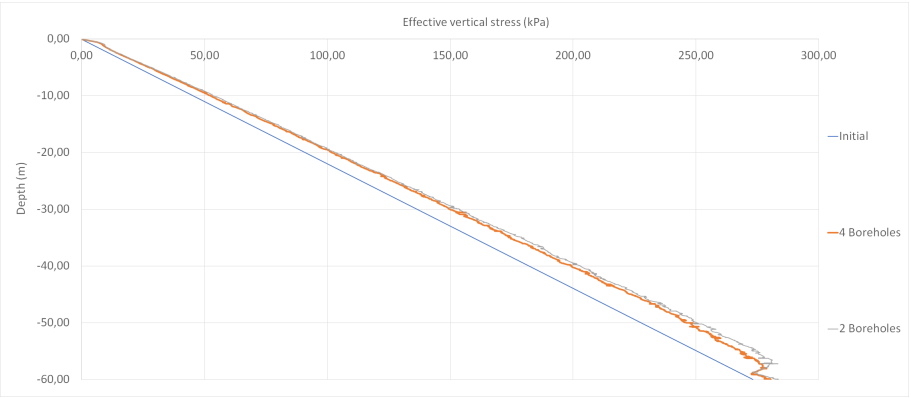

Figure E.6: Graph with the effective hoop stress versus the depth between two boreholes in an four borehole configuration

F

Appendix

F.1. 2D model mesh configurations for static pile load tests

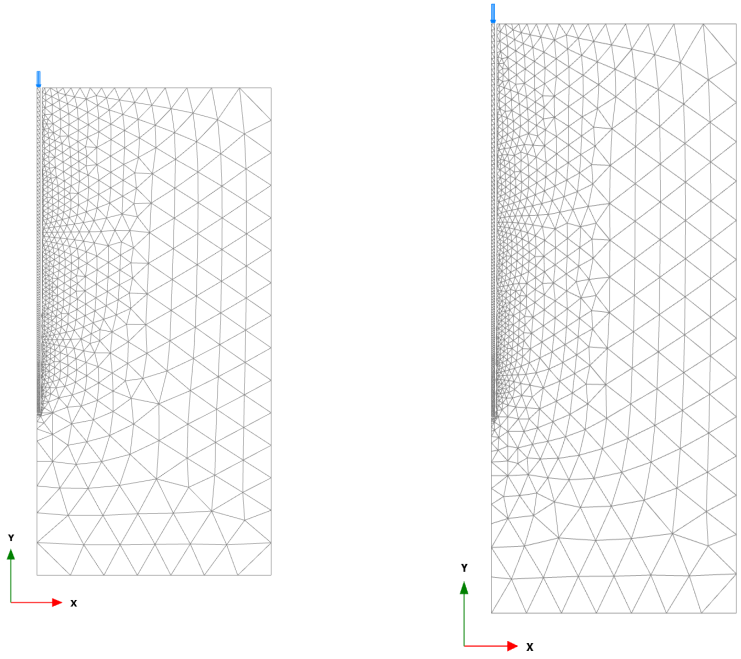

Figure F.1: Coarse mesh (left) and coarse mesh-moderately refined (right)

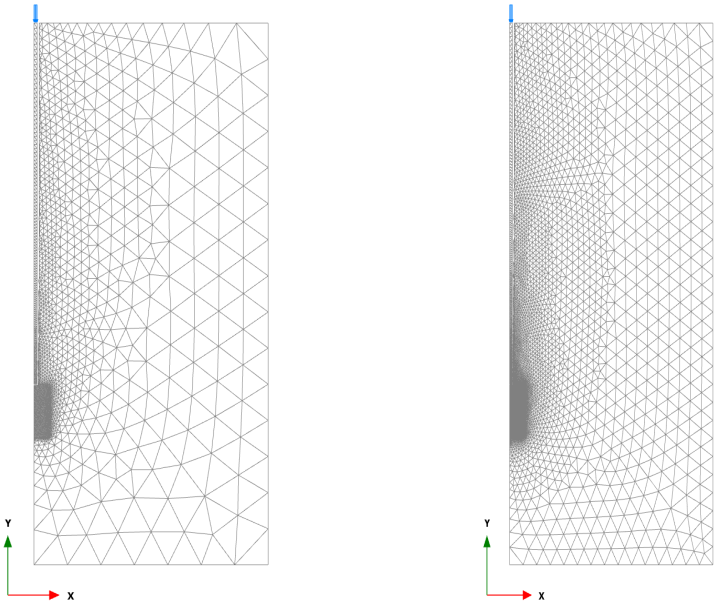

Figure F.2: Medium mesh - highly refined (left) and Very fine mesh - highly refined (right)

Bibliography

Aadnøy, B. S., & Looyeh, R. (2019). Stresses Around a Wellbore. *Petroleum Rock Mechanics*, 183–204. https://doi.org/10.1016/b978-0-12-815903-3.00011-x

Afzal, S., Shahzada, K., Fahad, M., Saeed, S., & Ashraf, M. (2014). Assessment of early-age autogenous shrinkage strains in concrete using bentonite clay as internal curing technique. *Construction and Building Materials*, *66*, 403–409. https://doi.org/10.1016/j.conbuildmat.2014.05.051

Austin, E. H., & Austin, E. H. (1983). Drilling Problems. *Drilling Engineering Handbook*, (2010), 58–121. https://doi.org/10.1007/978-94-009-7261-2{_}3

Beijer Lundberg, A., Dijkstra, J., & Van Tol, A. F. (2013). *Displacement pile installation effects in sand*.

Bloys, B., Davis, N., Smolen, B., Bailey, L., Houwen, O., Reid, P., Sherwood, J., Fraser, L., & Hodder, M. (1994). Designing and managing drilling fluid. *Oilfield Review*, *6*(2), 33–43.

Briaud, J. L. (2013). Deep Foundations, In *Geotechnical engineering: Saturated and unsaturated soils*. John Wiley & Sons Inc.

Brinkgreve, R. (1994). *Reference manual* (tech. rep.). PLAXIS. https://doi.org/10.1142/9789814343459{_}others04

Budhu, M. (2010). *Soil Mechanics and Foundations* (3rd). John Wiley & Sons. https://doi.org/10.1017/CBO9781107415324.004

Cabal, P. R., & K.L. (2015). *Guide to Cone Penetration Testing* (tech. rep.). Gregg Drilling.

CBS. (2019). Hernieuwbare energie in Nederland 2019. *Report number: 60115201401 C-89*, 1–106.

Dijkstra, J., Broere, W., & Van Tol, A. F. (2006). Numerical investigation into stress and strain development around a displacement pile in sand. *Proceedings of the 6th European Conference on Numerical Methods in Geotechnical Engineering - Numerical Methods in Geotechnical Engineering*, (February 2014), 595–600. https://doi.org/10.1201/9781439833766.ch86

Fleming, W. G. K., Weltman, A. J., & Randolph, M. (1985). *Piling Engineering* (2nd.). John & Wiley.

Fleuchaus, P., Schüppler, S., Godschalk, B., Bakema, G., & Blum, P. (2020). Performance analysis of Aquifer Thermal Energy Storage (ATES). *Renewable Energy*, *146*, 1536–1548. https://doi.org/10.1016/j.renene.2019.07.030

Gao, L., Zhao, J., & Tang, Z. (2015). A Review on Borehole Seasonal Solar Thermal Energy Storage, In *Energy procedia*. https://doi.org/10.1016/j.egypro.2015.02.117

Haimson, B., & Kovacich, J. (2003). Borehole instability in high-porosity Berea sandstone and factors affecting dimensions and shape of fracture-like breakouts. *Engineering Geology*, *69*(3-4), 219–231. https://doi.org/10.1016/S0013-7952(02)00283-1

Han, F., Salgado, R., Prezzi, M., & Lim, J. (2017). Shaft and base resistance of non-displacement piles in sand. *Computers and Geotechnics*, *83*, 184–197. https://doi.org/10.1016/j.compgeo.2016.11.006

Hogervorst, F., & Hoefsloot, F. (2020). Nieuwbouw appartementen Grevelingenweg Documentbeheer.

J. Desmedt, G. D. (2009). *Studie best beschikbare boortechnieken en evaluatie geschikte hydrothermische technieken in Brussel: aanvraag, kritische analyse en milieuexploitatievoorwaarden* (tech. rep.). BIM.

Javadi, H., Ajarostaghi, S. S. M., Rosen, M. A., & Pourfallah, M. (2018). A comprehensive review of backfill materials and their effects on ground heat exchanger performance. *Sustainability (Switzerland)*, *10*(12). https://doi.org/10.3390/su10124486

Lee, C., Lee, K., Choi, H., & Choi, H. P. (2010). Characteristics of thermally-enhanced bentonite grouts for geothermal heat exchanger in South Korea. *Science China Technological Sciences*, *53*(1), 123–128. https://doi.org/10.1007/s11431-009-0413-9

Lehane, B. M., & White, D. J. (2005). Lateral stress changes and shaft friction for model displacement piles in sand. *Canadian Geotechnical Journal*, *42*(4), 1039–1052. https://doi.org/10.1139/t05-023

Loukidis, D., & Salgado, R. (2008). Analysis of the shaft resistance of non-displacement piles in sand. *Geotechnique*, *58*(4), 283–296. https://doi.org/10.1680/geot.2008.58.4.283

Meyerhof, G. G. (1951). The ultimate bearing capacity of foundations. *Geotechnique*. https://doi.org/10.1680/geot.1951.2.4.301

Ministry of Economic Affairs and Climate Policy. (2020). Klimaatplan, 62.

Moor, M. (1994). Analysis of bored pile/diaphragm installation effects, (2), 341–347.

Nilsson. (2020). *Borehole Thermal Energy Storage Systems for Storage of Industrial Excess Heat* (Doctoral dissertation). Linköping University.

Normalisatie-Instituut., N. (1995). *Eurocode 7 : geotechnisch ontwerp. Dl. 1, Algemene regels (voornorm). LK - https://tudelft.on.worldcat.org/oclc/841725619*. Delft SE - 123 blz. ; .. cm., NNI.

Peels, J., & Dijkstra, O. (2010). Funderingsdag 2010 Thema-Uitgave. *Geotechniek*, (5), 22–26.

Phuong, N. T., van Tol, A. F., Elkadi, A. S., & Rohe, A. (2016). Numerical investigation of pile installation effects in sand using material point method. *Computers and Geotechnics*, *73*, 58–71. https://doi.org/10.1016/j.compgeo.2015.11.012

Plaxis. (2015). PLAXIS Material Models. *Plaxis Handbook 3D*.

Press, N. A., Committee, N., Mechanics, R., Board, G., & Systems, T. (1993). Stability, Failure, and Measurements of Boreholes and Other Circular Openings. *Stability, Failure, and Measurements of Boreholes and Other Circular Openings*. https://doi.org/10.17226/9177

Prezzi, M. (U., & Basu, P. (2005). Overview of construction and design of auger cast-in-place and drilled displacement piles. *Proceedings of the 30th Annual Conference on Deep Foundations, Chicago, Ill.*, *1*, 497–512. https://engineering.purdue.edu/~mprezzi/pdf/xxxxxxx1_overview_of_construction.pdf

Rad, F. M., & Fung, A. S. (2016). Solar community heating and cooling system with borehole thermal energy storage - Review of systems. https://doi.org/10.1016/j.rser.2016.03.025

Reuss, M. (2015). *Advances in Thermal Energy Storage Systems*. Woodhead Publishing Series. https://doi.org/10.1016/c2013-0-16453-7

Risnes, R., Bratili, R. K., & Horsrud, P. (1982). Sand Stresses Around a Wellbore. *Society of Petroleum Engineers journal*. https://doi.org/10.2118/9650-PA

Rostislav, D., & Magdaléna, K. (2018). Dataset on the innovation remediation technology of embankment dams by using suitable types of alternative raw materials. *Data in Brief*, *17*, 753–756. https://doi.org/10.1016/j.dib.2018.01.092

Schoemaker, F., Witkop, D., Schouten, F., Beerenhout, M., Groot, P., Vrisekoop, H., & Heynen, R. (2020). *Trendrapport* (tech. rep.). DNE Research.

SIKB. (2019). *Ontwerp, realisatie, beheer en onderhoud ondergronds deel van bodemenergiesystemen* (tech. rep.).

Spegelaere M. (2019). Richtlijnen en werkwijzen bodemenergie. *NVOE*, 37–45. https://nl.wikipedia.org/wiki/Civiele_techniek

Tomlinson, M. J., & Boorman, R. (1995). *Foundation design and construction LK - https://tudelft.on.worldcat.org/* (6th ed.). Harlow, England, Longman Scientific & Technical ;

USACE. (1977). Design of Pile Foundations. *Natl Coop Highw Res Program Synth Highw Pract*, (42). https://doi.org/10.1016/0148-9062(78)91390-6

Vaziri, H. H., & Byrne, P. M. (1990). Analysis of stress, flow and stability around deep wells. *Geotechnique*, *40*(1), 63–77. https://doi.org/10.1680/geot.1990.40.1.63

Verruijt, A. (2010). *Soil Mechanics*. Delft, TU Delft, Department Hydraulic Engineering SE -. https://tudelft.on.worldcat.org/oclc/7792828981

Vesic, A. B. (1975). Bearing Capacity of Deep Foundations in Sand.

Welsch, B., Rühaak, W., Schulte, D. O., Bär, K., & Sass, I. (2016). Characteristics of medium deep borehole thermal energy storage. *International Journal of Energy Research*. https://doi.org/10.1002/er.3570

WKO Nederland. (2020). Bodemenergie. https://wkonederland.nl/bodemenergie/

Zhang, J. J. (2019). *Borehole stability*. https://doi.org/10.1016/b978-0-12-814814-3.00010-1